THERMAL AND NUCLEAR DESIGN REVIEW OF THE NRX-A5 REACTOR
(Title Unclassified)

Astronuclear Laboratory

Westinghouse Electric Corporation

DISCLAIMER

This report was prepared as an account of work sponsored by an agency of the United States Government. Neither the United States Government nor any agency Thereof, nor any of their employees, makes any warranty, express or implied, or assumes any legal liability or responsibility for the accuracy, completeness, or usefulness of any information, apparatus, product, or process disclosed, or represents that its use would not infringe privately owned rights. Reference herein to any specific commercial product, process, or service by trade name, trademark, manufacturer, or otherwise does not necessarily constitute or imply its endorsement, recommendation, or favoring by the United States Government or any agency thereof. The views and opinions of authors expressed herein do not necessarily state or reflect those of the United States Government or any agency thereof.

DISCLAIMER

Portions of this document may be illegible in electronic image products. Images are produced from the best available original document.

DECLASSIFIED

Astronuclear
WANL-TME-758
May 15, 1964

THERMAL AND NUCLEAR DESIGN REVIEW OF THE NRX-A5 REACTOR
(Title Unclassified)

PREPARED BY:

D. L. Black

W. Minners

J. S. Stefanko

R. M. Vijuk

INFORMATION CATEGORY

C-R-D.

B. J. Riek 5/13/64
Authorized Classifier   Date

GROUP 1

Excluded from Automatic Downgrading
And Declassification

APPROVED BY:

J. G. Gallagher, Manager
Reactor Analysis

Westinghouse Electric Corporation

Astronuclear Laboratory

Large, Pennsylvania

May 15, 1964

DECLASSIFIED

THIS PAGE

WAS INTENTIONALLY

LEFT BLANK

DECLASSIFIED

Astronuclear

TABLE OF CONTENTS

DECLASSIFIED

THIS PAGE

WAS INTENTIONALLY

LEFT BLANK

DECLASSIFIED

Ⓦ Astronuclear

LIST OF ILLUSTRATIONS

v

DECLASSIFIED

Astronuclear

LIST OF ILLUSTRATIONS (Cont)

CONFIDENTIAL
RESTRICTED DATA
Atomic Energy Act 1954

DECLASSIFIED

Astronuclear

LIST OF ILLUSTRATIONS (Cont)

Astronuclear

LIST OF TABLES

Astronuclear

ABSTRACT

A thermal and nuclear NRX-A5 Design Review was held at WANL on April 10, 1964. Analyses and planning performed to date on the NRX-A5 and subsequent reactors were presented. Systems analyses were performed on various "cooled periphery" and "hot periphery" seal configurations. A number of inner reflector designs were examined, as well as means for cooling the lateral support springs.

Core component redesign included methods for controlling inter-element pressure distribution by undercutting or chamfering of fuel elements. Changes in tie rod diameters, use of as-extruded fuel elements, and performance analysis of the various systems were also described.

Nuclear analysis was confined to parametric studies on excess reactivity and control drum span for inner reflector material combinations of graphite, aluminum, and/or beryllium. Changes required to more precisely define the NRX-A5 were discussed together with the effects associated with the twice power reactor capability envisioned for subsequent reactors.

DECLASSIFIED

Astronuclear

SECTION 1

INTRODUCTION

The first NRX-A5 Design Review Meeting was held at WANL on April 9th and 10th, 1964.*   The purpose of the meeting was to review the work already accomplished and to formulate plans for the final design of the NRX-A5.   This report documents the thermal and nuclear portions of that meeting.

The scope of the NRX-A5 redesign was limited to changes in the core-periphery inner-reflector area to eliminate uncertainties associated with the NRX-A2 design.   A second major objective was to evaluate the KIWI B-4D wrapper seal concept.   A basic ground rule was that all redesigned components be interchangeable with the NRX-A1, NRX-A2, NRX-A3 and NRX-A4 reactors.   Additionally, NRX-A5 was to be power rated at 1100 MW with the same flow capability as the NRX-A2.

Based on these ground rules, studies were initiated to improve the reactor thermal and mechanical design.   No nuclear changes were anticipated except as a result of mechanical design changes.   Areas of improvement considered were reduction of possible core in-leakage from the support system, inner reflector lift-off, and inner reflector cylinder buckling.

The possibility of inner reflector lift-off from the nozzle flange can be reduced by the inclusion of heavier pre-load hold down springs.   The inner reflector cylinder buckling can be reduced by increasing the graphite thickness or by changing to a stronger metal design. In this connection, the nuclear effects of various inner reflector combinations of graphite, aluminum, and beryllium on reactivity and control drum span have been evaluated.

Two opposite approaches were taken in an attempt to solve the core in-leakage problem. The first was the "cooled periphery" approach which uses a metal seal or mechanical barrier, such as the wrapper on KIWI B-4D, to separate the core inter-element flow from the seal leakage flow.   The use of metal seals to prevent core in-leakage requires convective cooling; thus the name "cooled periphery".

---

* A list of attendees at the April 10th meeting is given in Appendix A.

DECLASSIFIED

Astronuclear

The second or "hot periphery" approach eliminates all cooling in the periphery-lateral support region, elevating the filler strips and seal rings to near core temperature. With this method, no special attempt is made to eliminate the in-leakage. It is assumed that any in-leakage will approach fuel element temperature and no thermal stresses will be induced; thus the term "hot periphery".

Design improvement studies were also made in the NRX-A5 core components. These include such items as the use of as extruded fuel elements, tie rod diameters, core internal pressure distributions, and possible effects on core performance of various proposed reactor designs.

Astronuclear

SECTION 2

THERMAL ANALYSIS

2-1   COOLED PERIPHERY CONCEPT

The cooled periphery concept for eliminating core in-leakage consists of the providing of a positive flow barrier between the core and the lateral support system. One type of flow barrier is provided by a wrapper of thin metallic foil for the core and filler strips. This wrapper method was pioneered by LASL for the KIWI B-4D program. Another type of flow barrier is provided by a metal reed which seals the interface of adjacent filler strips. In both cases these are mechanical type seals for which cooling must be furnished.

A.   Wrapper Seal

The first studies were based on the KIWI B-4D design, modified to meet NRX-A5 requirements. Six different wrapper configurations were considered, each varying in core diameter, inner reflector thickness, or number of springs. From a system point of view, these six configurations reduce to only two, a distributed seal and a nozzle end seal. A distributed seal refers to an axially distributed pressure profile on the periphery of the core. The nozzle end seal refers to an axially constant pressure profile. The variations in the configurations have little effect on temperature distribution and system analysis.

A plan view of a typical section of the core periphery and inner reflector is shown in figure 2-1. This section closely resembles the KIWI B-4D design in that it has small inner filler strips, internally cooled large outer filler strips (432 Invar lined tubes, 0.117 inch inside diameter), and a 5 mil metallic foil wrapper in 48 segments surrounding the filler strip outer periphery.

(W) Astronuclear

OUTER REFLECTOR

REFLECTOR ANNULUS

GRAPHITE CYLINDER (INNER REFLECTOR)

PLUNGER

STAGNANT   HYDROGEN

SEAL (OR LOAD) RING

WRAPPER

SEAL LEAKAGE

FILLER STRIP

FILLER STRIP COOLANT

PYRO TILES

INNER FILLER STRIP

FUEL ELEMENT

TYPICAL CROSS SECTION   597859A
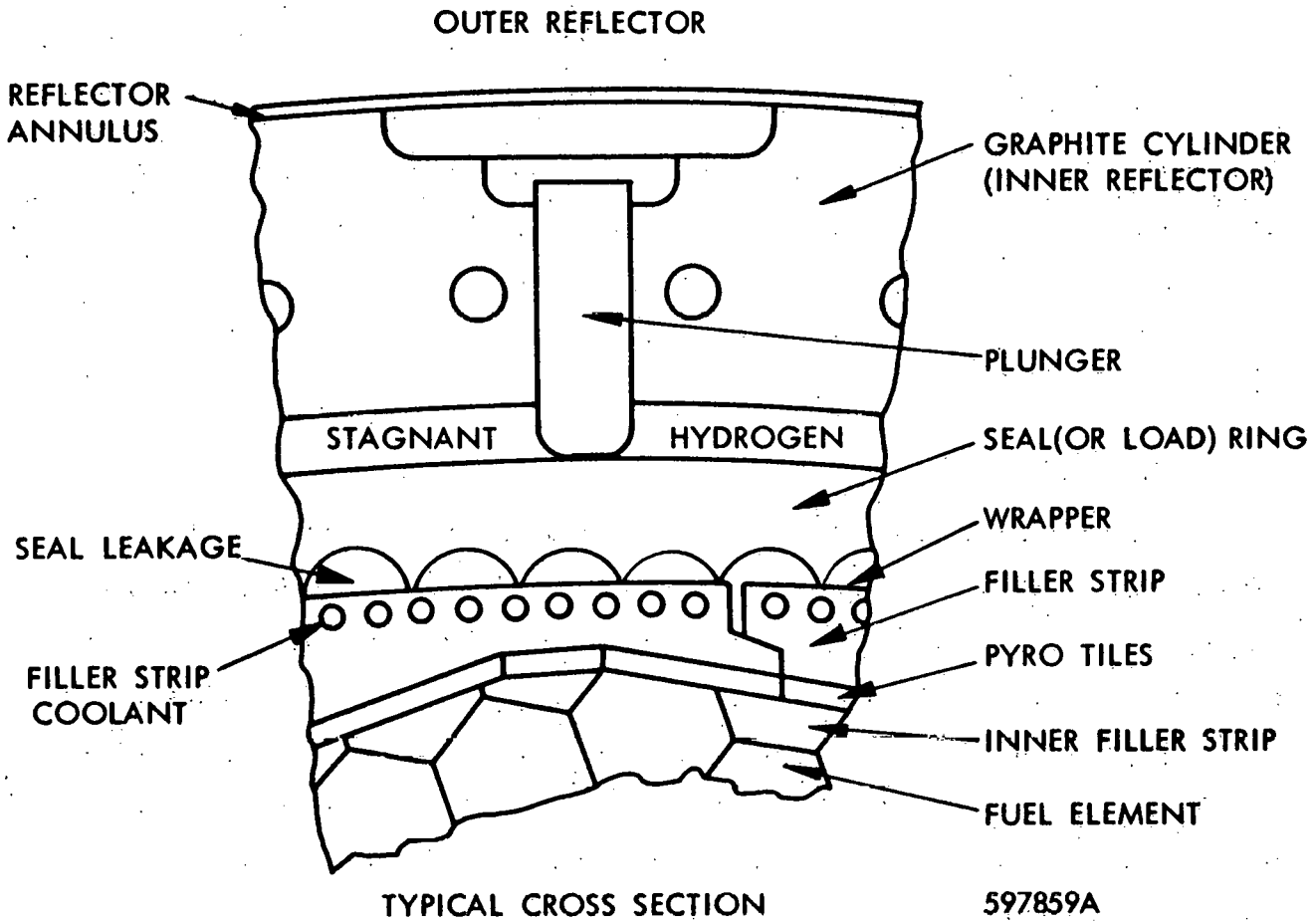
Figure 2-1 Cooled Periphery Concept with Wrapper – Typical Cross Section

-4-

The temperature distribution was calculated using THT-B (Transient Heat Transfer – Version B), a finite difference digital computer code. The model was a one-dimensional radial conduction solution in conjunction with a one-dimensional axial compressible flow solution. Azimuthal symmetry was assumed, with the rings of coolant holes, as in the filler strips, being modeled as a flow annulus. The average inner filler strip thickness was taken as 0.10 inch; the average outer filler strip thickness as 0.50 inch. Stagnant hydrogen was assumed to exist in the seal cavity between the seal ring and the inner reflector. Heat transfer across this gap was by molecular conduction. The gap thickness was adjusted axially to account for radial core expansion. The only differences in the model for nozzle end and distributed seal configurations were the flow rates and fluid boundary conditions of bulk temperature and film coefficient. The magnitude and distribution of radiation heating in the components were assumed to be the same as for the NRX-A2 reactor operating at 100 percent power.

The axial distribution of average material temperatures is shown in figures 2-2 and 2-3, for the nozzle end seal and the distributed seal respectively. The fluid temperature profile in each of the four streams (filler strip and seal leakage coolant in parallel with core flow, and the graphite cylinder and reflector annulus coolant counter-current with core flow) is shown in figure 2-4 for the nozzle end seal and in figure 2-5 for the distributed seal. The radial temperature profile through a seal or load ring at midplane (Station 26) is given for the nozzle end seal in figure 2-6 and for the distributed seal in figure 2-7. The shape of these curves is typical of all the other axial positions.

The axial pressure distribution for inter-element, filler strip and seal leakage flows is shown in figure 2-8. This curve provides the maximum and minimum hydraulic bundling pressures (radial ΔP) that the core might experience. The two curves labeled inter-element are the maximum and minimum pressures anticipated. Both nozzle end and distributed seal pressure distributions are given. The core pressure drop of 129 psi was assumed to be the same as the NRX-A2. The axial pressure distribution in the reflector annulus and in the graphite cylinder coolant holes is shown in figure 2-9 for a reflector pressure drop of 44 psi.

Astronuclear
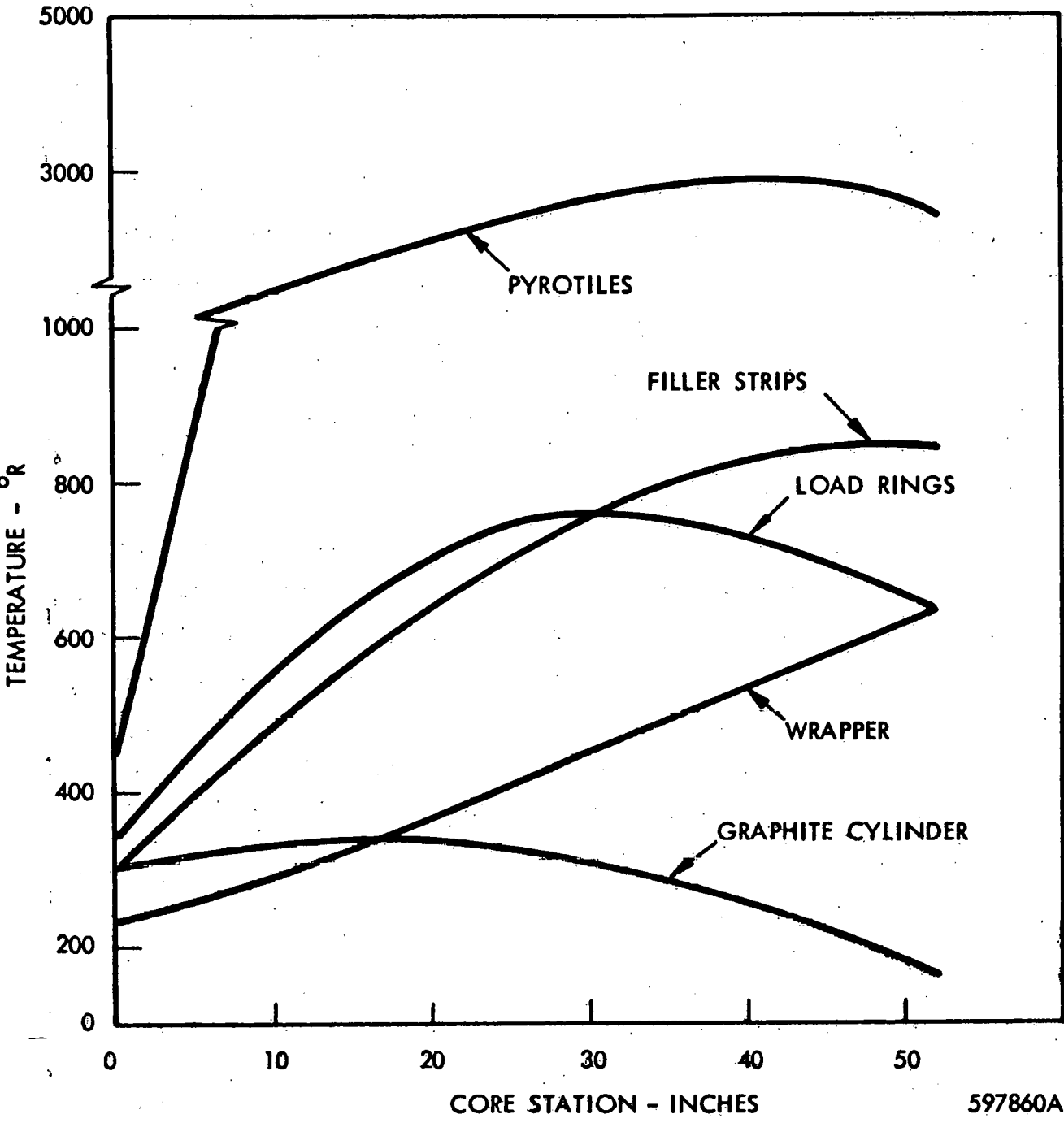
Figure 2-2 Average Material Temperatures, Cooled Periphery Concept
with Wrapper Nozzle End Seal

Astronuclear
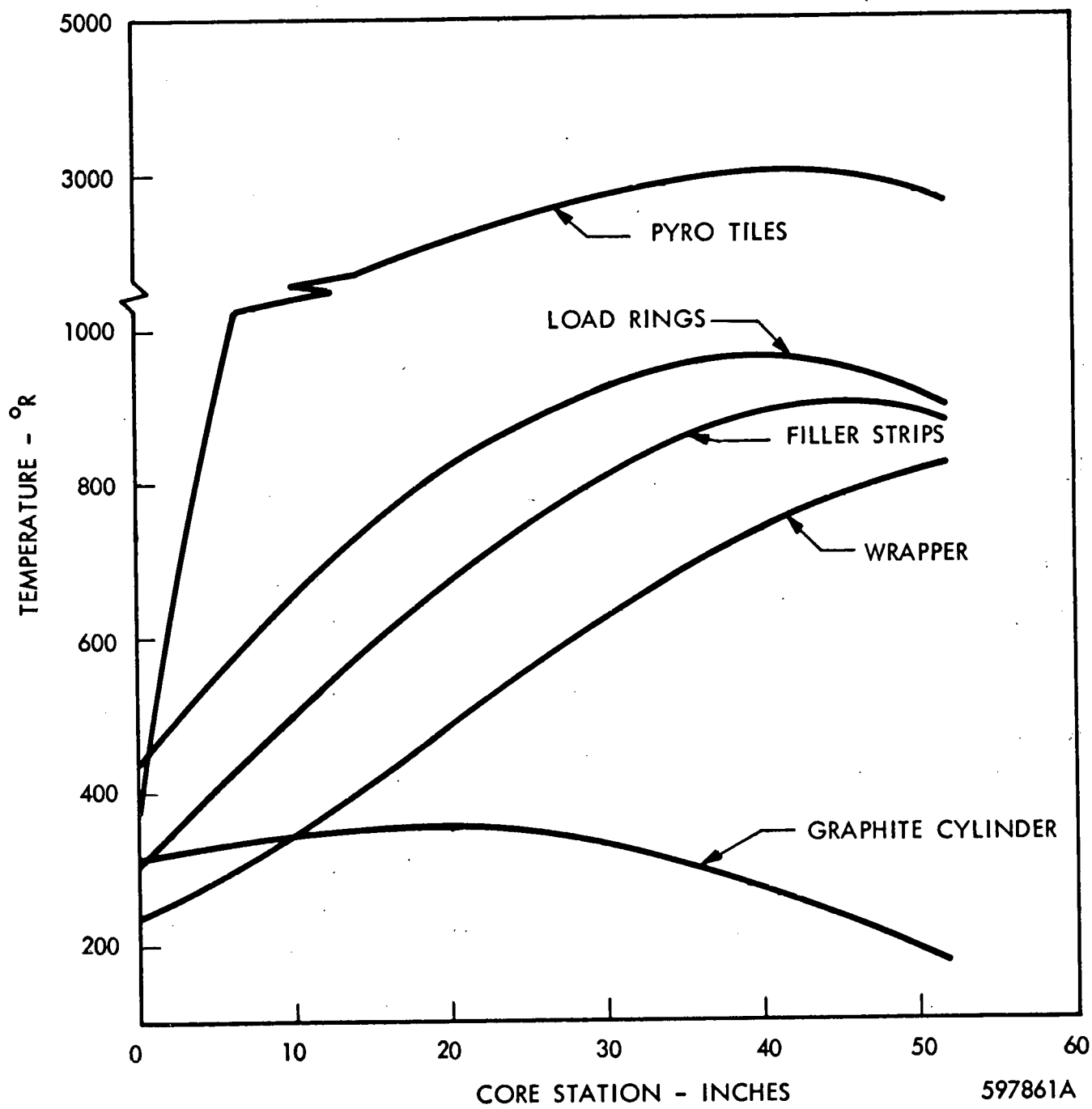
Figure 2-3 Average Material Temperatures, Cooled Periphery Concept
with Wrapper Distributed Seal

Astronuclear
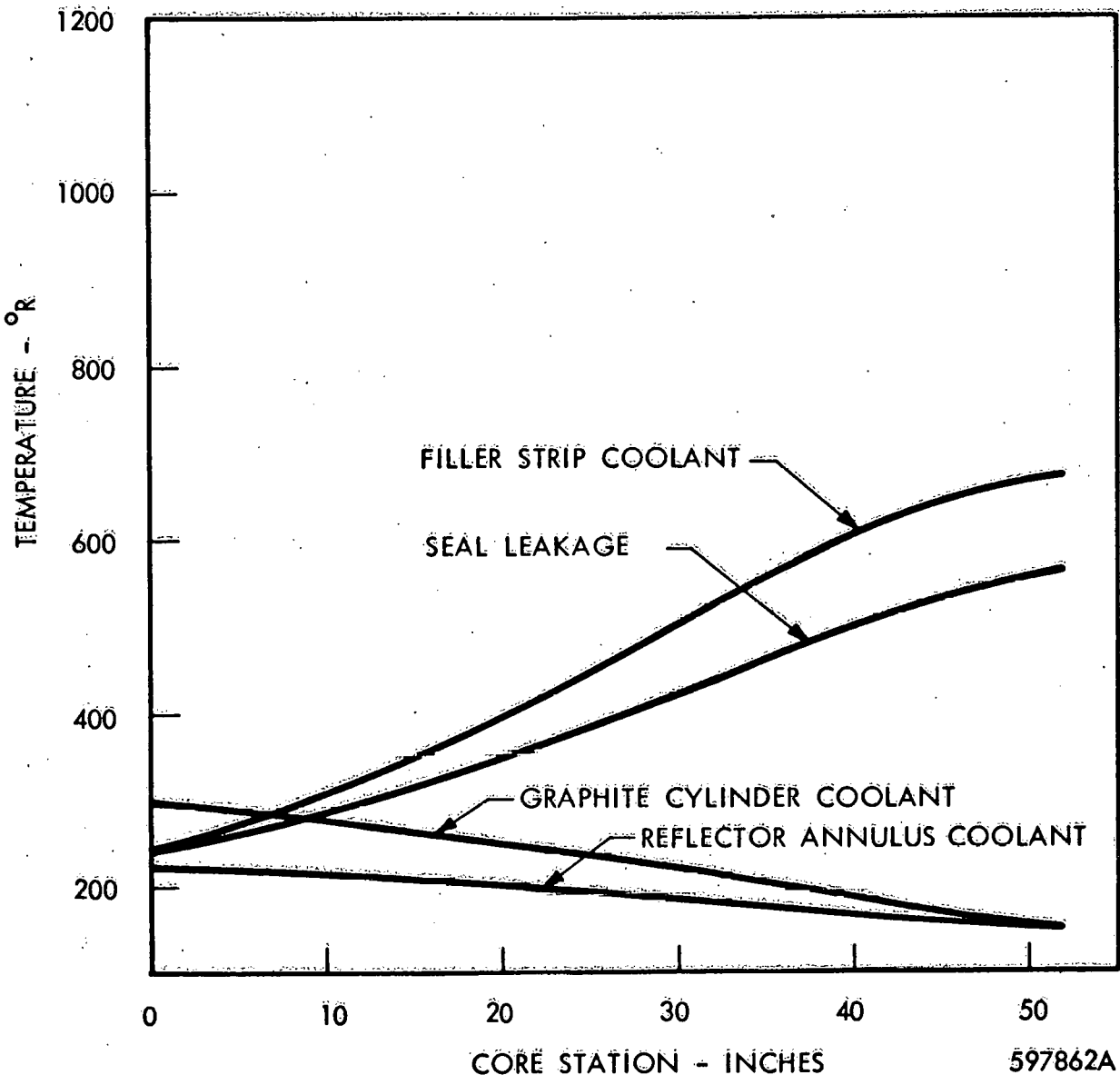
Figure 2-4 Fluid Temperatures, Cooled Periphery Concept with Wrapper
Nozzle End Seal

-8-

DECLASSIFIED

(W) Astronuclear
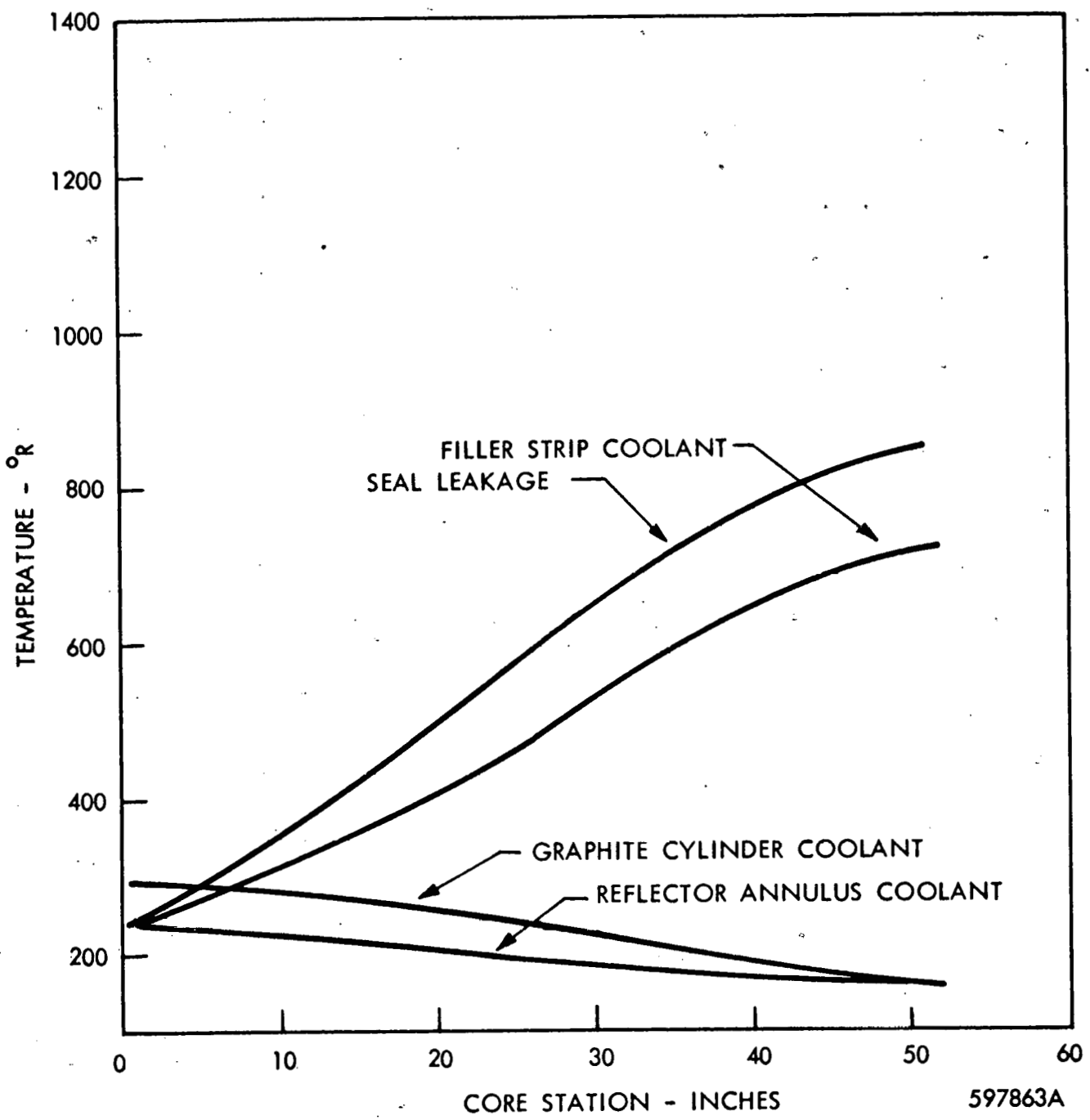
Figure 2-5 Fluid Temperatures, Cooled Periphery Concept with Wrapper
Distributed Seal

DECLASSIFIED
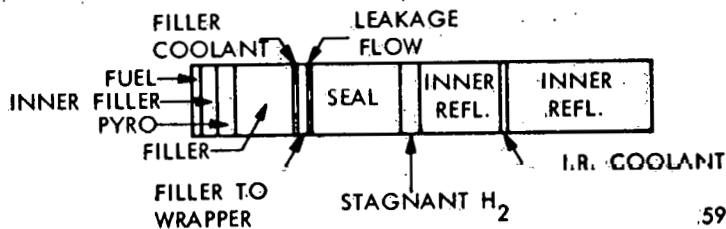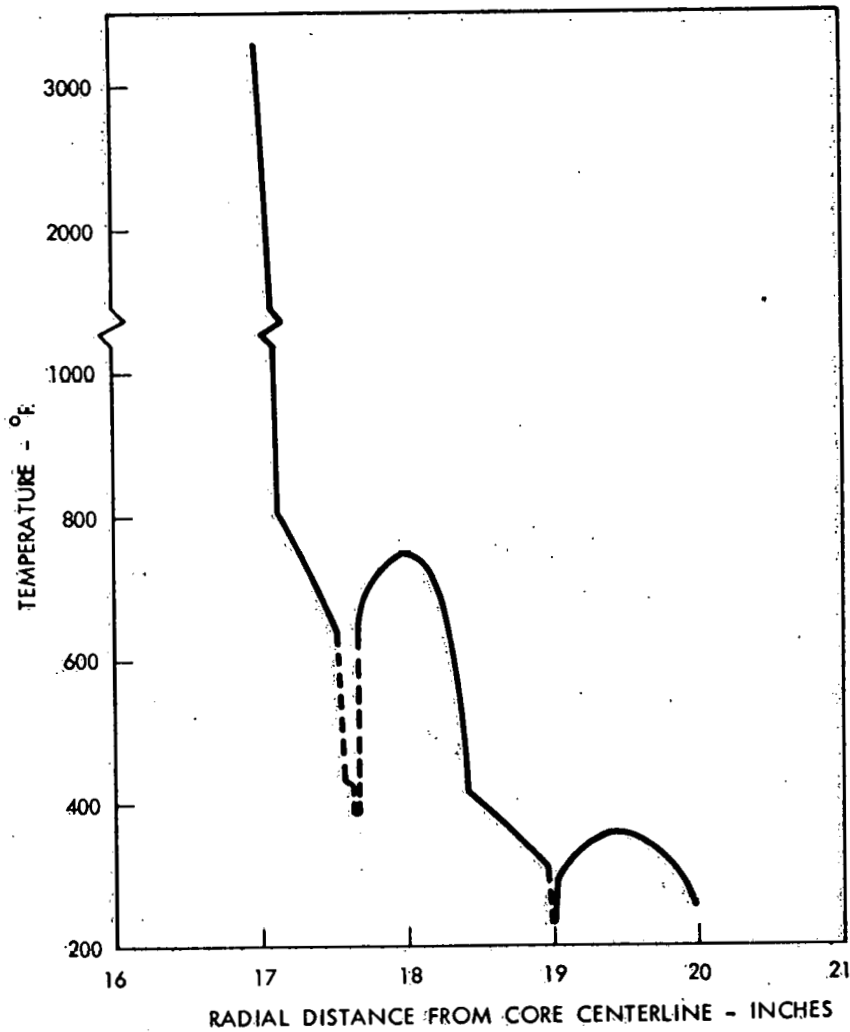
Figure 2-6 Radial Temperature Profile, Core Station 26, Cooled Periphery
Concept with Wrapper Nozzle End Seal

Astronuclear
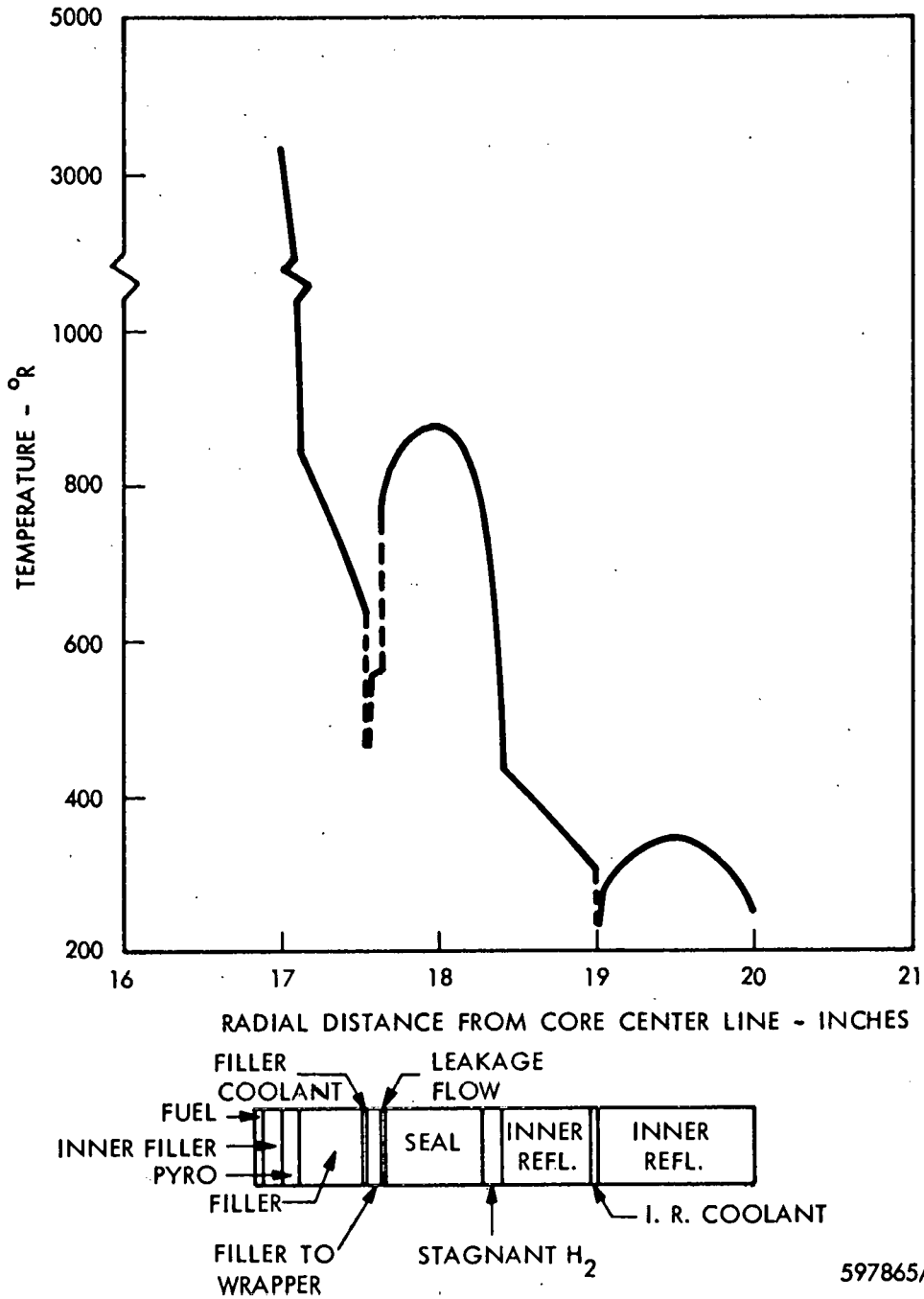
Figure 2-7 Radial Temperature Profile, Core Station 26, Cooled Periphery
Concept with Wrapper Distributed Seal

597865A

Astronuclear
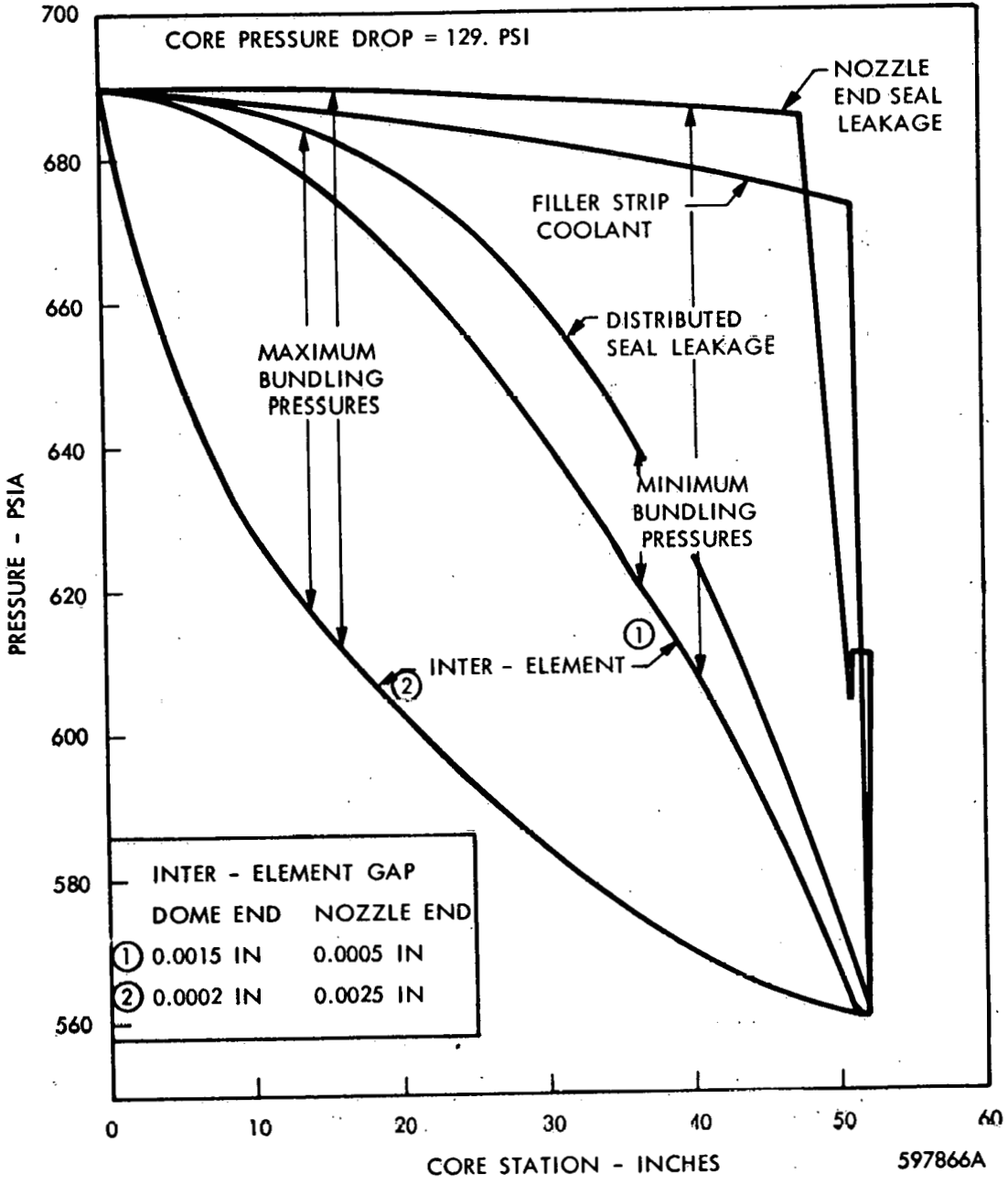
Figure 2-8 Axial Pressure Profiles, Cooled Periphery Concept with
Wrapper Nozzle End Seal and Distributed Seal Systems

Astronuclear
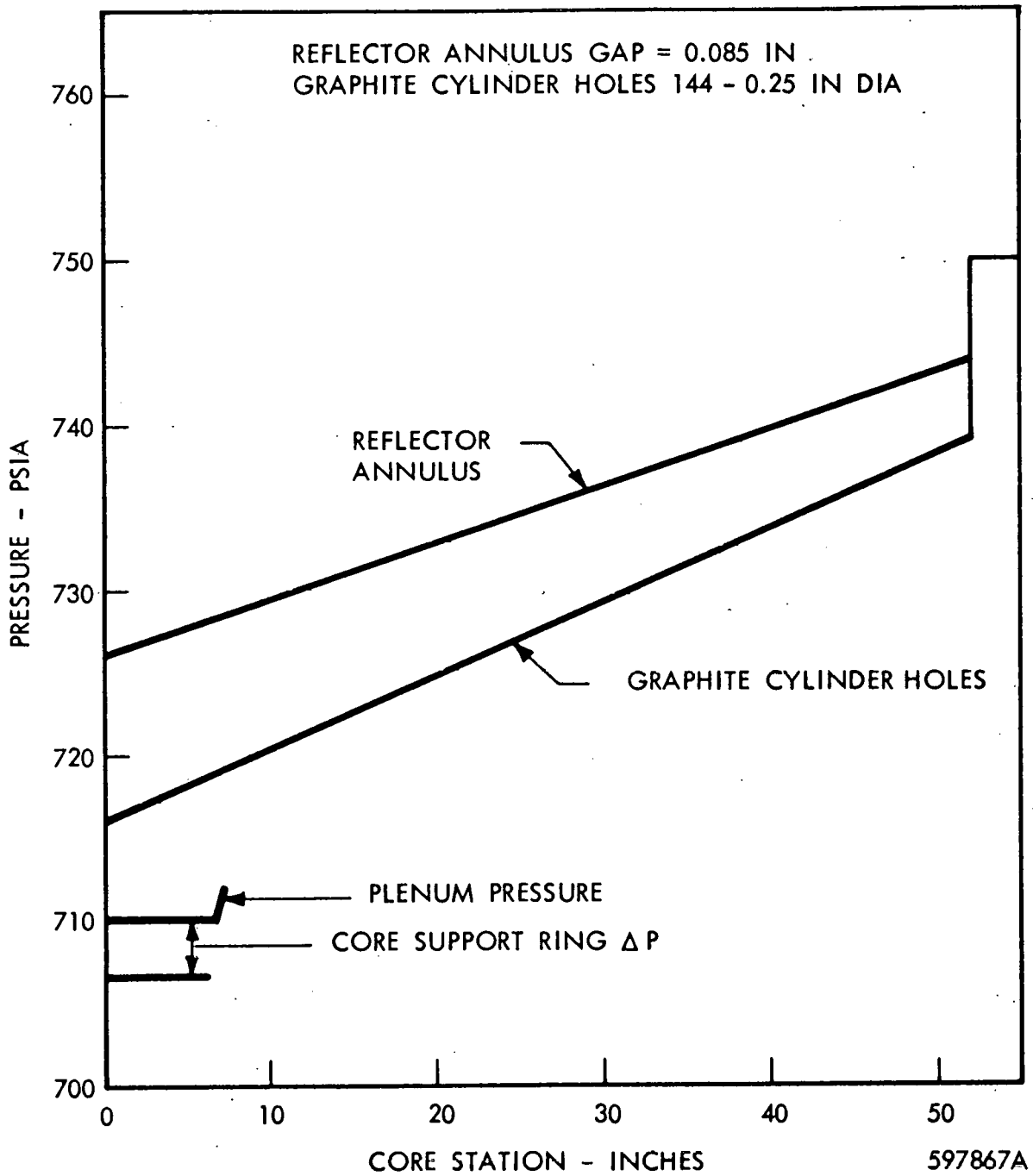
Figure 2-9 Inner Reflector Axial Pressure Profiles Cooled Periphery
Concept with Wrapper

The two cooled periphery seal designs are compared in Table 2-1. Performance data indicates a decrease relative to the NRX-A2 in specific impulse for the nozzle end seal of 2.1 percent and for the distributed seal of 1.3 percent. These values were calculated by holding the core and tie rod mixed exit temperatures constant and the total system flow constant. Nozzle chamber temperature dropped 171°R and 106°R for the nozzle end and distributed seals respectively.

Temperature levels and differences are similar for both systems. Radial temperature differences in the pyro are slightly greater, 50°R, with the nozzle end seal. The maximum difference is 3390°R at Core Station 45. Maximum seal ring and wrapper temperatures are nearly 200°R hotter with the distributed seal from the effect of the hotter leakage flows. From a pressure bundling standpoint, the nozzle end seal provides an additional 29 psi radial ΔP based on average axial pressures. From a reliability standpoint, the single nozzle end seal is inferior to a multiple seal system.

The wrapper seal works well but does not entirely eliminate the core in-leakage. Fluid entering the dome end plenum can flow axially behind the wrapper in the area between adjacent filler strips. The total flow may be in the order of 0.02 lb/sec. A portion of this fluid at the temperature of the filler strips (less than 1000°R) can flow radially into the core depending on the inter-element radial pressure difference.

B.   Metal Reed Seal

Because of this limitation, another method for sealing the periphery was analyzed. This method, called the metal reed seal, is illustrated in figures 2-10 and 2-11. Figure 2-10 compares the wrapper concept (KIWI B-4D periphery) with the metal reed seal concept. The filler strips of the latter are tie rod supported and hung from the core support plate. The filler strip junction is sealed by a pressure seated metallic foil. This is shown more clearly in figure 2-11. An axial flow path is provided on the reflector side of the reed which pressure communicates with the lateral support seal leakage. Tie rods are cooled externally by flow in an annulus between the tie rods and the filler strips. Axial flow behind the reed is impeded by a small graphite cylinder inserted from the core side at the

Astronuclear

TABLE 2-1

COOLED PERIPHERY CONCEPT WITH WRAPPER

PARAMETER	NOZZLE END SEAL	DISTRIBUTED SEAL
Specific impulse relative to NRX–A2	0.979	0.987
Nozzle chamber temperature $^\circ$R (A2 = 4087)	3916	3981
Total flow into nozzle chamber, lb/sec	4.2	2.8
Mixed temperature of filler strip and leakage coolant, $^\circ$R	612	752
Reflector annulus flow, lb/sec	12.5	12.5
Graphite cylinder flow, lb/sec	6.5	6.5
Filler strip flow, lb/sec	2.0	2.0
Seal leakage flow, lb/sec	2.2	0.8
Maximum axial average pyro temperature, $^\circ$R	2800	2800
Maximum radial ΔT in pyro, $^\circ$R	3390	3340
Maximum average seal ring temperature, $^\circ$R	760	950
Maximum wrapper temperature, $^\circ$R	640	810
Axial average radial ΔP between seal and inter-element flow, psi		
Maximum	84	55
Minimum	41	12

KIWI FILLER SLAT

PYRO TILE

COOLING HOLES

PYRO CUP

MODIFIED FILLER SLAT

PYRO TILE
RETENTION PIN

PYRO TILE

TIE ROD
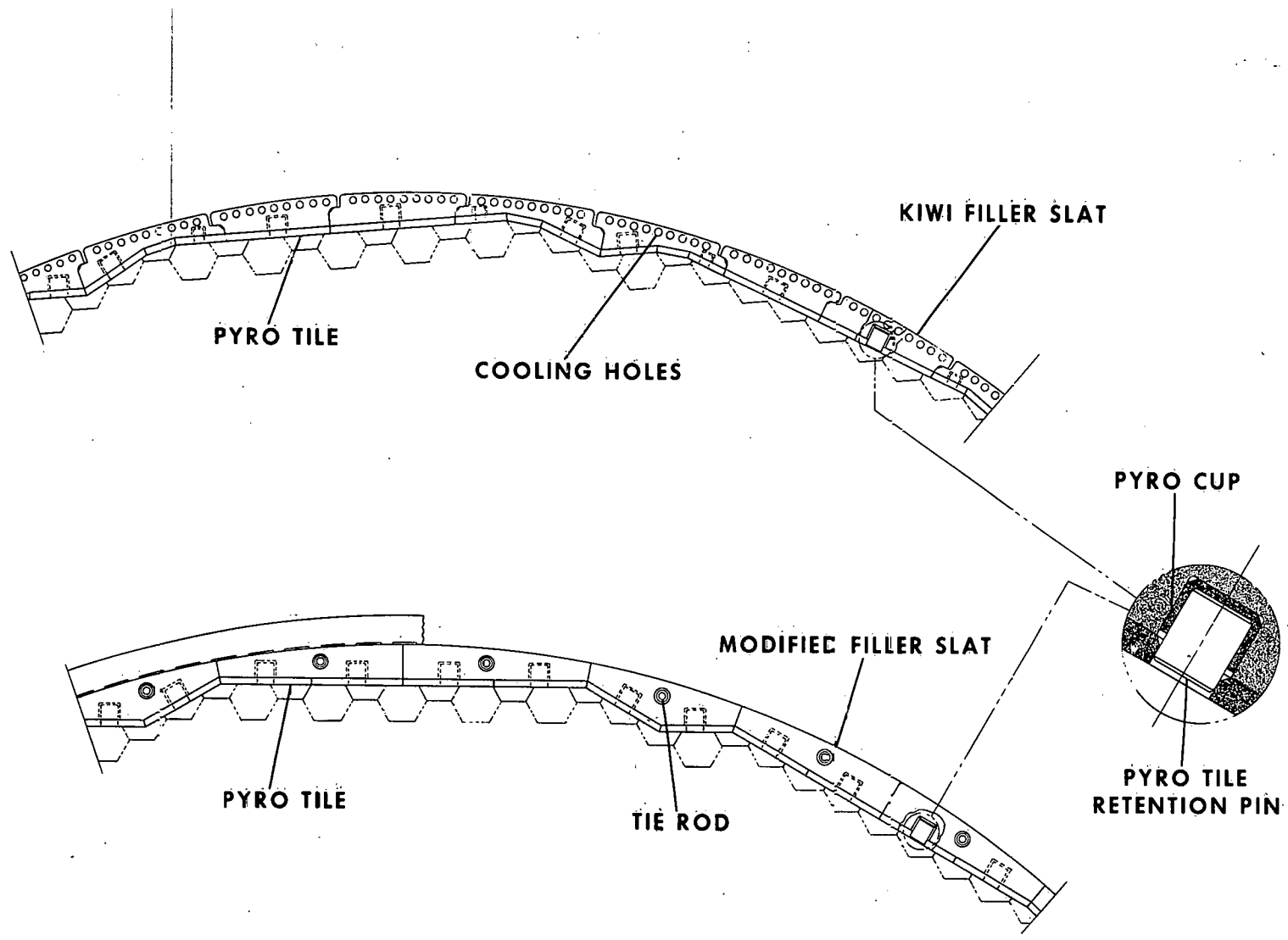
Figure 2-10 Comparison of Wrapper Seal with Metal Reed Seal

Astronuclear

Astronuclear

HOLD DOWN ARM

FILLER SLATS

METAL RADIAL
FLOW IMPEDANCE

GRAPHITE AXIAL
FLOW IMPEDANCE

TIE ROD
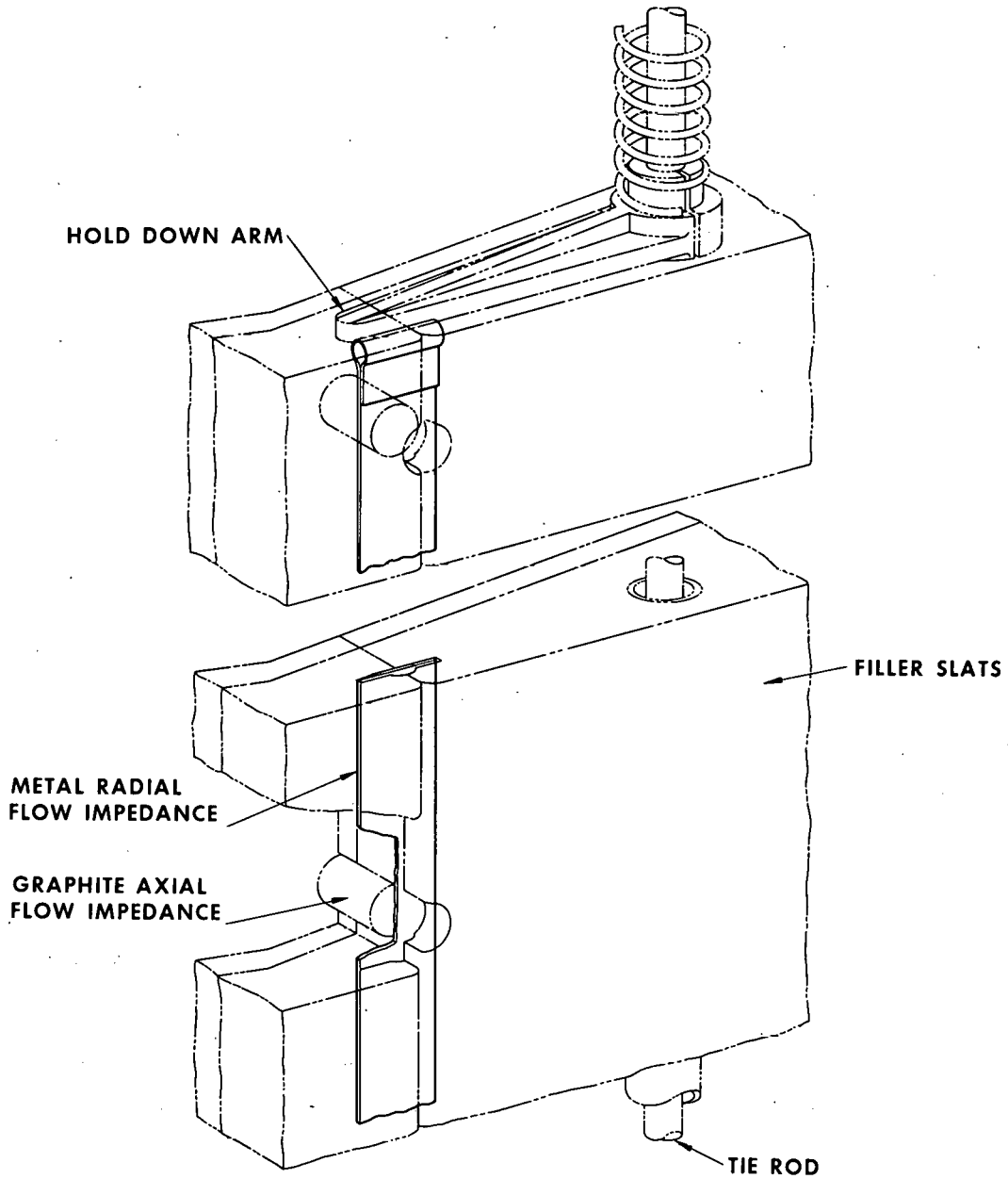
Figure 2-11 Metal Reed Seal Flow Impedance at Core Periphery

junction of filler strips. The required number of these cylinders has not as yet been determined.

The metal reed concept was analyzed to determine feasibility from a temperature level point of view. A two-dimensional (r, θ) model of an average filler strip was constructed for use with the THT-B code. Core Stations 26 and 45 were studied and typical results are shown in figures 2-12 and 2-13 respectively. A full systems analysis on this concept has not been performed to date; that is, no calculations of flow balancing in the tie rod, metal reed, and seal leakage channels have been made. For this reason, parametric studies were made covering a range of fluid temperatures; the results given are for the estimated fluid temperature indicated on the figures.

Thermal analysis of the metal reed design shows that temperature levels are comparable with the wrapper design. The radial temperature difference in the filler strip is approximately twice that of the wrapper design, or $400^{\circ}R$. From a performance standpoint, although exact values have not been calculated, it is believed that the metal reed system will result in less of a specific impulse loss. While feasibility has been demonstrated additional analysis is required to establish all system parameters.

In summary, it is concluded that:

1) The wrapper concept utilizing either the nozzle end or distributed seal system, is feasible from the thermal and hydraulic point of view.

2) The distributed seal is considered more reliable than the single nozzle end seal.

3) The wrapper seal will do an efficient but not wholly complete job of eliminating cold in-leakage to the core from the lateral support system.

4) Other peripheral core designs, such as the metal reed seal, show that radial in-flow leakage may be effectively reduced in other ways.

2-2   HOT PERIPHERY CONCEPT

The "hot periphery" concept is another method for preventing cold gas in-flow into the reactor core; an in-flow which would cause adverse temperature gradients to develop in the fuel elements. Ideally, a hot periphery design would accomplish this by eliminating

DECLASSIFIED

Astronuclear

450   INNER REFLECTOR

500

750

1000   STAGNANT HYDROGEN

1100

1200

1100

SEAL SEGMENT

1000

METAL REED
SEAL

700

1200

1250

1300   FILLER STRIP

TIE ROD
COOLANT

1400

2750

PYROGRAPHITE

FUEL

3320

597870A

TEMPERATURES IN °R
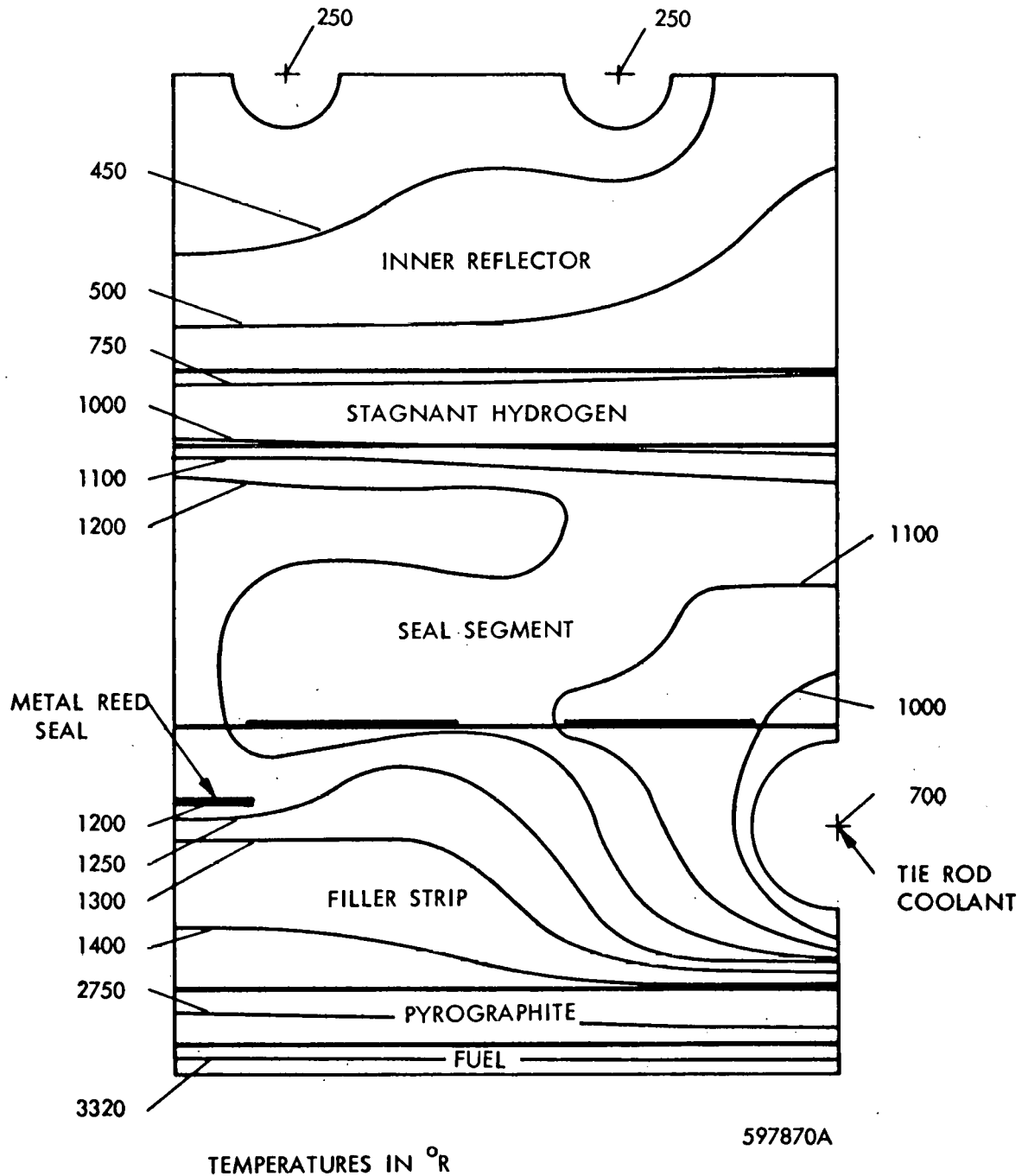
Figure 2-12 Cooled Periphery Concept with Tie Rod Supported Fillers and
In-Flow Seal, Core Station 26

DECLASSIFIED

Astronuclear
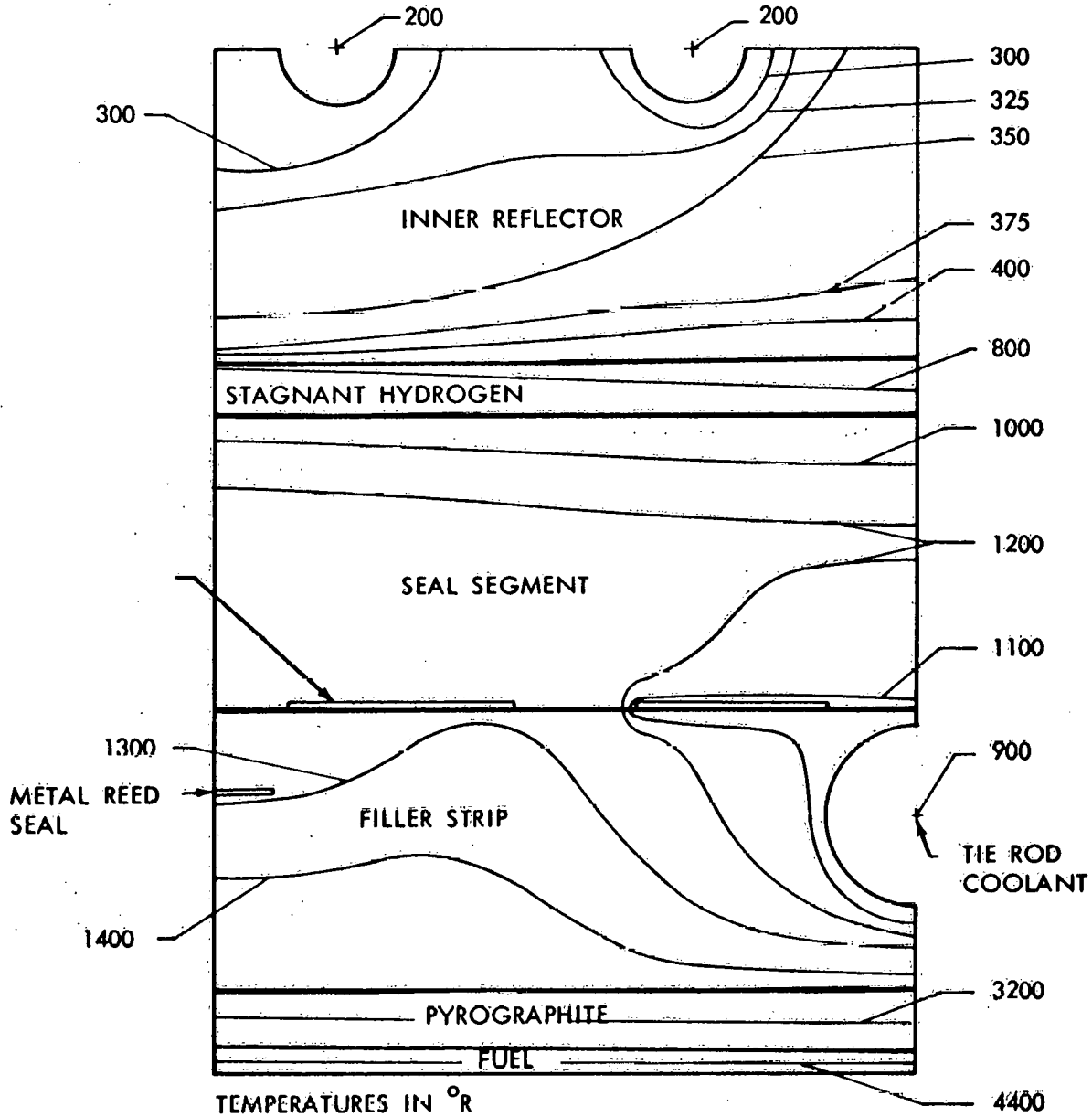
Figure 2-13 Cooled Periphery Concept with Tie Rod Supported Fillers and In-Flow Seal, Core Station 45

Astronuclear

all coolant flow from the core periphery. However, a more realistic approach is a design which maintains the core periphery coolant flow at a minimum, with the coolant temperature nearly equal to the core temperature at all axial positions. In this way, radial in-flow of coolant will not jeopardize the mechanical integrity of the fuel elements.

A feasibility study of the hot periphery design was performed which considered:

1) the temperature levels and distribution in the periphery region,

2) the graphite corrosion process and its effects, and

3) the axial pressure distribution available for bundling the core.

A. Periphery Region Temperatures

The temperature distributions in the core periphery region were determined for three core periphery-inner reflector configurations. Each configuration was analyzed using three-dimensional nodal models and either the THT-B Code or the TOSS Code. Coolant flow in the periphery region was assumed to be neglible. Surface contact between components was assumed to be intimate and the void regions in the lateral support system to be filled with stagnant hydrogen. Heat transfer through these voids was considered to be by means of molecular conduction and surface-to-surface radiation. Coolant flow rates and bulk temperatures in the inner reflector cooling channels, reflector annulus, and fuel element cooling channels were assumed to be the same as for the NRX-A2 at full power operation. Convective film coefficients were taken from NRX-A2 solutions and modified by the channel dimensions of the designs analyzed. The volumetric heat generating rates assumed were also taken from the NRX-A2 operating at full power.

The first core periphery-inner reflector configuration analyzed was identical with the NRX-A2 design except for the lateral support seal rings which were not grooved on their inner circumference. The temperature distribution in this configuration is shown in figure 2-14 for Core Station 26 where the heating rates are at a maximum. The two curves on this figure are the radial temperature profiles at two slightly different core stations, one station being at the center of the seal ring and the other centered between seal rings. The radial and axial temperature gradients are readily observable from the figure. Temperature

Figure 2-14 Temperature Distribution in an NRX-A2 Type Inner Reflector Having Stagnant Hydrogen in the Seal Region Voids, Core Station 26 at Full Power

Astronuclear

gradients in the azimuthal direction were found to be neglible. It should be noted that the temperature levels in the pyrolytic tiles, filler strips, and seal rings are strong functions of the width of the stagnant hydrogen regions because a major portion of the radial temperature drop appears across these regions.

The second core periphery-inner reflector configuration analyzed is shown in figure 2-15. This arrangement consisted of pyrolytic graphite tiles and graphite filler strips identical to those used in NRX-A2, but employed an aluminum inner reflector having a repeating "Z" shaped cross section and seal rings having a triangular cross section. Rings of graphite felt were located between the inner reflector and seal rings to provide lateral support for the core. The temperature distribution for the design at Core Station 26 is shown by the isotherms plotted on figure 2-15. As in the preceding configuration, the azimuthal temperature gradients were negligible compared to the axial and radial gradients. The major portion of the radial temperature drop appeared in the stagnant hydrogen and graphite felt. Therefore, the temperature levels in the core periphery region were strongly dependent on the radial thickness of these materials. The temperature distribution in the seal rings and inner reflector are discussed in Section 2-3.

The third core periphery-inner reflector configuration is shown in figure 2-16. The temperature distribution shown is at Core Station 26. In this design, in which an aluminum inner reflector is utilized, lateral support of the core is provided by metallic springs and graphite plungers. Radial in-flow of coolant along the plungers is prevented by containing the springs in sealed pockets. These pockets were assumed to be filled with stagnant hydrogen and the springs were not included in the conduction model of the system. The temperature distribution does not differ significantly from that in the previous configuration.

The temperature distributions were also determined at Core Station 48 where the core temperature is at its maximum value. However, because the heating rates and reflector coolant temperatures were significantly less at this point than they were at Core Station 26, the temperature levels and gradients in the core periphery and inner reflector were found to be significantly reduced compared to those at Core Station 26.

Astronuclear

GRAPHITE FELT
ALUMINUM BARREL
OUTER REFLECTOR
COOLANT TEMP = 206 °R

300 °R
COOLANT TEMP = 240 °R
300 °R
1000 °R
1500 °R
2000 °R
2700 °R
3000 °R
4000 °R
4600 °R

SURFACE TEMP = 870 °R

GRAPHITE SEAL
GRAPHITE FILLER STRIP
PYROLYTIC GRAPHITE
STAGNANT HYDROGEN
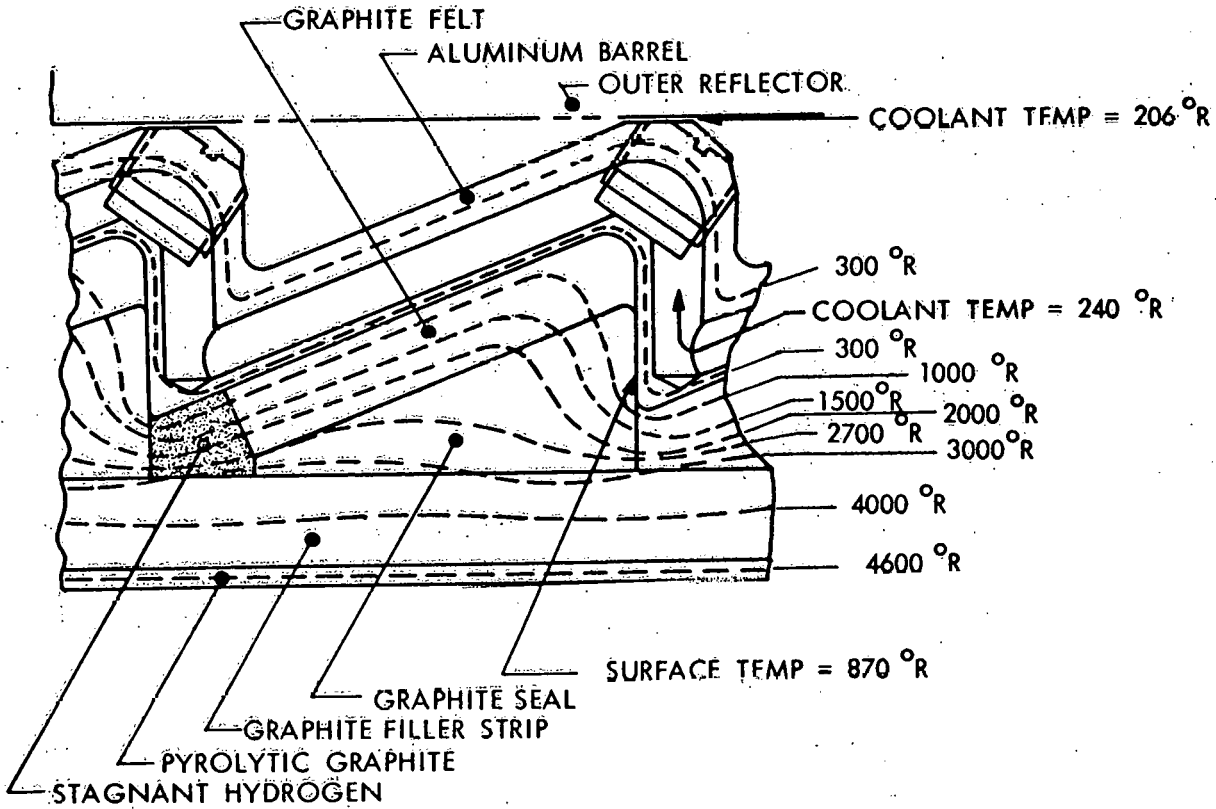
597871A

Figure 2-15 Temperature Distribution in an Aluminum Inner Reflector with Stagnant Hydrogen in the Seal Region Voids, Core Station 26 at Full Power, Surface Temperature 870°R
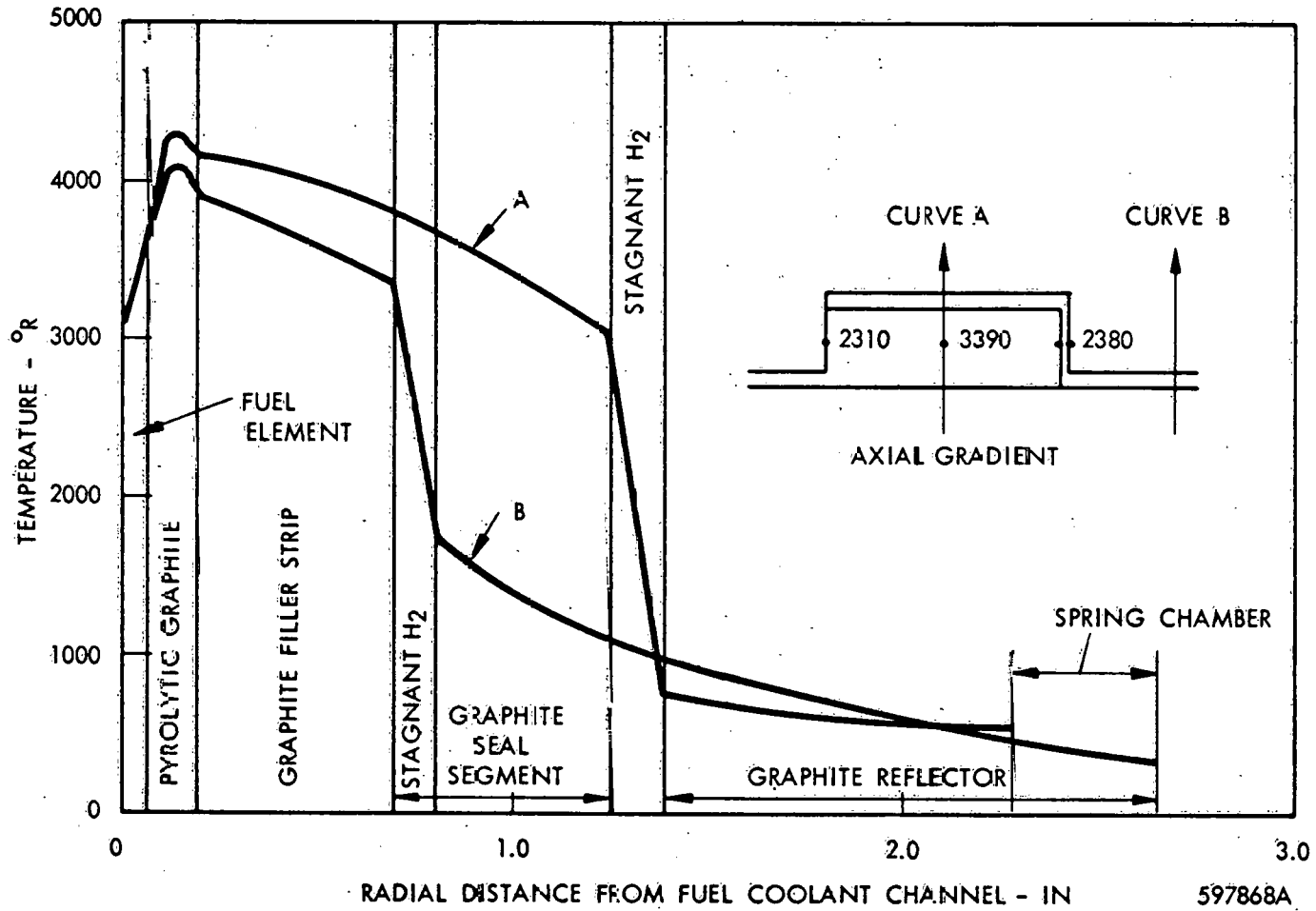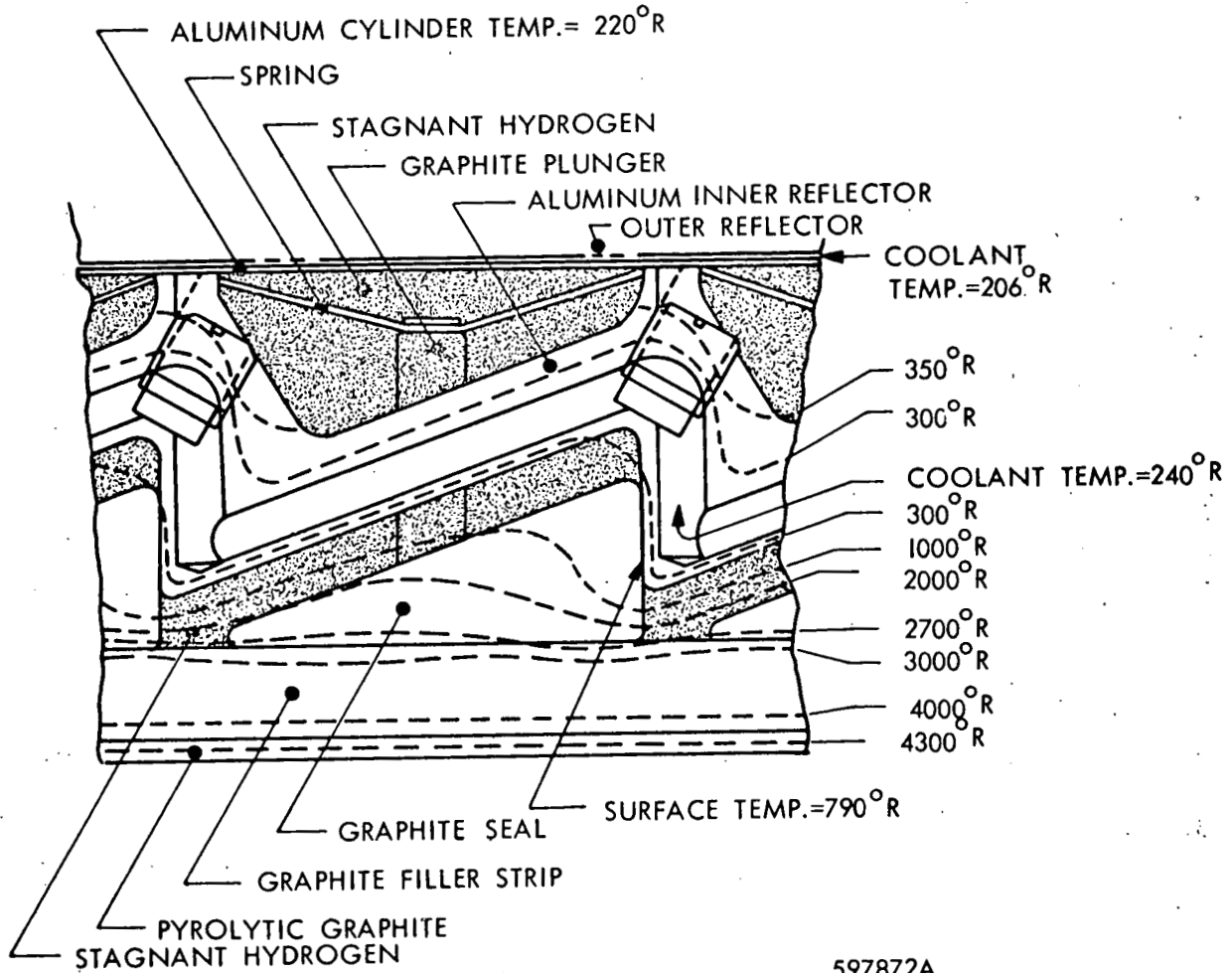
Figure 2-16 Temperature Distribution in an Aluminum Inner Reflector with Stagnant Hydrogen in the Seal Region Voids, Core Station 26 at Full Power, Surface Temperature 790°R

Astronuclear

B.   Graphite Corrosion Process

The graphite corrosion which takes place in a hydrogen atmosphere is another important factor in the hot periphery concept. Figure 2-17 shows the effect of temperature on the equilibrium constants for the carbon-hydrogen reactions which produce methane and acetylene. Noting that the abscissa of this figure is the reciprocal of temperature, it can be reasoned that the reaction products will be predominately methane at low temperatures and acetylene at high temperatures. It is of interest that for a pressure of 50 atmospheres the equilibrium constants of these two competing reactions become equal at a temperature of $4050^\circ R$ ($1000/T = 0.444$ ($^\circ K^{-1}$)).

Figure 2-18 shows the measured dynamic effect of the combination of these two reactions as a function of temperature. This figure is applicable when the hydrogen velocity is in excess of 0.5 ft/sec. Upon noting that the abscissa of this plot is also the reciprocal of temperature, it may be observed that the corrosion rate increases rapidly with temperature for temperatures in excess of $2291^\circ R$. Figures 2-17 and 2-18 were taken from WANL-TME-432.

The effect of graphite corrosion on the design of the core periphery may now be examined. Experimental results indicate that the flow rate which occurs at the interface of two flat pieces of graphite is the same as the flow rate which would occur if the graphite plates were separated by a 0.001 inch gap. Then, considering this to be the case in the region of contact between the lateral support-seal rings, it can be shown that the leakage flow through the lateral support region will be approximately 0.0004 lb/sec and the average velocity of the flow at the seal ring-filler strip interface will be approximately 13 ft/sec. This represents the minimum leakage rate which will occur assuming that there are no observable gaps between adjacent filler strips and that the contour of the outer periphery of the filler strips is identical to that of the inner diameter of the seal rings. Assuming that the hydrogen remains stagnant in the voids between and behind the seal rings, figures 2-14, 2-15, and 2-16 show that the temperature at the seal ring-filler strip interface is approximately $3000^\circ R$. Then, referring to figure 2-18, the expected corrosion rate in this area is found to be approximately 18 mils/hr. In contrast, the maximum temperature in the lateral support-seal ring region for the NRX-A2 design is $2400^\circ R$, corresponding to a corrosion rate of approximately 1.8 mils/hr.
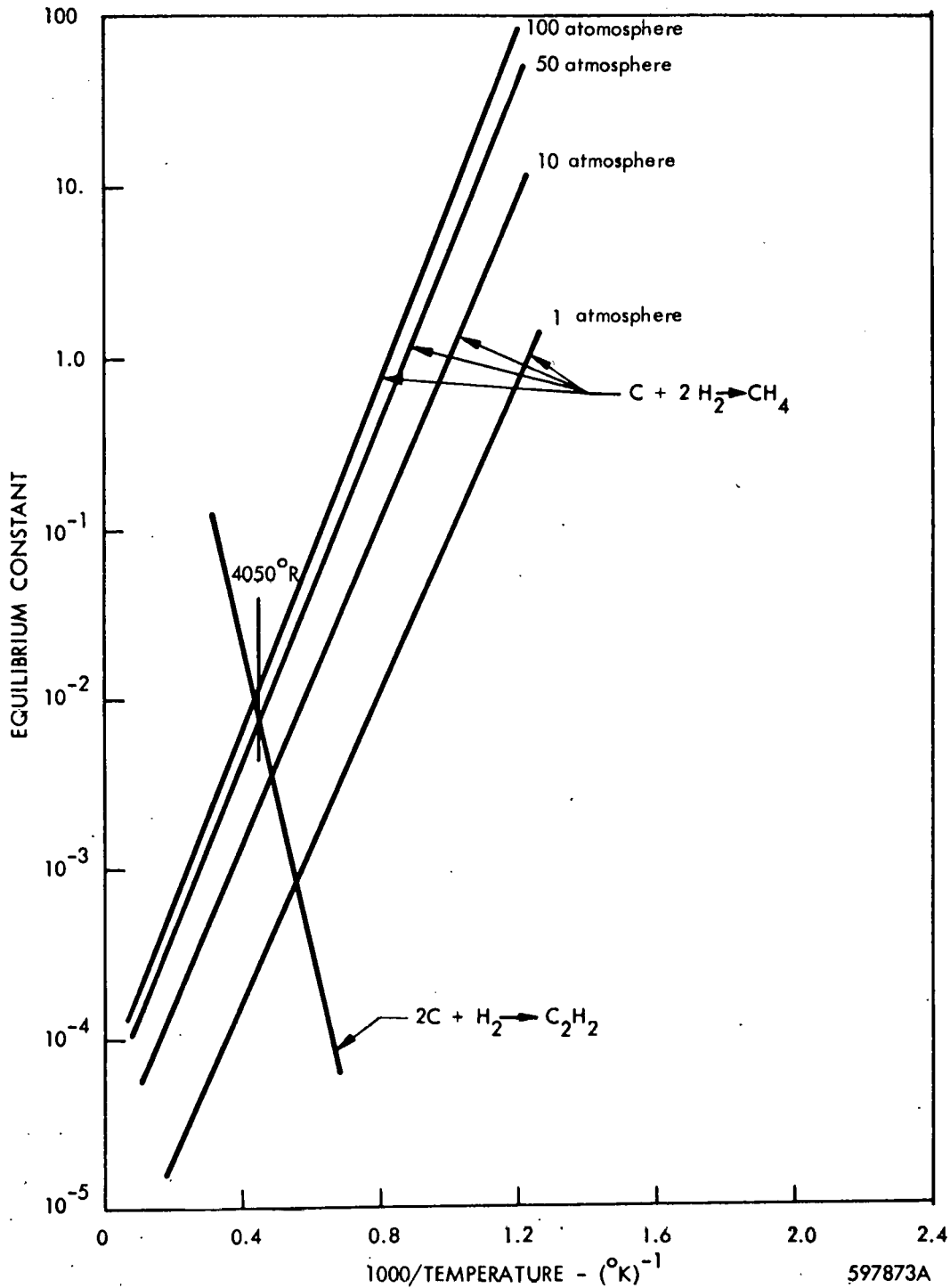
Figure 2-17 Effect of Temperature and Pressure on the Equilibrium
Constants for the Formation of Methane and Acetylene

Astronuclear

EFFECT OF PRESSURE:

$$C_p = C_{550} \ (p/565)$$

C_p = CORROSION RATE
      AT PRESSURE p

p = PRESSURE (PSIA)

C_{550} = CORROSION RATE
         AT 550 PSIG

ACTIVATION ENERGY OF 31,300 CAL/MOL (LASL DATA)

ACTIVATION ENERGY OF 10,000 CAL/MOL

3000 °R

2400 °R

2291 °R

CORROSION RATE - MILS/HR

1000/TEMPERATURE . (°K)⁻¹

597874A
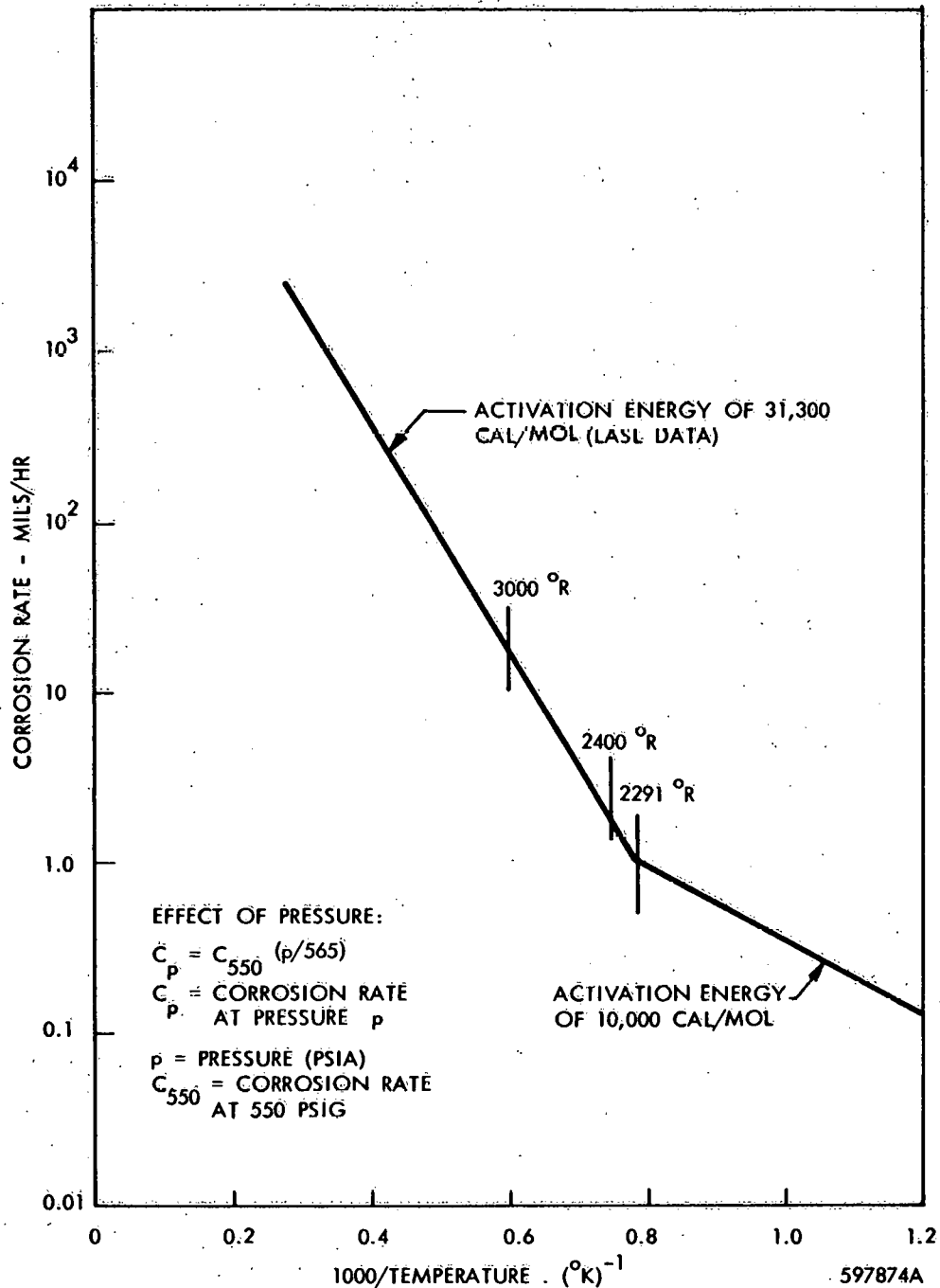
Figure 2-18 Effect of Temperature on the Corrosion Rate of Graphite in a
Hydrogen Atmosphere at 550 psig

It may be argued that for an operating time of one hour the configuration and the flow impeding characteristics of the seal system can change significantly due to corrosion. Because of temperature variations, flow gaps will begin to grow between adjacent filler strips, and at points between the seal rings and the filler strips. The corrosion cannot be expected to occur evenly around the periphery. It appears possible that these gaps could eventually produce leakage flow rates similar to those for NRX-A2.

C.   Pressure Distribution for Core Bundling

During initial reactor operation the pressure distribution is determined by the gaps between adjacent filler strips, and between the filler strips and the seal rings. These gaps, resulting from core expansion and manufacturing tolerances, change with continued operation and the onset of corrosion. As the corrosion process affects these gaps, the pressure distribution becomes unpredictable. Therefore, to assure that positive bundling of the core will be achieved during the operating life of the reactor, it will be necessary to provide a means of bundling which is independent of the pressure distribution in the seal region. In contrast the pressure distribution in the NRX-A2 lateral support region is much more predictable because the seal grooves were made large as compared with the component tolerance gaps, and the material temperatures in the periphery components are low enough to limit the corrosion rate to 1.8 mils/hour.

In summary, it is concluded that:

1)   The "hot periphery" design concept is feasible based on thermal considerations, but additional design effort is required to assure its practicality.

2)   The "hot periphery" design concept would eliminate thermal stresses in the peripheral fuel elements due to radial inflow by assuring that high temperature hydrogen exists in the seal regio

3)   Corrosion of graphite in the seal region at high materials and fluid temperatures may occur at rates such that control of the peripheral pressure distribution cannot be assured.

4)   Manufacturing tolerance for the core and associated lateral support-seal system components become important in determining the operating characteristics of the "hot periphery".

5)   The "plugged core" test facility could be used in conjunction with additional design analyses to investigate the practicality of "hot periphery" designs.

Astronuclear

2-3   REFLECTOR COMPONENT DESIGN

A.   Lateral Support Spring Design

The principal source of cold in-flow from the lateral support region is spring plunger or pin leakage. Elimination of this leakage, in conjunction with the hot periphery design, would reduce cold in-flow to the core. The various corrective methods considered are described in the following paragraphs.

1.   Conduction and Radiation Cooled Springs

The NRX-A2 cantilever type springs were analyzed to find their operating temperature limits without external convective cooling. One-dimensional heat balance equations were derived for the case of conduction to or from the inner reflector through a region of stagnant hydrogen to a spring having infinite conductivity and internal generation. The heat was then conducted through another layer of stagnant hydrogen to the aluminum barrel, which acts as a heat sink. The spring thickness was then calculated for a given inner reflector surface temperature, reflector annulus coolant temperature, and spring internal heat generation. Figure 2-19 shows the results for an Inconel spring at Core Station 26, the region of highest radiation heating, 12420 BTU/hr in.^{3} Maximum thickness for a spring operating at 1600°R is approximately 20 mils for an inner reflector temperature of 500°R and an aluminum barrel temperature of 250°R.

The same calculations were performed every 5 inches along the core length to obtain the maximum permissible spring thickness as a function of core station. This curve is shown in figure 2-20 for an Inconel spring having a maximum temperature of either 1400 or 1600°R.

Other candidate spring materials having a high thermal conductivity were also investigated. A two-dimensional (r, θ) model, as shown in figure 2-21, with conduction and radiation was made of the spring area for use with the THT-B code. Boundary conditions of fluid temperatures, film coefficients, and surface fluxes were extracted from NRX-A2 design information. Two materials, one a high temperature molybdenum alloy (TZM), and the other a low temperature copper-beryllium alloy, were selected for analysis. For purposes

Astronuclear
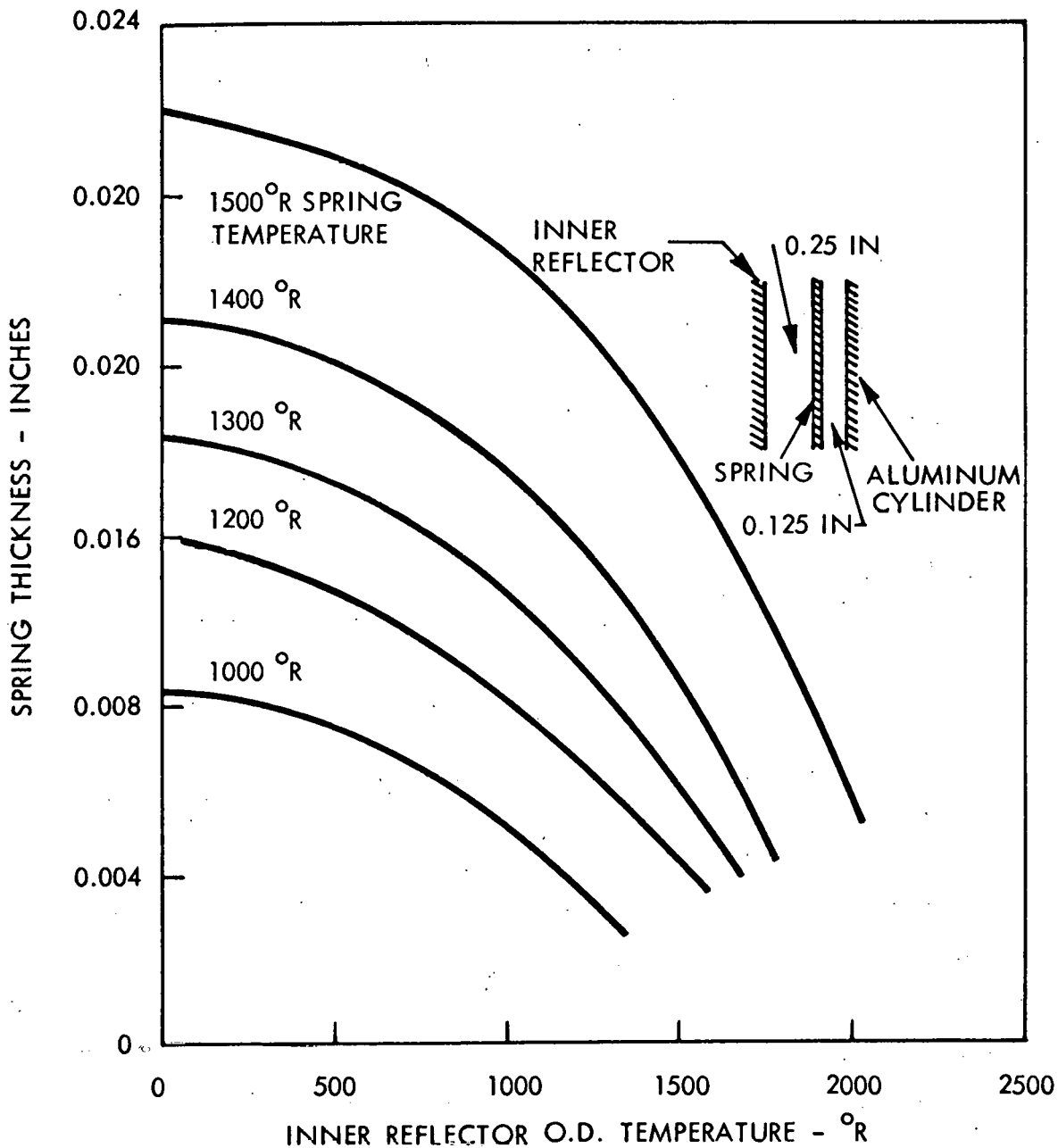
Figure 2-19 Spring Temperature Study with no Convective Cooling – Spring Located
on OD of Inner Reflector – Sink Temperature 250°R, Core Station 26

597875A

Astronuclear
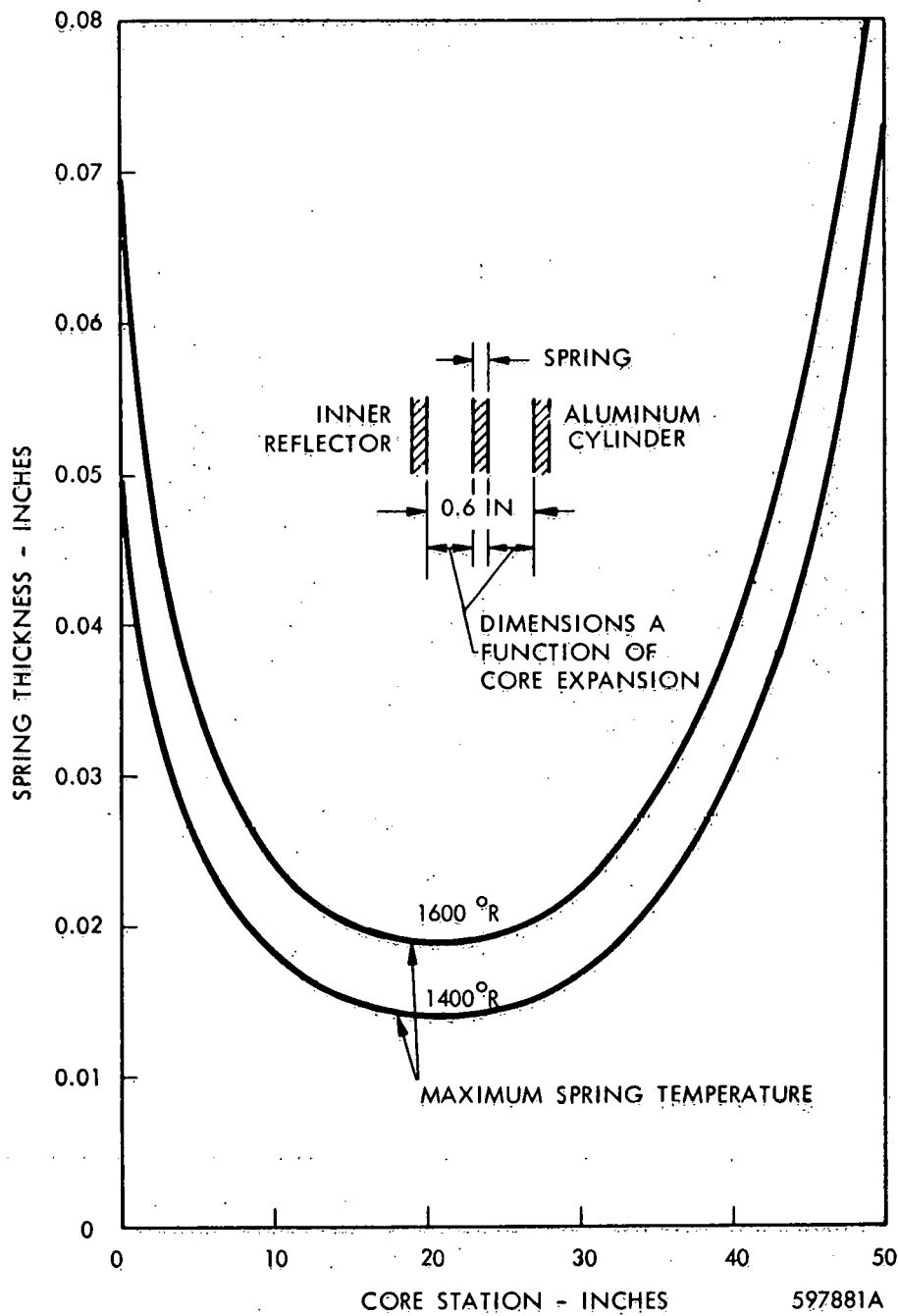
Figure 2-20 Maximum Thickness of Inconel Spring as a Function of Core Station

-32-

Astronuclear

$T_b = 210 \, °R \qquad h = 4280 \, BTU/HR \, FT^2 \, °R$
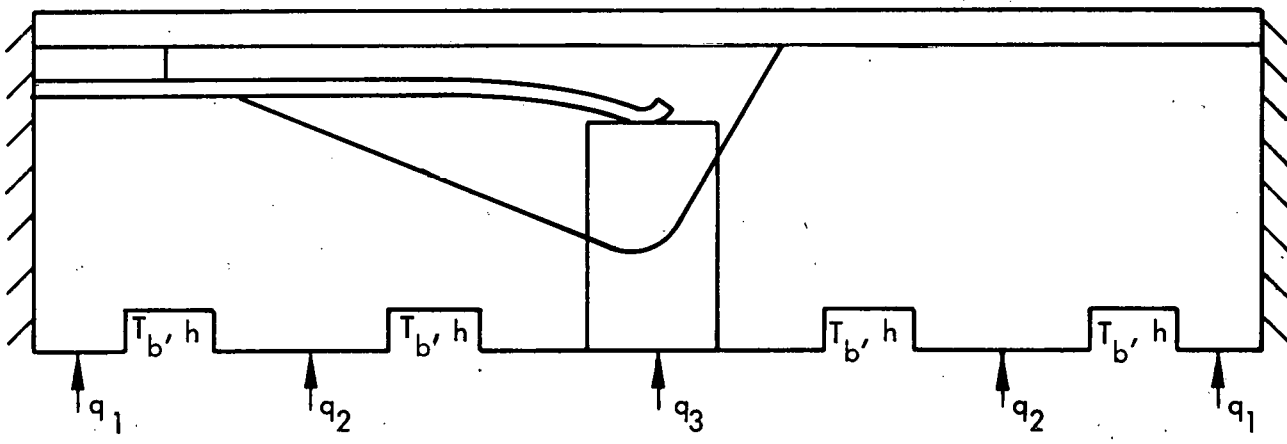
$T_b = 242 \, °R$

$h = 3470 \, BTU/HR \, FT^2 \, °R$

$q_1 = 3655 \, BTU/HR \, FT^2$

$q_2 = 11,963 \, BTU/HR \, FT^2$

$q_3 = 183,102 \, BTU/HR \, FT^2$

597877A

Figure 2-21 Cross Section of Spring at Core Station 26

of comparison, thermal conductivities at ambient conditions were 63 and 105 BTU/hr ft °R respectively. A two dimensional solution for Inconel was also performed as a check on the one dimensional model. The ambient temperature conductivity of Inconel is 8.5 BTU/hr ft°R.

The maximum and minimum spring temperatures at Core Station 26 for the three materials are shown in figure 2-22 as a function of spring thickness. Maximum temperatures for a 60 mil spring are 1905, 1830, and 1360°R for Inconel, TZM and copper-beryllium respectively. Minimum temperatures were approximately 390°R. Since TZM becomes brittle at cryogenic temperatures, the minimum temperature is also of interest.

Of interest is the difference in maximum temperature for the one and two-dimensional solutions for an Inconel spring. At a thickness of 20 mils, the one-dimensional solution is approximately 250°R hotter. This difference is greater for thicker springs.

A twisted end spring, located in the cavity on the inner reflector seal eliminates the need for a plunger, see figure 2-23. This case was analyzed one-dimensionally for several inner reflector surface temperatures. The results in figure 2-24 show the concept to be marginally acceptable for a cooled periphery but unacceptable for use with a hot periphery.

A third spring design, the non-linear lay down spring, shown in figure 2-25, was analyzed in conjunction with an aluminum inner reflector and a hot periphery. A two dimensional (r, θ) model shown in figure 2-26 was analyzed at Core Station 26. Isotherms are plotted in the figure. Zero seal leakage and intimate contact between the seal segment and filler strip were assumed. Maximum temperatures reached 5700°R and the radial difference across the seal and filler strip combined was approximately 1000°R. Maximum aluminum temperatures were slightly in excess of 800°R.

(W) Astronuclear
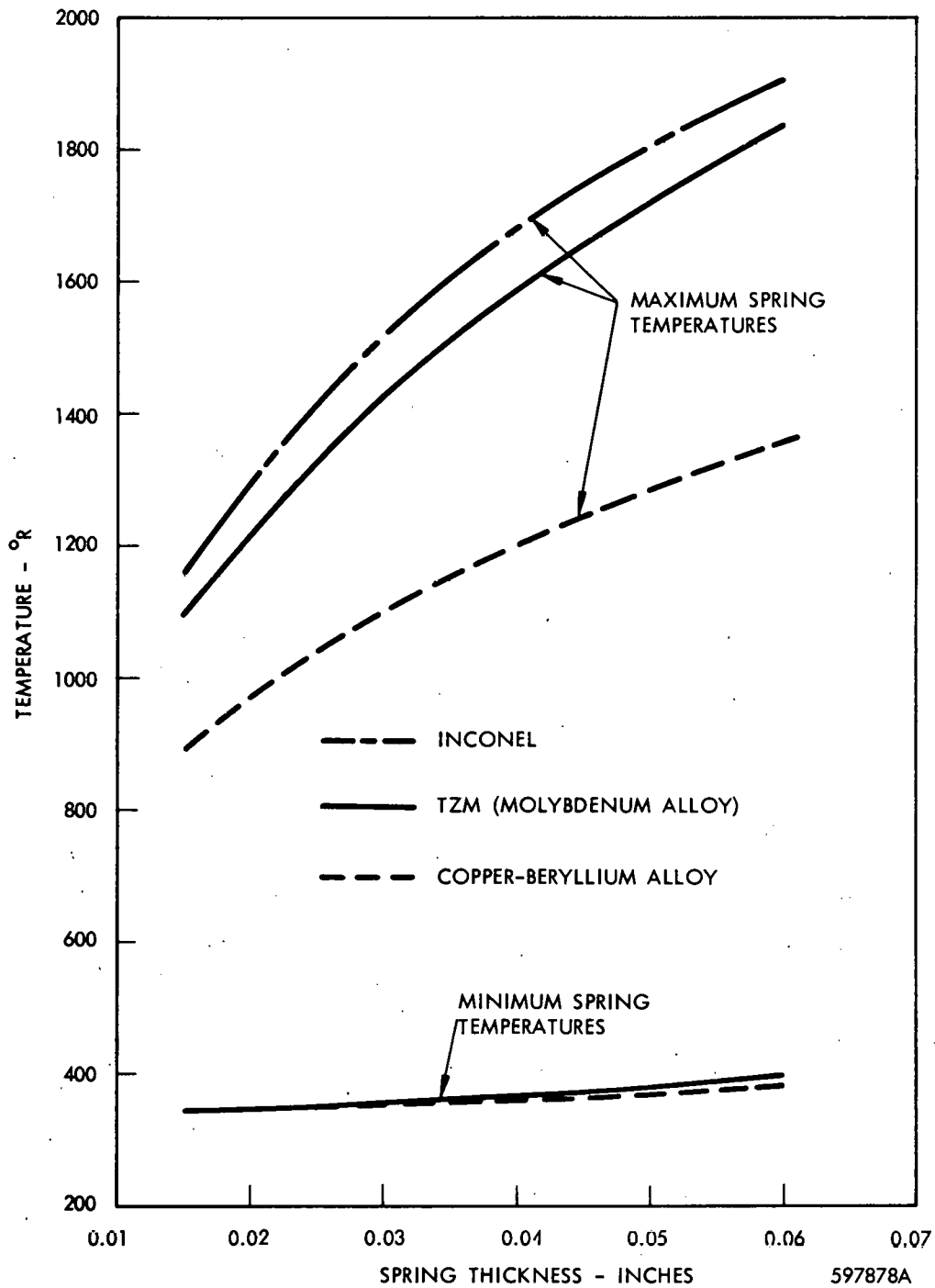
Figure 2-22 Spring Temperatures at Core Station 26

Astronuclear

FILLER STRIP

PYROGRAPHITE

TWISTED END SPRING

GRAPHITE INNER
REFLECTOR

SEAL SEGMENTS
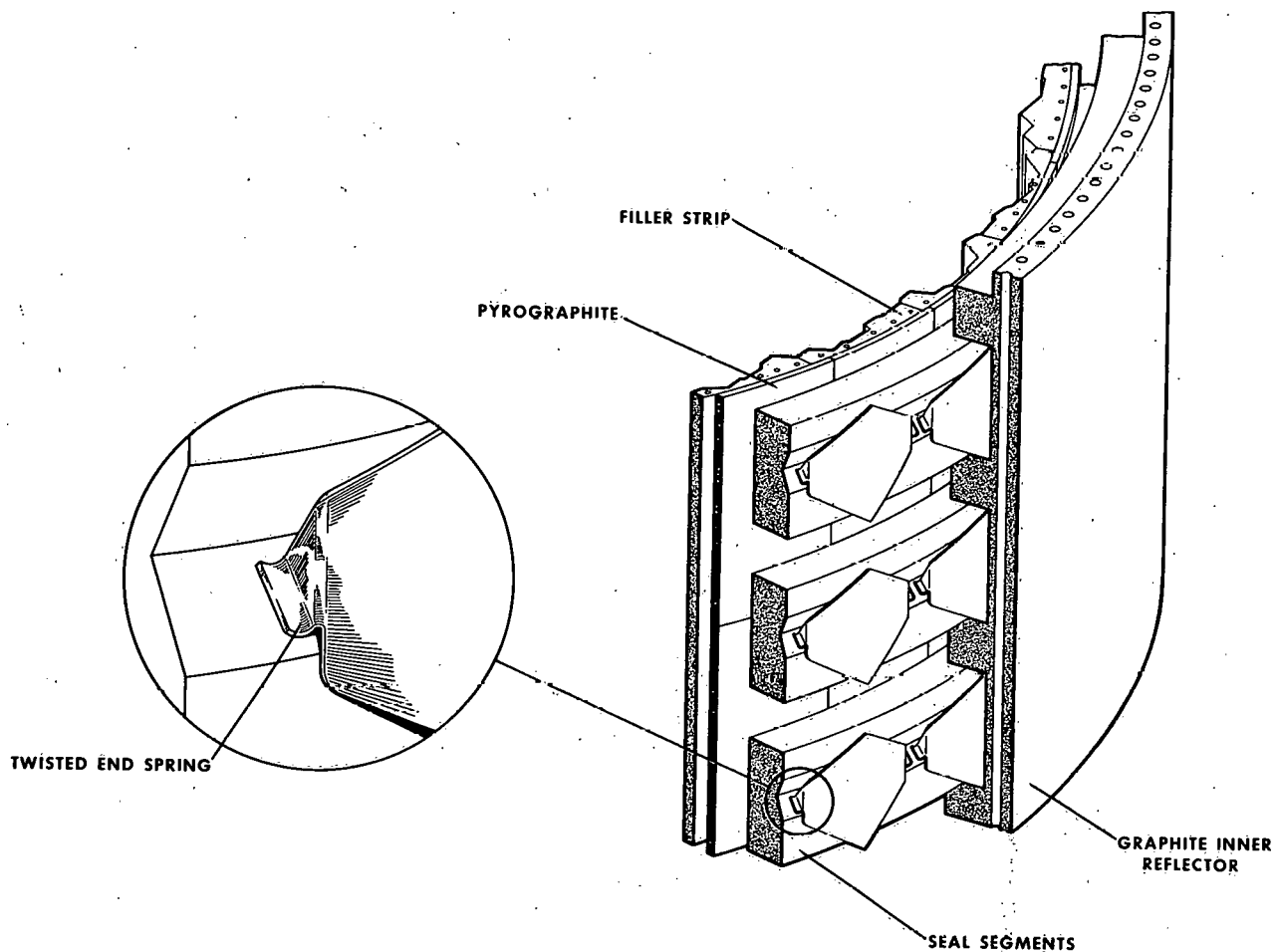
Figure 2-23 Twisted End Spring (Without Plunger)

INNER REFLECTOR I.D.
TEMPERATURE

——— 500 °R
- - - 700 °R
-·-·- 900 °R

SEAL — SPRING

.046 .126 INNER REFLECTOR

SPRING TEMPERATURE - °R

SPRING THICKNESS – INCHES

0.040

0.032

0.024

0.016

0.008

0

1400

1200

1000

800

SEAL RING O.D. TEMPERATURE - °R

400   800   1200   1600   2000   2400

597879A
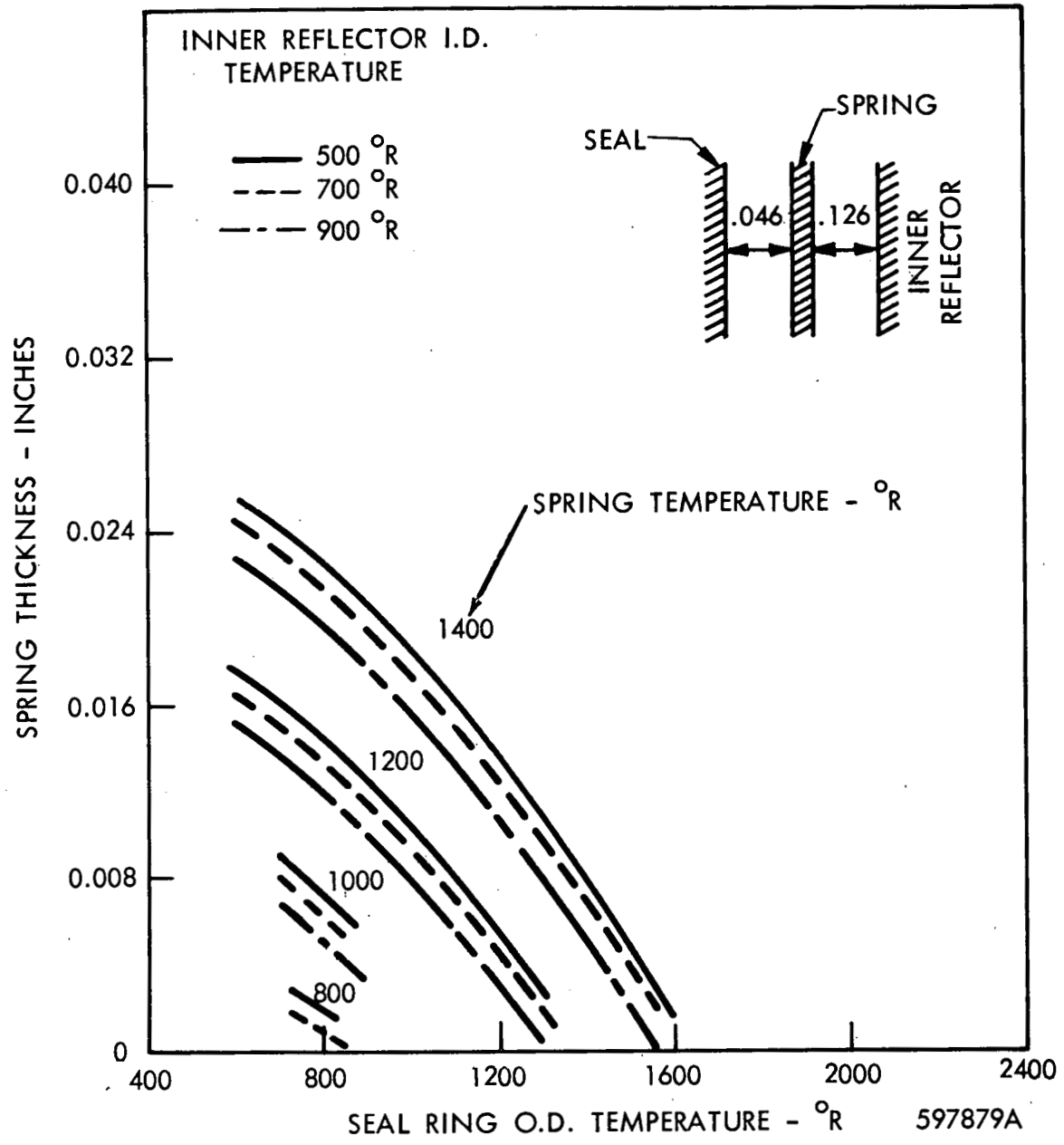
Figure 2-24 Uncooled Twisted End Spring Temperature, Core Station 26

STEADY STATE DESIGN POSITION

ASSEMBLY PRELOAD

FREE STATE
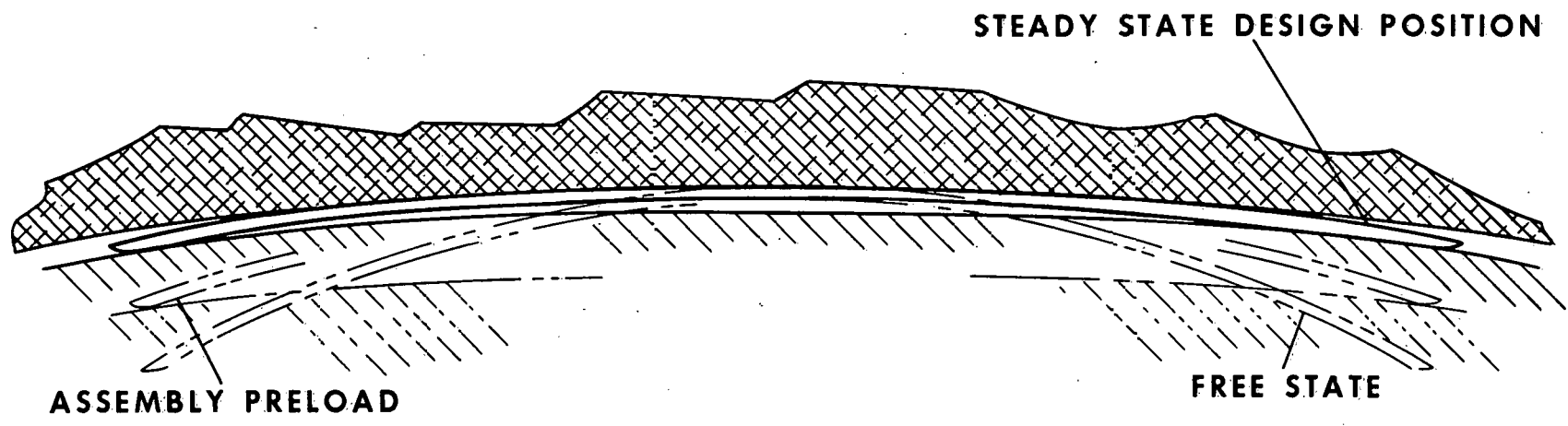
Figure 2-25 Non Linear Laydown Spring

Astronuclear

Astronuclear
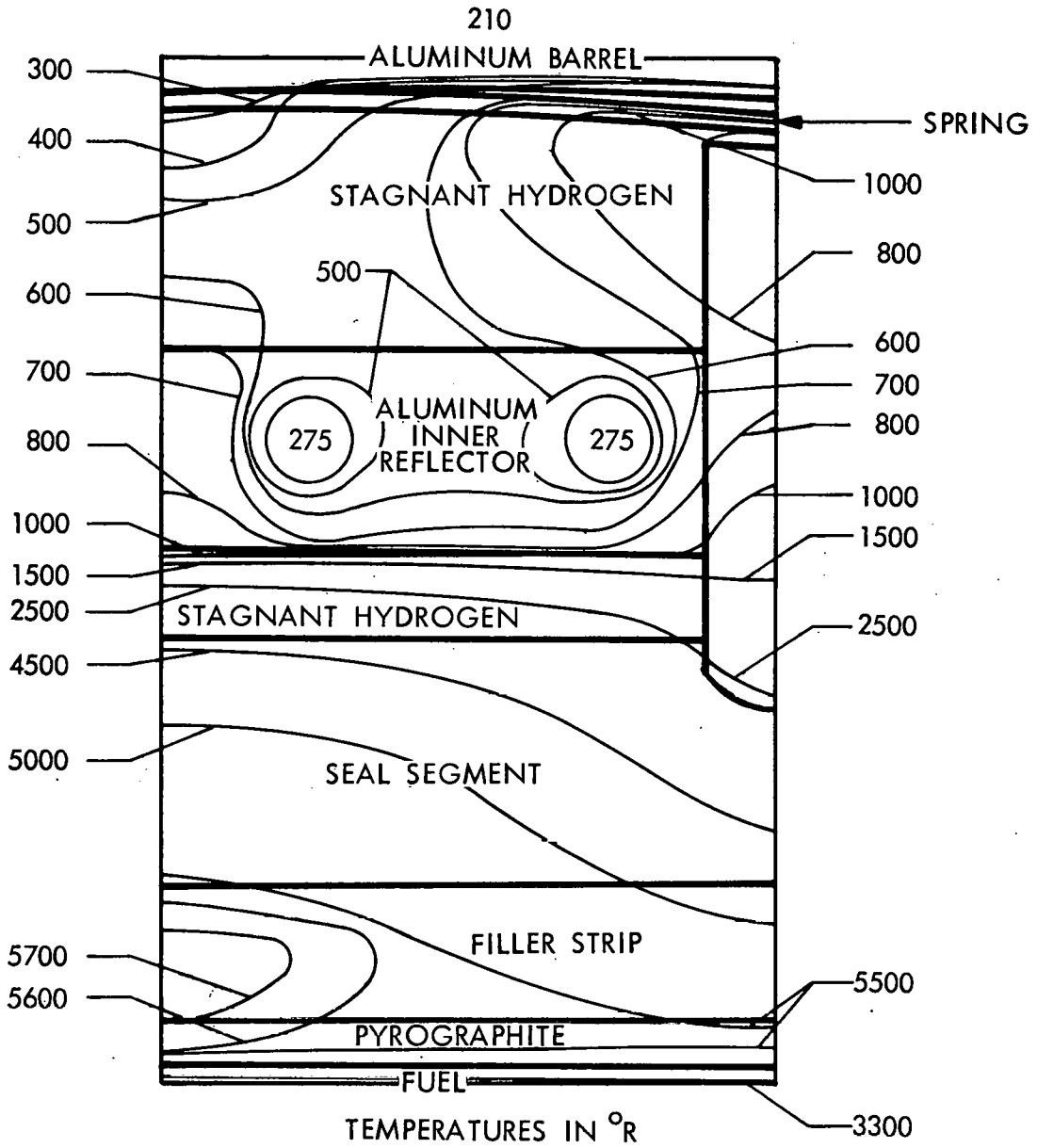
Figure 2-26 Hot Periphery Concept with Laydown Stainless Steel Springs
and Aluminum Inner Reflector, Core Station 26

597880A

Only one spring thickness was studied, 0.042-inch. At operating conditions, the maximum distance between the spring and the aluminum barrel was 0.048 inch and was in contact with the barrel for 1.15 inches of its 2.50 inch length. With this configuration, the stainless steel spring reached a maximum temperature of 1000°R.

2. Other Spring Pin Leakage Corrective Measures

Various cooled spring concepts were considered ranging from the bellows sealed plunger to a leaf spring with an internally cooled box section. The most promising design is the tubular coil spring shown in figure 2-27. Flow is taken from the reflector annulus, fed through several coils in series, and dumped into the inner reflector cooling holes. The pressure differential available is from 5 to 10 psi from figure 2-9. Approximately 0.002 lb/sec would cool four 18-inch coils in series.

Another scheme, that of scavenging pin leakage, as shown in figure 2-28, has been mentioned as a possible solution. Holes would be drilled axially in the inner reflector providing a low resistance flow path, and thus a low pressure sink, to the nozzle chamber. Both seal leakage and pin leakage would be vented to the core exit pressure. Studies performed a year ago are shown on figures 2-29 and 2-30 for comparison of three flow schemes, no pin leakage, with pin leakage, and with pin leakage scavenging the last five seals.

The axial pressure distribution with scavenging, figure 2-29, is intermediate to the other two schemes. Wall temperatures of the filler strips and seals, figure 2-30, are several hundred degrees higher over the last 12 inches of the core with pin leakage scavenging. Seal leakage exit temperature is 1700°R with scavenging and 1150°R without scavenging.

The conclusions drawn from the spring study are:

1) Inconel or stainless steel springs of the NRX-A2 type and thickness (0.064 inch) not convectively cooled would not operate within the mechanically imposed maximum temperature limitation near the midplane of the core.

Figure 2-27 Internally Cooled Spring

CORE

AXIAL COOLANT PASSAGES

GRAPHITE INNER REFLECTOR

GRAPHITE
SEAL
SEGMENTS

COOLANT EXHAUST

LATERAL
SUPPORT
SPRINGS

COOLANT INLET AND SEAL

SEAL
SEGMENT
SEATING
FORCE

LATERAL
SUPPORT
FORCE

LATERAL
SUPPORT
FORCE

SEAL
SEGMENT
SEATING
FORCE

VIEW A

Astronuclear
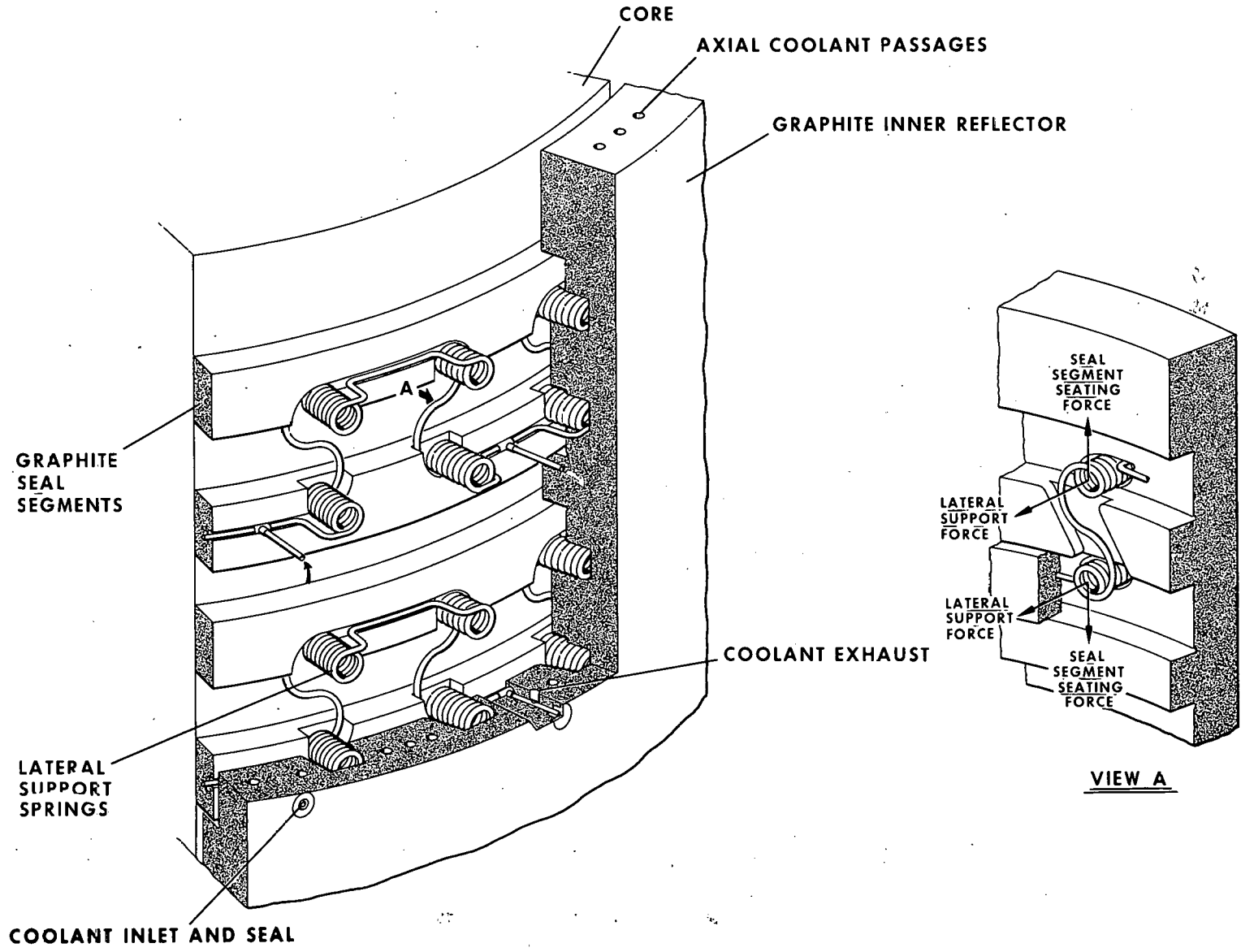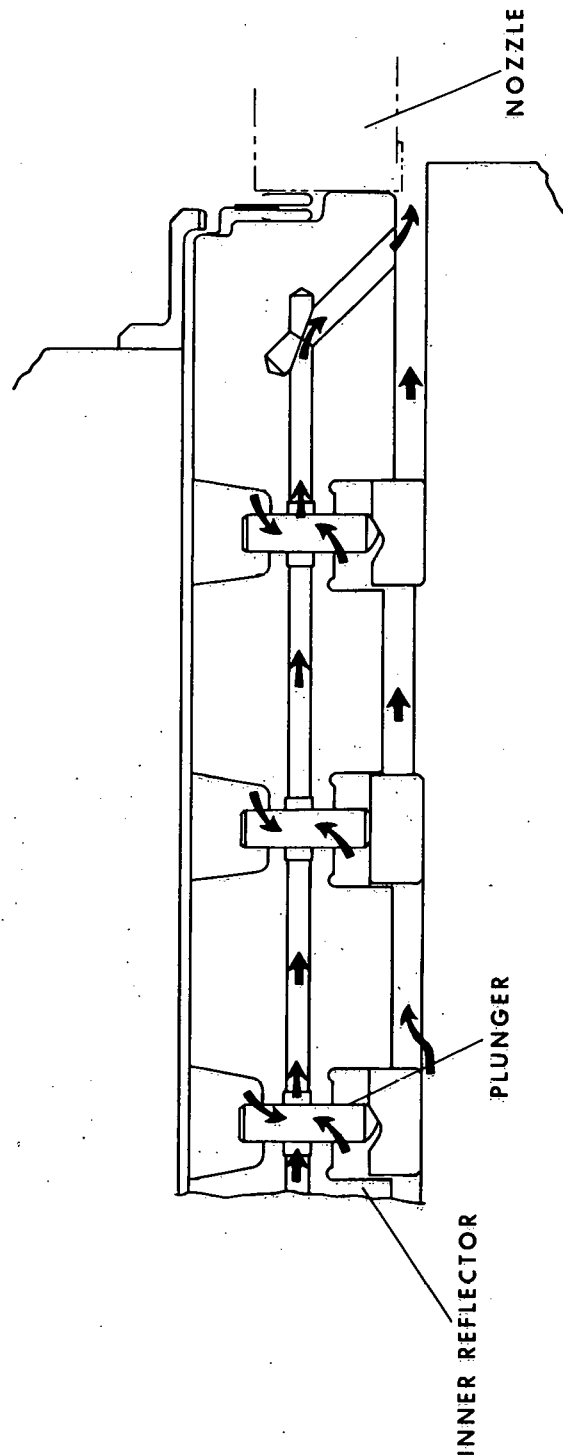
Figure 2-28 Plunger Leakage Scavenge

Astronuclear

SEAL GAP = 0.008 IN
PIN GAP = 0.0006 IN
16 EFFECTIVE SEALS (18 TOTAL)
ΔP TOTAL = 140 PSI
SCAVENGE PRESSURE = 560 PSI
INLET TEMPERATURE = 200 $^{\circ}$R
INLET PRESSURE = 700 PSIA
CORE LEAKAGE NOT INCLUDED

PRESSURE - PSIA

- - - NO PIN LEAKAGE

.... PIN LEAKAGE; NO SCAVENGING

—— PIN LEAKAGE; LAST 5 PINS WITH SCAVENGING

CORE STATION - INCHES

597876A
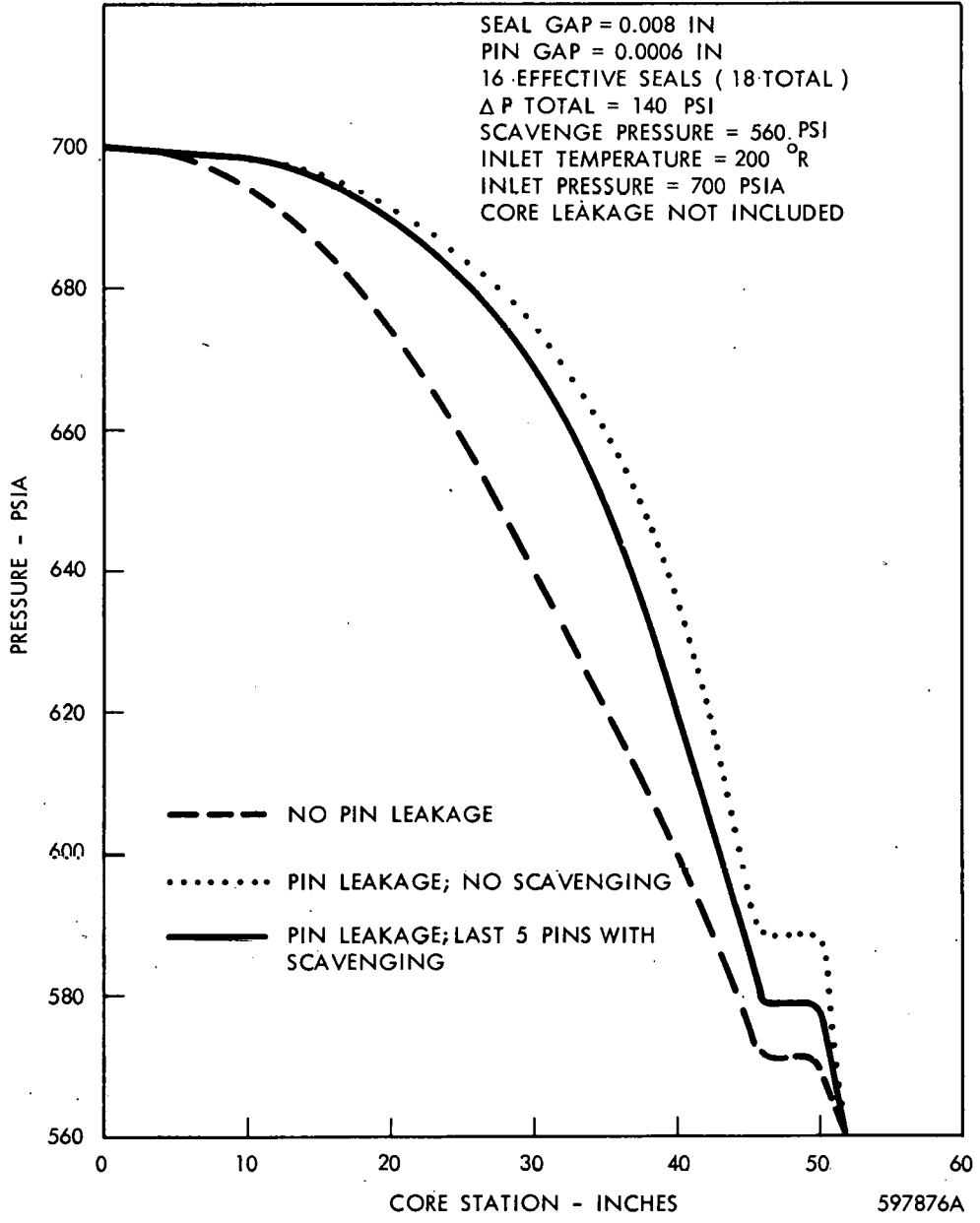
Figure 2-29 Seal Study - Effect of Pin Leakage - Axial Pressure Profiles

-43-

Astronuclear
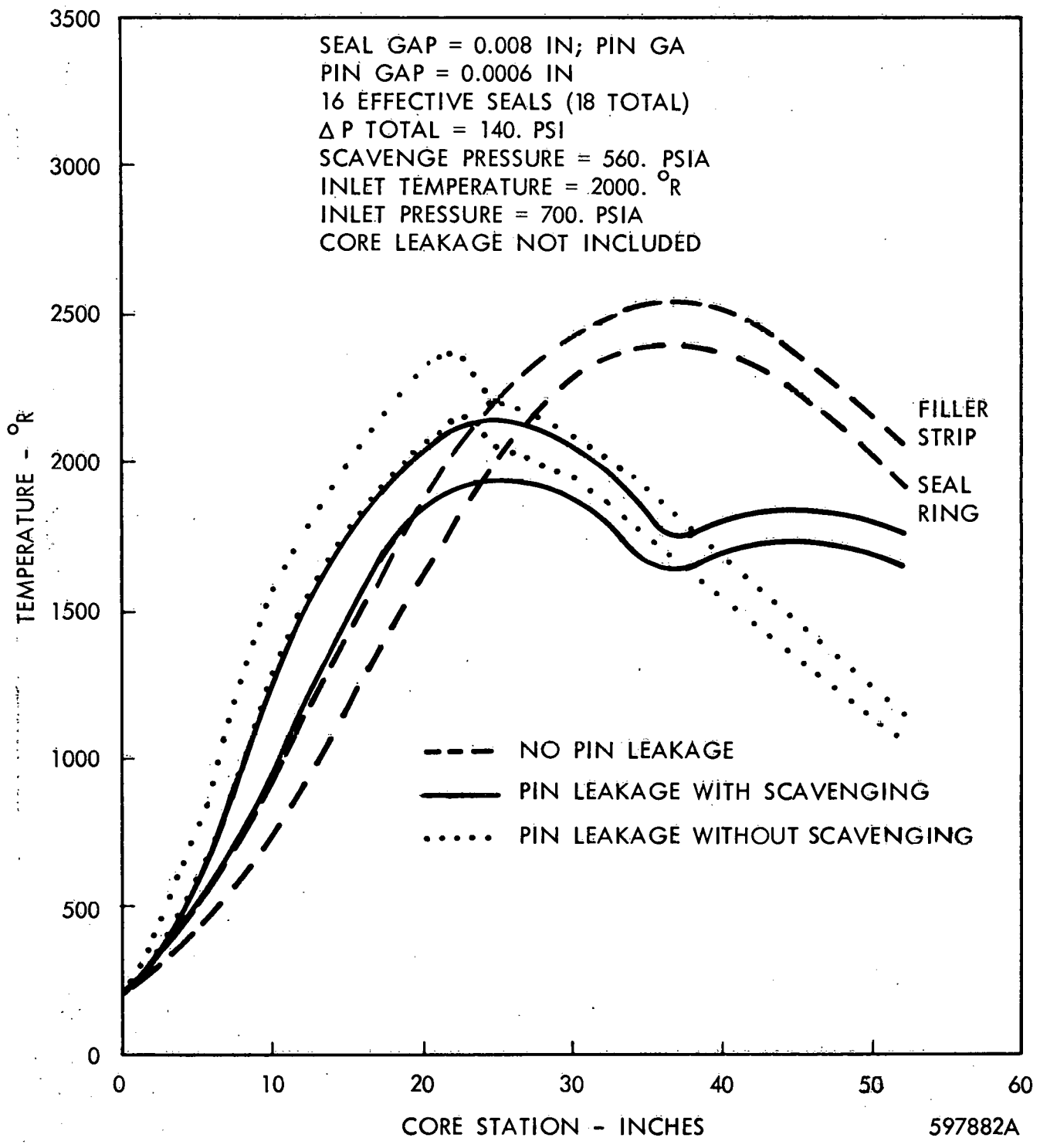
Figure 2-30 Seal Study – Effect of Pin Leakage Axial Wall Temperature
Profile at Seals

Ⓦ Astronuclear

2) Thinner springs of the NRX-A2 type have permissible temperatures but large uncertainties in radiation heating ($^{+1.6}_{-0.6}$) make their use unadvisable.

3) A high temperature alloy capable of withstanding a 2000°R hydrogen atmosphere and low temperature could be used without convective cooling. Neither TZM or copper-beryllium meet both these criteria.

4) Internally cooled tubular coil springs are thermally feasible and will eliminate pin leakage.

5) The scavenging of pin leakage can be used as an alternate method of eliminating cold in-flow to the core without substantially sacrificing thermal performance.

6) Convection cooled springs are recommended for the NRX-A5.

B.   Inner Reflector Design

Five inner reflector designs which would provide increased strength were subjected to thermal analysis. Three reflectors were aluminum and two were composite structures of aluminum and graphite. The studies included the effects of both a hot periphery design and the NRX-A2 periphery design.

1.   Aluminum Reflectors

Two similar aluminum reflectors and their temperature distributions at Core Station 26 are shown in figures 2-15 and 2-16. The temperature distributions shown here are those which occur in conjunction with a hot periphery design and were determined using the analytical models and procedures described in Section 2-2. It should be noted that these temperature distributions were evaluated using heating rates equivalent to those occurring in NRX-A2 at full power.

Both these designs utilized 144 internal cooling holes 0.25 inch in diameter equally spaced around the circumference and following the "Z" shaped contour of the inner reflector. This configuration was necessary to limit the aluminum temperatures along the inside surface of the reflector to values that would not adversely affect the strength of the reflector. The temperatures at the interface between the seal ring and reflector and those at the inside surface of the reflector behind the seal rings were found to be greatly dependent on the thickness of

- 45 -

the wall between the coolant channel and the inner surface of the reflector. The results shown in figures 2-15 and 2-16 were obtained using a wall thickness of 0.10 inch in the area where the seals seat and a thickness of 0.08 inch behind the seal rings. The effect of free convection heat transfer in the seal region on the aluminum surface temperature behind the seals was also examined. It was found that this surface temperature would not exceed $800^{\circ}R$ for a convective heat transfer coefficient of 100 BTU/hr $ft^{2 \circ}R$ if the hydrogen temperature in the seal region did not exceed $4300^{\circ}R$.

In figures 2-15 and 2-16, it may be seen that the seal rings exhibit a temperature difference of approximately $2000^{\circ}R$ along their diagonals. These high temperature differences are a result of the insulating properties of the graphite felt and stagnant hydrogen behind the seals forcing the core heat to pass diagonally through the seal ring and into the aluminum barrel.

Figures 2-31 and 2-32 show the temperature distribution in the same reflector that is shown in figure 2-16, but with a periphery design similar to NRX-A2. This distribution was obtained assuming that the coolant flowing through the seal region has the same properties as those for NRX-A2. However, the power density was double that at Core Station 26 in NRX-A2 under full power conditions. The hydrogen behind the seal rings was assumed to be stagnant, but forced convection heat transfer was assumed to exist on the inner surface of the reflector between seals. Figure 2-31 shows the temperature distribution at a cross section through one of the 144 cooling holes in the reflector and figure 2-32 shows the distribution at a cross section midway between cooling holes. A comparison of these two figures shows that the temperature gradients in the azimuthal direction are negligible. Upon comparing figure 2-31 with figure 2-16, it may be noted that the temperature differences in the seal rings are much less when the periphery design is of the NRX-A2 type.

The unrealistic temperatures shown for the pyrolytic graphite are a result of the high power density used in the analysis. Some redesign will be required if higher power densities than those of the NRX-A2 are to be used.

ALUMINUM CYLINDER TEMP = 230°R

COOLANT TEMP = 206°R

STAGNANT HYDROGEN

450 °R

400°R

300°R

ALUMINUM INNER REFLECTOR

STAGNANT HYDROGEN

1000°R

1500°R

COOLANT TEMP = 240°R

300°R

GRAPHITE SEAL

1900°R

1500°R

2000°R

2150°R

SEAL LEAKAGE 2100°R

3450°R

GRAPHITE FILLER STRIP

8800°R

PYROLITIC GRAPHITE

SURFACE TEMP = 850°R

SURFACE TEMP = 800°R

SURFACE TEMP = 800°R

598237A
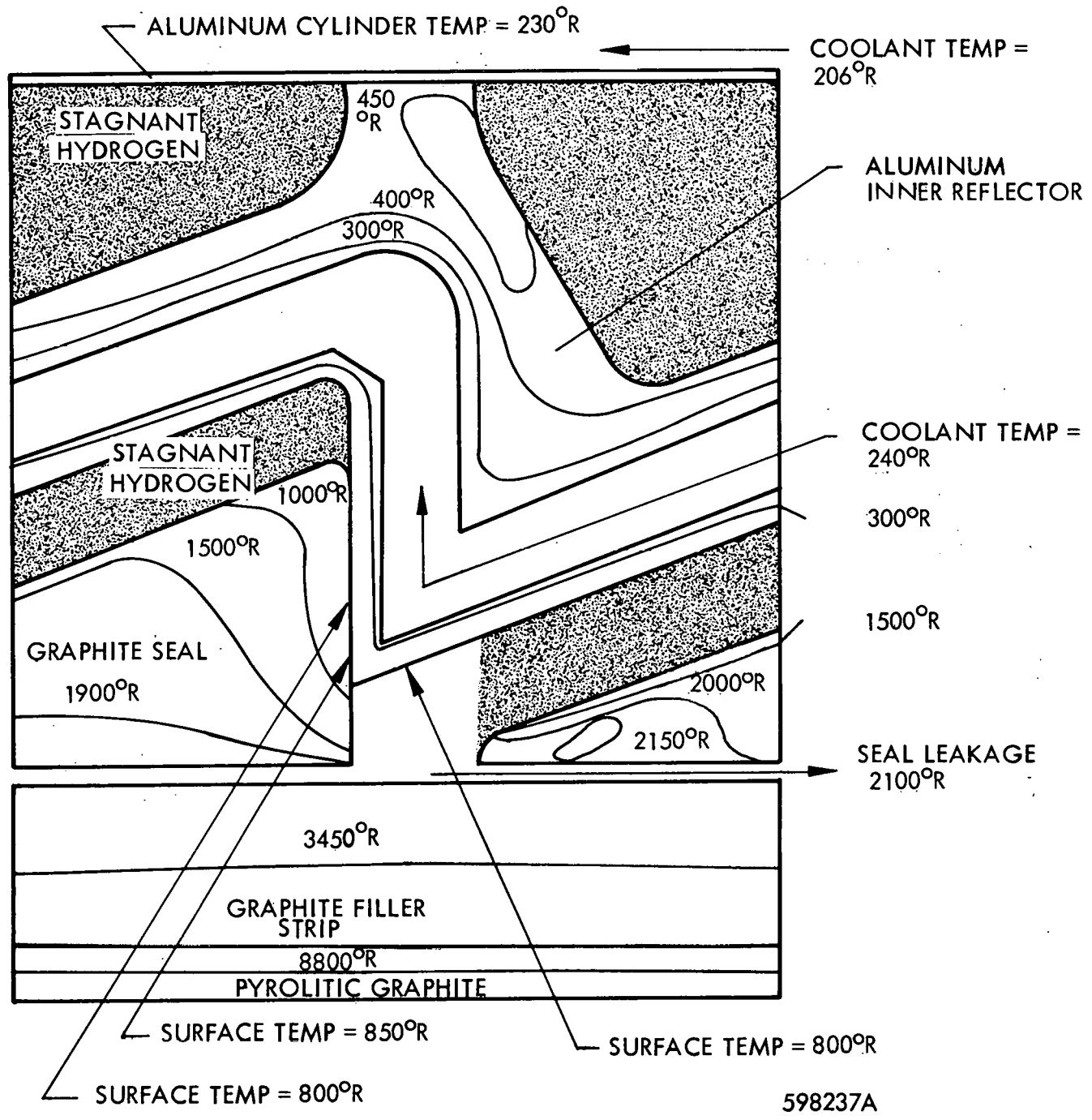
Figure 2-31 Temperature Distribution in an Aluminum Inner Reflector Having NRX-A2 Seal Region Boundary Conditions, Core Station 26 at Twice NRX-A2 Power Density, Cross Section at Cooling Hole

Astronuclear
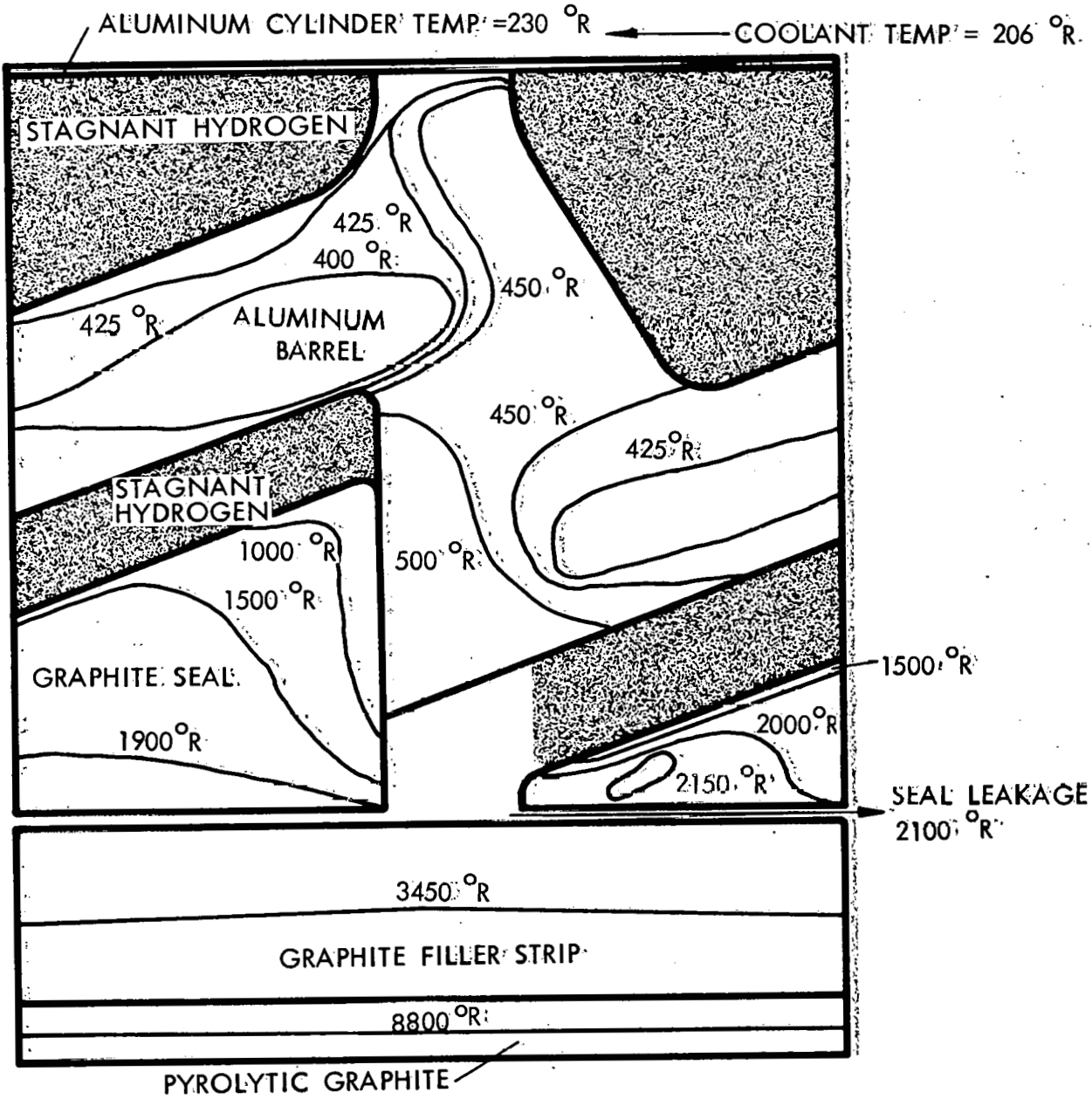
Figure 2-32 Temperature Distribution in an Aluminum Inner Reflector Having NRX-A2 Seal Region Boundary Conditions, Core Station 26 at Twice NRX-A2 Power Density, Cross Section Midway Between Cooling Holes

597884A

-48-

The other aluminum inner reflector design is basically an aluminum version of the NRX-A2 inner reflector. As would be expected from the preceding discussion, the temperatures in the thick aluminum sections between the seal rings were found to be excessive.

2. Composite Reflectors

The composite reflector structure shown in figure 2-33 was designed to eliminate the above-mentioned excessive temperature problem by replacing the thick aluminum sections between seals with graphite rings. These rings are held in position by smaller aluminum support rings and provide seating surfaces for the graphite seal segments. Internal cooling of the structure is provided by coolant channels which pass axially through the aluminum.

Analysis of this design in conjunction with NRX-A2 periphery conditions showed that the temperature distributions in the graphite parts would not differ significantly from those of the NRX-A2. The maximum aluminum temperatures were found to occur at the inside surface of the aluminum barrel and were primarily dependent on the positioning of the cooling holes. It was found that 144 cooling holes of 0.25 inch diameter spaced evenly around the circumference would maintain the maximum aluminum temperature below $800^{\circ}R$ if the wall thickness between the inner surface of the aluminum barrel and the coolant channel surface did not exceed 0.08 inch.

A second composite reflector structure which was considered is shown in figure 2-34. This reflector design uses a convoluted flow path to provide cooling for the aluminum sections between the seal rings. When used with NRX-A2 periphery conditions, it was found that the maximum aluminum temperature in this design would not exceed $800^{\circ}R$ if the thickness of the aluminum between the cooling channels and the inner periphery of the structure is the same as in the NRX-A2. However, preliminary fluid flow analyses for this irregular flow path have indicated that it may not be possible to provide a coolant flow rate as large as that used in the temperature analysis. Lower flow rates in this channel would result in higher bulk and material temperatures.

Astronuclear
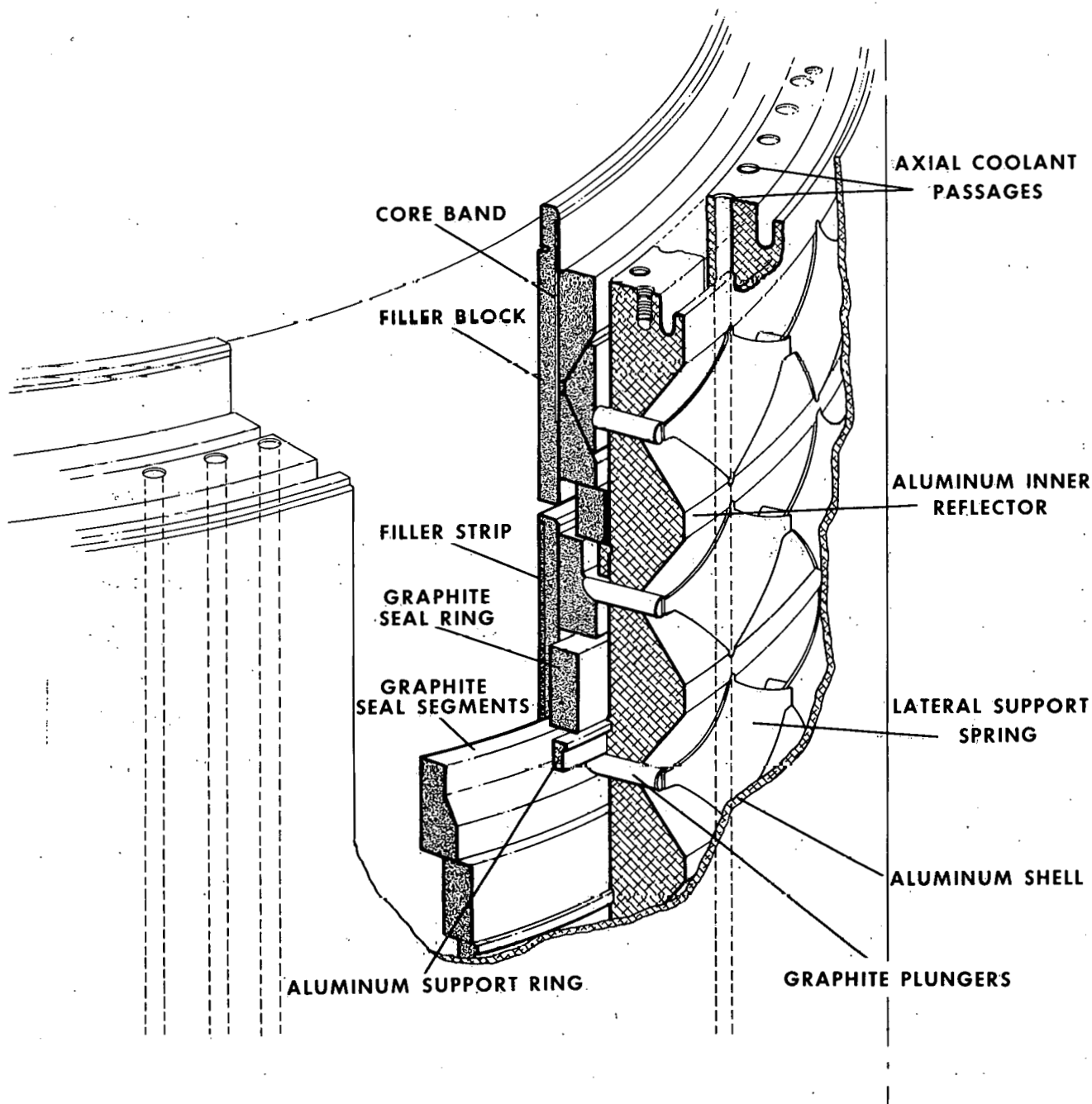
Figure 2-33 Composite Reflector Structure with Axial Coolant Passages

-50-

(W) Astronuclear

ALUMINUM BARREL

GRAPHITE INSERTS

PLUNGER

RETAINER BAR

GRAPHITE SLATS

LEAF SPRING

SEAL SEGMENTS

ALUMINUM CYLINDER
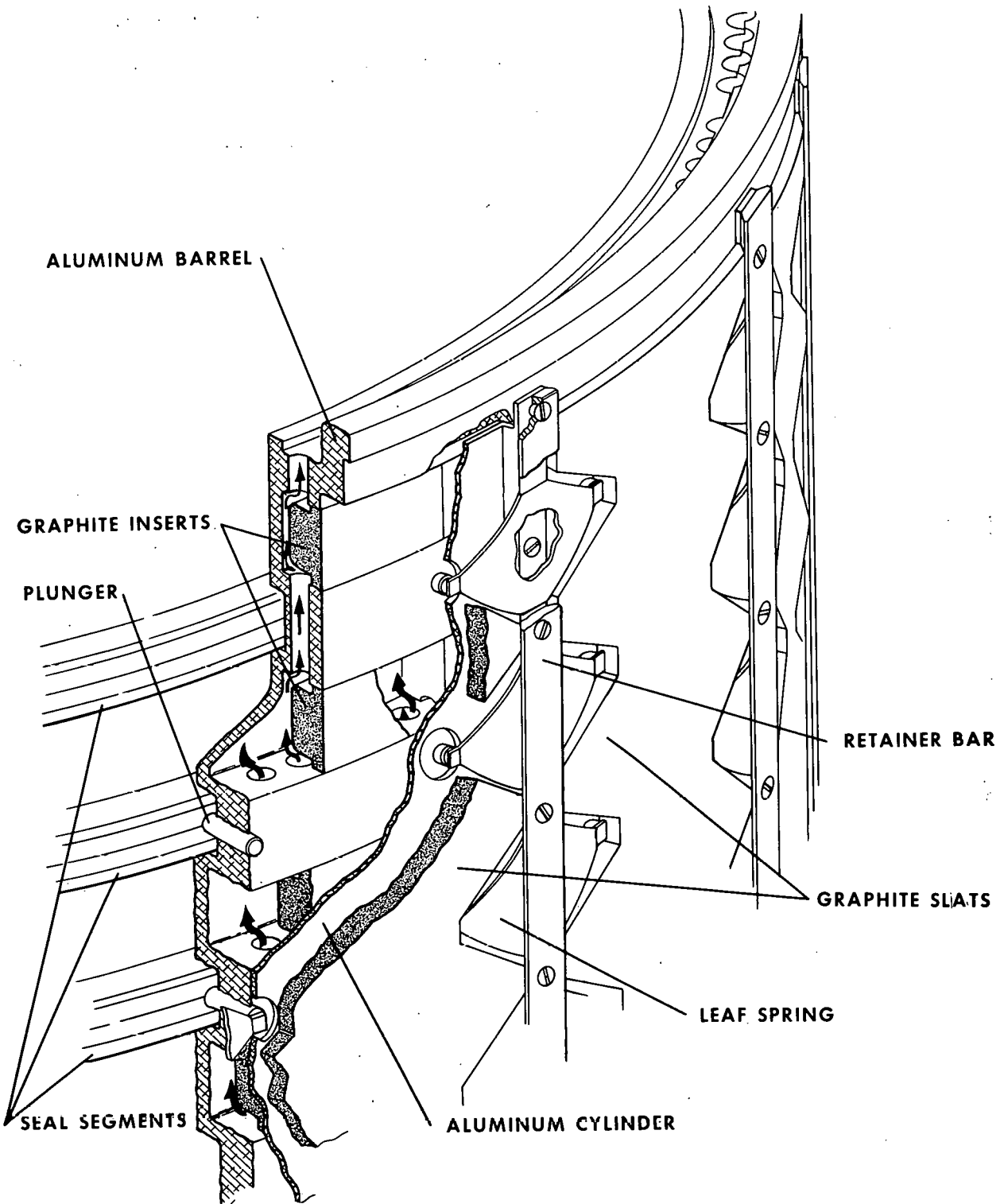
Figure 2-34 Composite Reflector Structure with Convolute Coolant Passages

An additional investigation made in conjunction with the inner reflector studies considered the elimination of the flow annulus between the inner and outer reflectors. This would strengthen the inner reflector by allowing the outside diameter to be increased and by mechanically reinforcing it with the outer reflector. The analysis was made by using the NRX-A2 configuration, but the coolant which flows through the reflector annulus in the NRX-A2 was routed through the inner reflector cooling holes. This arrangement would involve enlarging the 144 cooling holes in the inner reflector to a diameter of 0.35 inch if the pressure drop and flow distribution through the reflector is to remain unchanged. In addition, it was assumed that there would be no in-flow of coolant from the lateral support spring chambers to the lateral support seal region.

Assuming the interface of the two reflectors to be an adiabatic surface, the analysis showed that when compared with NRX-A2 (a) the temperature level in the core periphery will increase a negligible amount at Core Station 0, approximately $500^\circ R$ at Core Station 26, and approximately $700^\circ R$ at the nozzle end; (b) the radial temperature difference in the inner reflector will be significantly reduced because of an increase in the temperature at the outer diameter of the reflector of approximately $200^\circ R$; (c) the radial difference in the outer reflector will increase slightly because of an increase in the temperature at the inner diameter of the sectors of approximately $50^\circ R$; and (d) the nozzle end and dome end support ring temperatures will not change significantly.

In summary it can be said that, for the configurations analyzed:

1)   The material temperatures in an aluminum inner reflector can be maintained at a satisfactory level if the material between the coolant channels and the inner surface of the aluminum does not exceed 0.08 to 0.10 inch in thickness.

2)   Although this applies to both hot periphery designs and designs having a periphery similar to that of the NRX-A2, the temperature gradients in the seal segments become excessive when the hot periphery design is used in conjunction with an aluminum inner reflector.

3)   If the flow is eliminated from the reflector annulus and rerouted through the inner reflector cooling holes in the NRX-A2 design, the temperature distribution throughout the system is not adversely affected.

Astronuclear

2-4 CORE COMPONENT DESIGN

For the NRX-A5 program four areas of core component redesign and improvement were investigated. These areas were (a) controlling inter-element pressure, (b) effect of peripheral cooling on core performance, (c) effect of increasing the tie rod diameter, and (d) the use of un-machined fuel elements.

A. Controlling Inter-Element Pressure

Two methods for controlling inter-element pressure distribution were considered; these were undercutting and chamfering, see figure 2-35.

The first method, that of undercutting the element, provides radial paths between elements so that the pressure difference between the seal system and the core is always small. This technique would only be used with a hot periphery seal design. In this case the temperature of the gas in the seal system is very nearly the same as the fuel element temperature, and gas flowing radially into the core would not cause appreciable temperature gradients in the fuel elements.

In the hot periphery design flow in the lateral support system is held to a minimum and seal clearances are made as small as possible. The axial pressure profile is then determined by tolerance buildup and corrosion rate. A possibility exists that the core inter-element pressure could be greater than the seal system pressure in this case.

However, if the elements are undercut, any pressure rise in the core will be radially vented to the seal system and the inter-element and the seal pressures will remain nearly equal. Figure 2-36 shows some possible inter-element pressures for the case of elements with a 0.002 by 2.0 inch undercut every four inches. The figure is for NRX-A2 full power conditions (689 psia core inlet, 560 psia core outlet).

The pressure distributions for three axial inter-element gaps are given in figure 2-36. One distribution is for an axial gap which tapers from 0.2 mils at the core inlet to 2.5 mils at the core exit. A second distribution is for a gap tapered from 0.2 mils at the core inlet to 1.5 mils at the core exit. These two gaps represent the limits of the estimated probable gap sizes. This range is based on calculations of the tolerance buildups and measurements

of gaps in a bundle of 9-inch long elements.   The band around the core at the inlet end causes the gaps to be small at the inlet end and have an increasing width toward the core exit.   The third pressure distribution is for a gap which is large at the core inlet (1.5 mils) and small at the core exit (0.5 mils).   This gap is possible, but not probable, and produces the highest inter-element pressures.

The second method for controlling inter-element pressure distribution is by chamfering elements at the corners along the lower 10 or 20 inches.   In the assembled core these chamfers would form low resistance paths to the core exit, and thereby tend to keep the inter-element pressure lower than the seal pressure.

The inter-element pressure distributions for three types of inter-element gap with chamfered elements are shown in figures 2-37, 2-38 and 2-39.   Figure 2-37 illustrates the case where the bundling force is greatest due to the gaps being tapered from 0.2 mils at the core inlet to 2.5 at the core exit.   The distribution for three lengths of chamfer, varying from zero to 20 inches, is shown together with a possible range of seal pressures.   Chamfering the elements has only a small effect on the inter-element pressure.

Figure 2-38 shows the inter-element pressure for the case of predicted average gap. The gap varies from 0.5 mils at the core inlet to 1.5 mils at the core exit.   Increased lengths of chamfer decrease the core inter-element pressure and increase the bundling force.

Figure 2-39 shows the pressure distribution for the possible, but not probable case, in which the gap tapers down from 1.5 mils at the core inlet to 0.5 mils at the core exit. With no chamfer the inter-element pressure exceeds the highest expected seal pressure from Core Station 35 to the core exit.   Increasing the length of chamfer reduces the axial length over which the core pressure exceeds the seal pressure, but does not eliminate it completely.

It can be seen that undercutting and chamfering of elements are effective methods for controlling inter-element pressure distribution.   However, there is no conclusive evidence that positive measures need to be taken to control inter-element pressures.   Additionally, there are various undesirable side effects resulting from undercutting and chamfering, namely,

1) strength of fuel elements is decreased as a result of reducing the cross section,

2) sharp corners cause stress concentrations,

Astronuclear
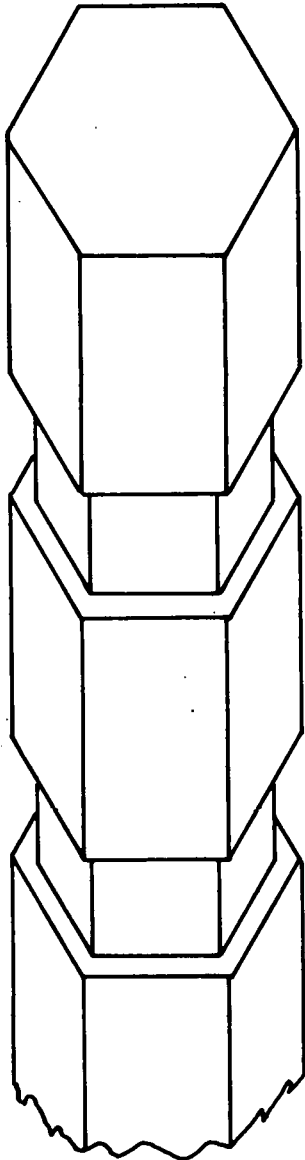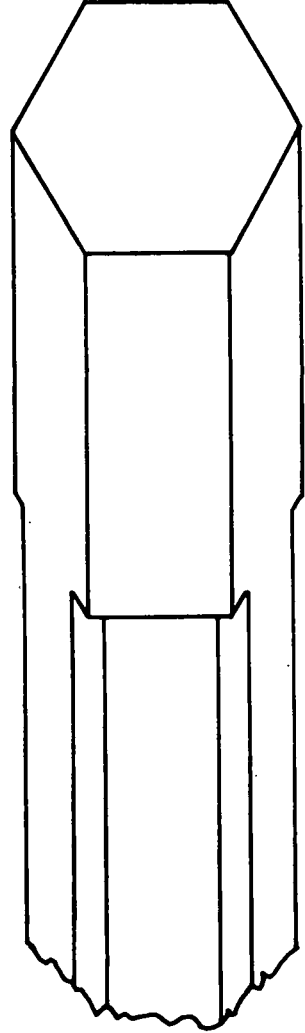
UNDERCUT ELEMENT   CHAMFERED ELEMENT

597885A

Figure 2-35 Undercut and Chamfered Fuel Elements

Astronuclear

Figure 2-36 Inter-Element Pressure for Undercut Element, Full Power,
No Seal Leakage

597886A

Astronuclear
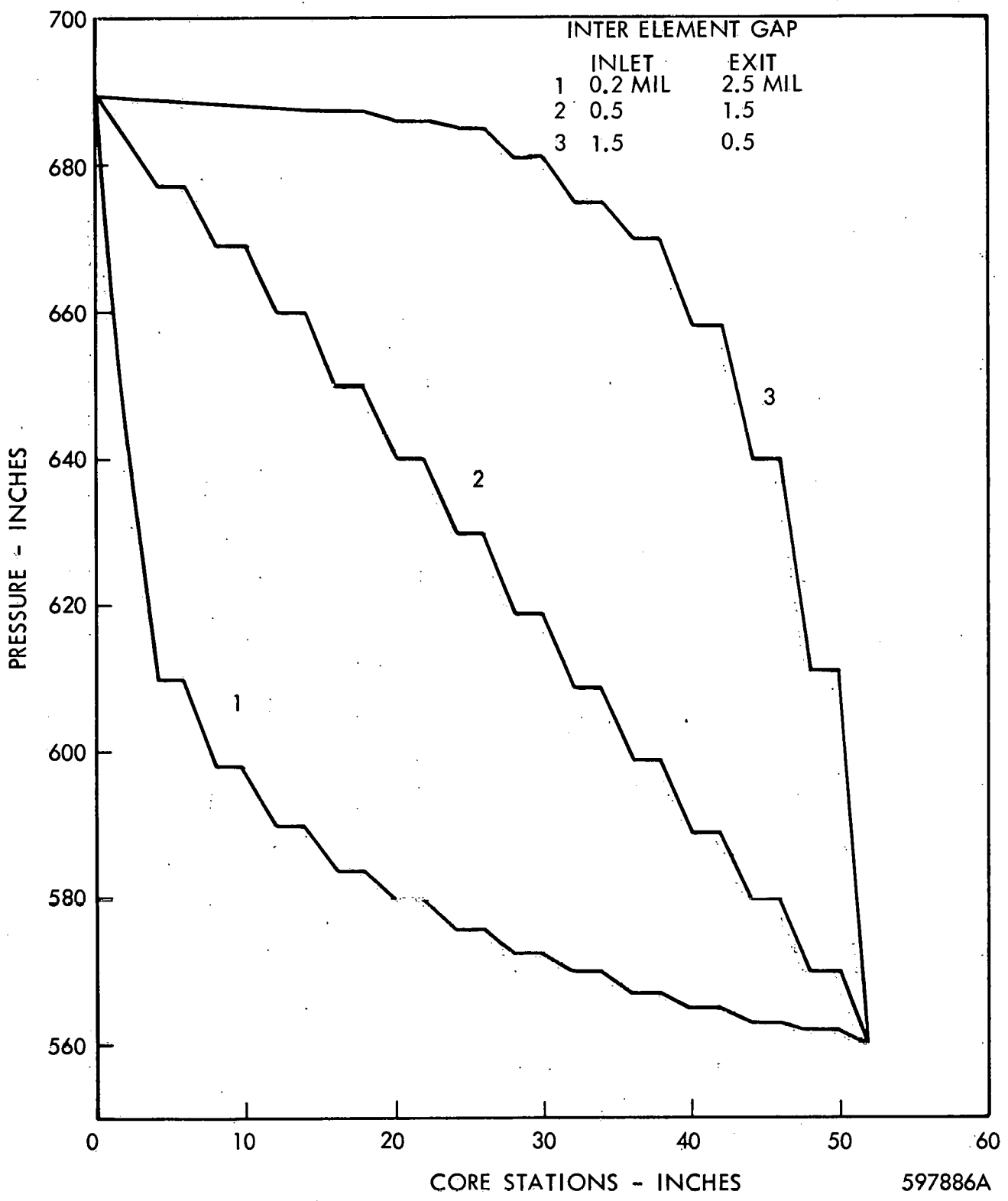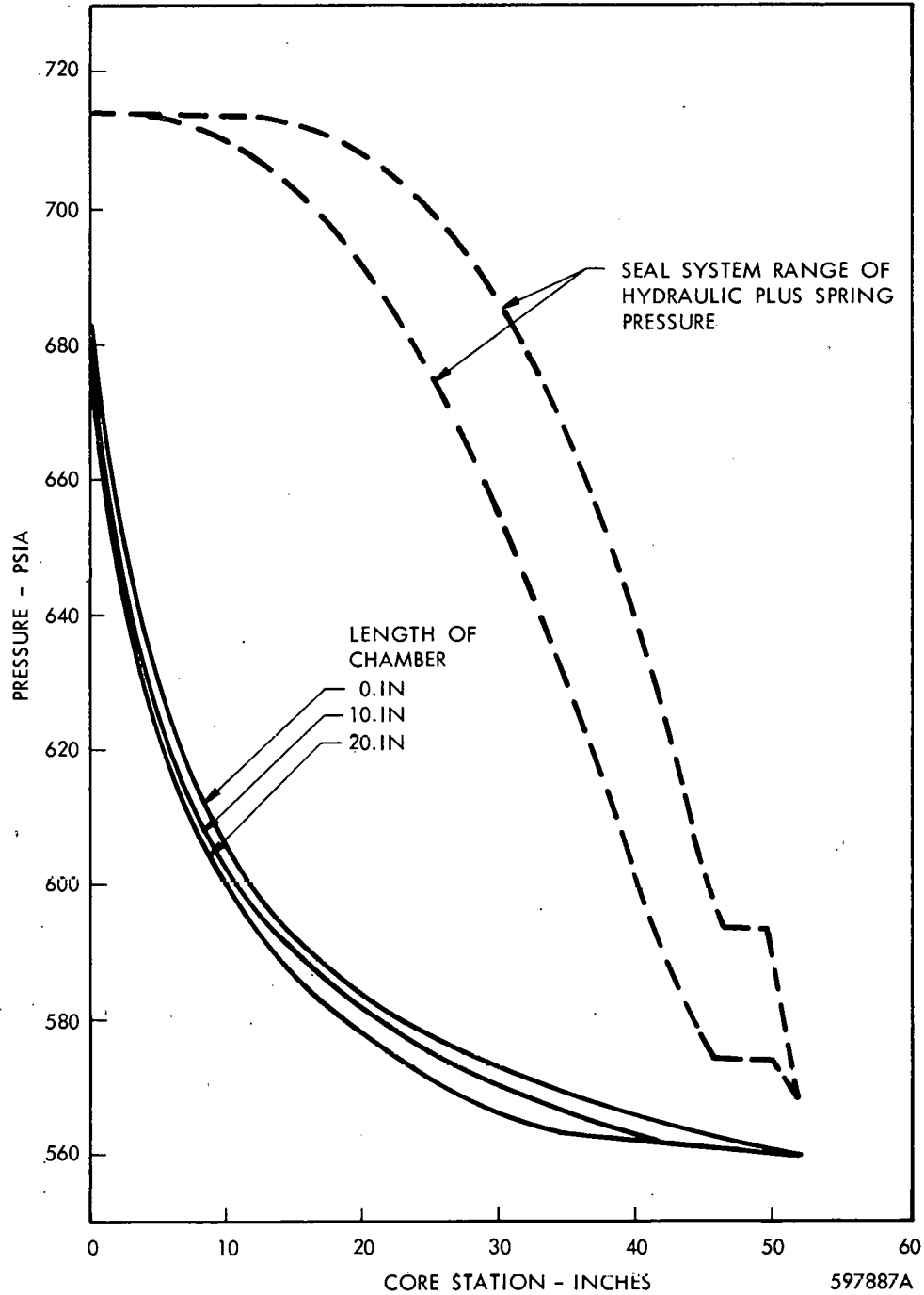
Figure 2-37 Inter-Element Pressure for Chamfered Element, Full Power
No Radial Flow (0.2 Mil Inlet Gap, 2.5 Mil Exit Gap)

Astronuclear
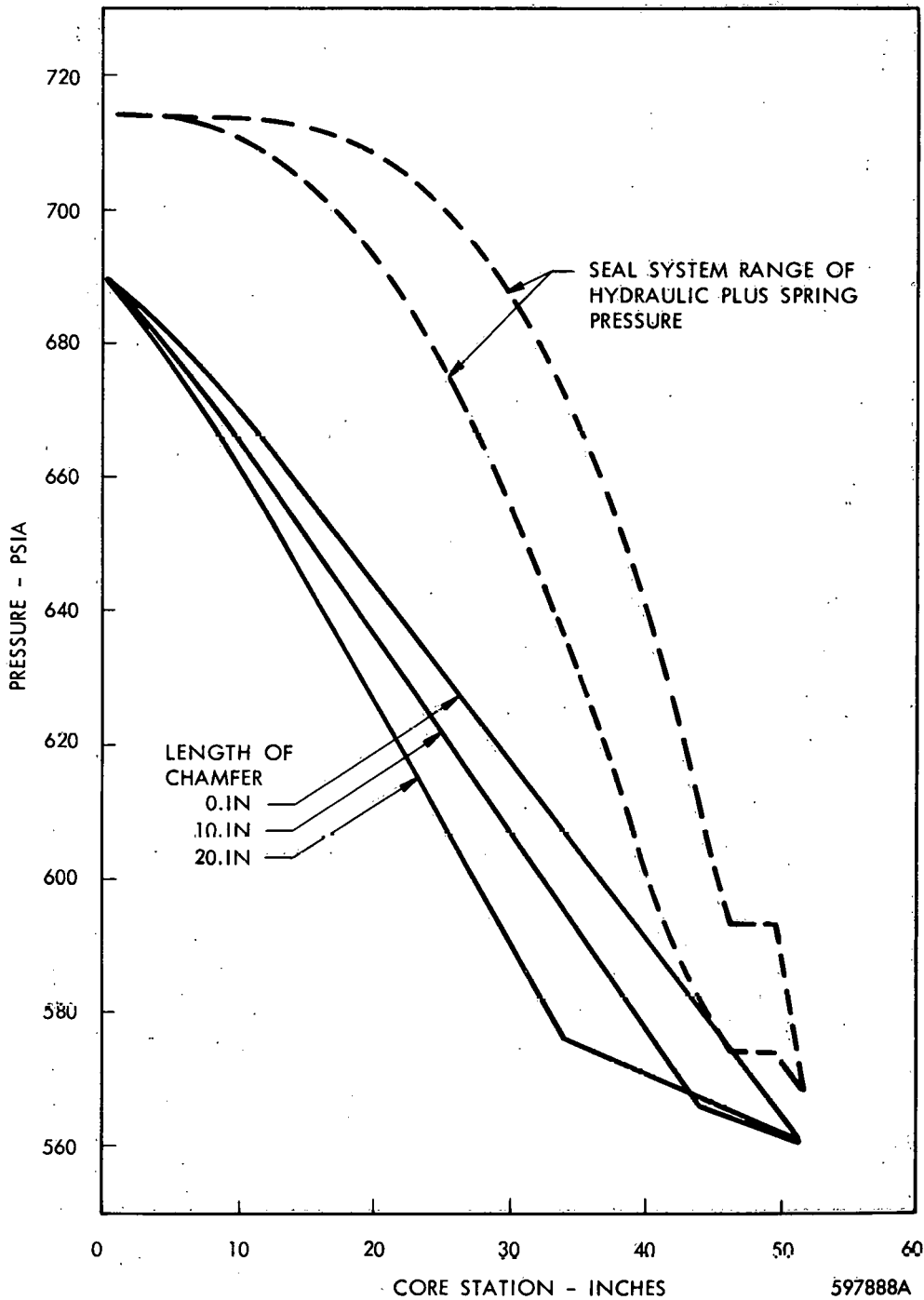
Figure 2-38 Inter-Element Pressure for Chamfered Element, Full Power
No Radial Flow (0.5 Mil Inlet Gap, 1.5 Mil Exit Gap)

Astronuclear
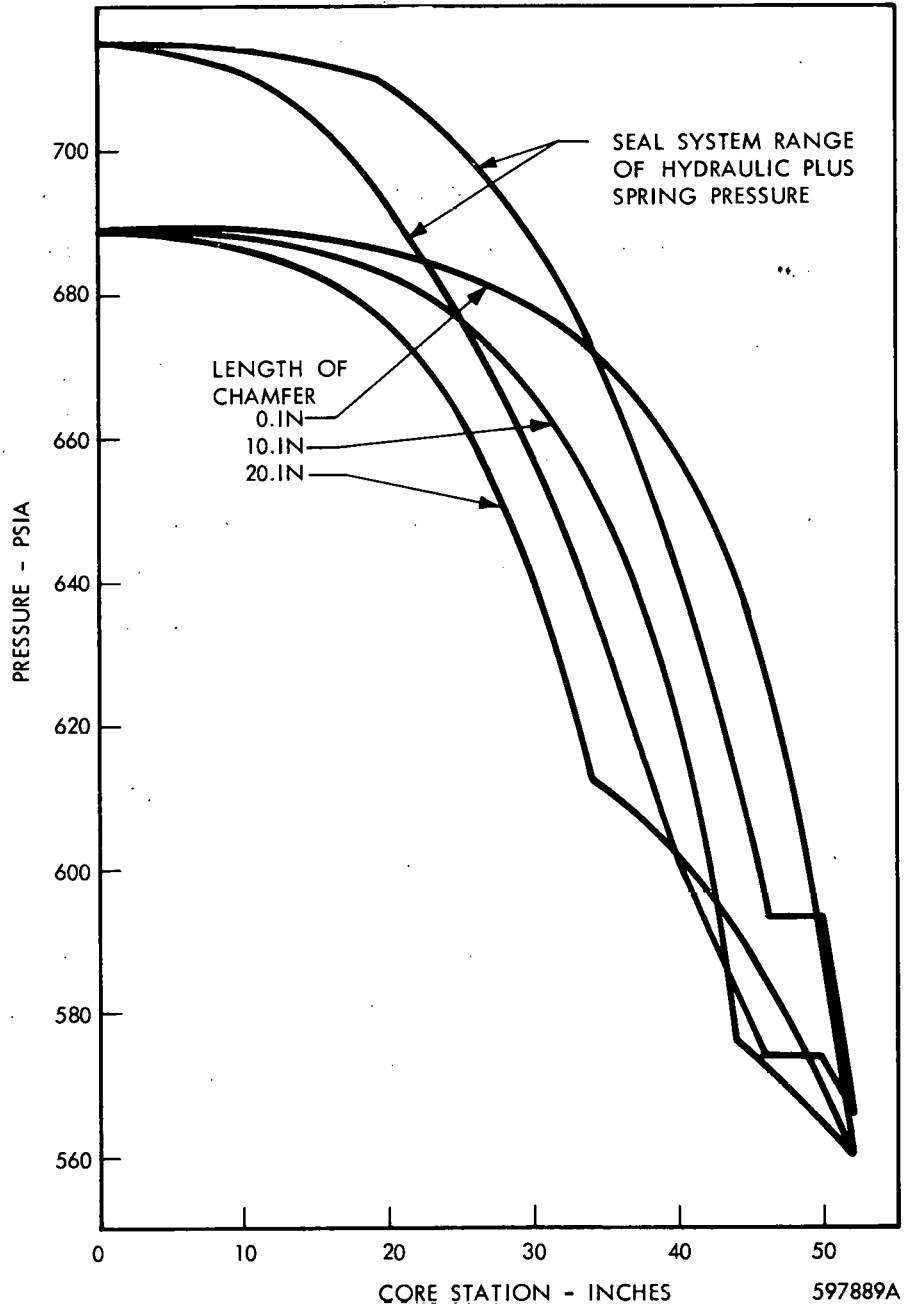
Figure 2-39 Inter-Element Pressure for Chamfered Element, Full Power
No Radial Flow (1.5 Mil Inlet Gap, 0.5 Mil Exit Gap)

DECLASSIFIED

Astronuclear

3)   as-extruded structure is destroyed, and

4)   inter-element flow and therefore corrosion is increased.

B.   Effect of Peripheral Cooling on Core Performance

The change in specific impulse as a function of core periphery coolant and leakage exit temperature and flow rate is given in figure 2-40. In this study the total flow was assumed to be 71.3 lb/sec. Of this, a varying amount either cooled the core periphery or leaked through the seal system and a constant 0.035 lb/sec flowed through the gaps. The remainder flows through the core fuel element and tie rod channels. The exit temperatures of the gases from the fuel elements, tie rods, and interstitial gaps were assumed to remain constant for all variations in peripheral flow. The assumed exit temperatures were, respectively, 4300, 545, and 4300°R. For varying peripheral flows the mixed mean enthalpy of the fuel element and tie rod channel flows was held constant. Over the narrow range considered, the loss in specific impulse is linear with both peripheral flow rate and peripheral flow exit temperature.

It can be concluded that:

1)   Changes in specific impulse are small over the range of core peripheral flow rates which were considered.

2)   For maximum core performance the core peripheral flow rates should be as small as possible and the exit temperature as high as possible. This necessitates a balance between the requirements of maximum core performance and the necessity, in some designs, of cooling the core periphery.

Astronuclear

	EXIT TEMP °R	EXIT PRESS. PSIA
CORE	4299	560
TIE ROD	545	560
CORE LEAKAGE	4300	560
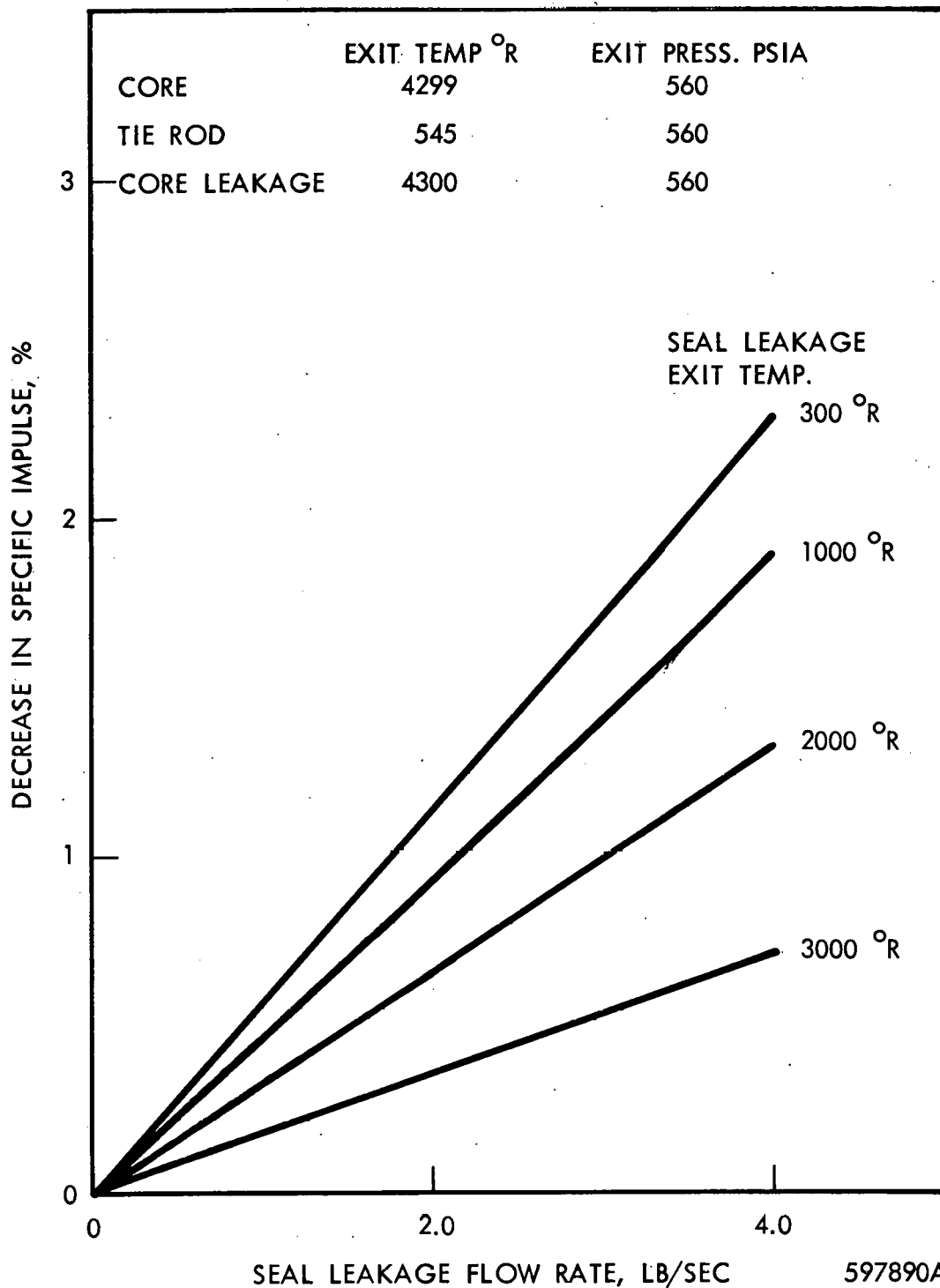
Figure 2-40 Reactor Performance versus Lateral Support Seal Leakage Flow
and Exit Temperature

597890A

-61-

C.   Effect of an Increase in Tie Rod Diameter

It has been suggested that increasing the diameter of the tie rod might reduce stress levels and increase core reliability.   To evaluate this possibility, tie rod temperature as a function of tie rod diameter has been calculated.   The results of this calculation are presented in figure 2-41 as tie-rod centerline and surface temperature versus tie rod diameter.   The temperatures are calculated for two axial positions, the first position at the point of maximum internal heat generation near the core midplane and the second at the channel exit where the maximum coolant temperature occurs.

Two assumptions are made in this analysis, the first being that the coolant exit bulk temperature is 882°R for all tie rod diameters and the second that the pressure drop across the inlet and exit orifices is constant for all tie rod diameters.   All temperature drops are ratioed to the temperature drops of a nominal 0.110-inch diameter rod at the point of maximum radial power factor.

The tie rod temperature calculation does not include provisions for deviations from the nominal conditions.   A qualitative analysis of these variations may be made by classifying them into two groups.   The first group includes the following:

1) width of the hydrogen gap between the pyrographite insulating sleeve and the stainless steel liner,

2) heat generation between unfueled elements with reactivity shims and without reactivity shims,

3) pyrographite thermal conductivity, and

4) temperature of the fuel surrounding the unfueled elements.

The parameters in this group affect only the quantity of heat added to the coolant from the tie rods.   Since the fraction of the total heat added to the coolant through the outer wall decreases with increasing tie rod diameter, changes in this first group of parameters will have less effect on the coolant temperature as the diameter of the tie rod is increased and more surface area is available for heat transfer.

(W) Astronuclear
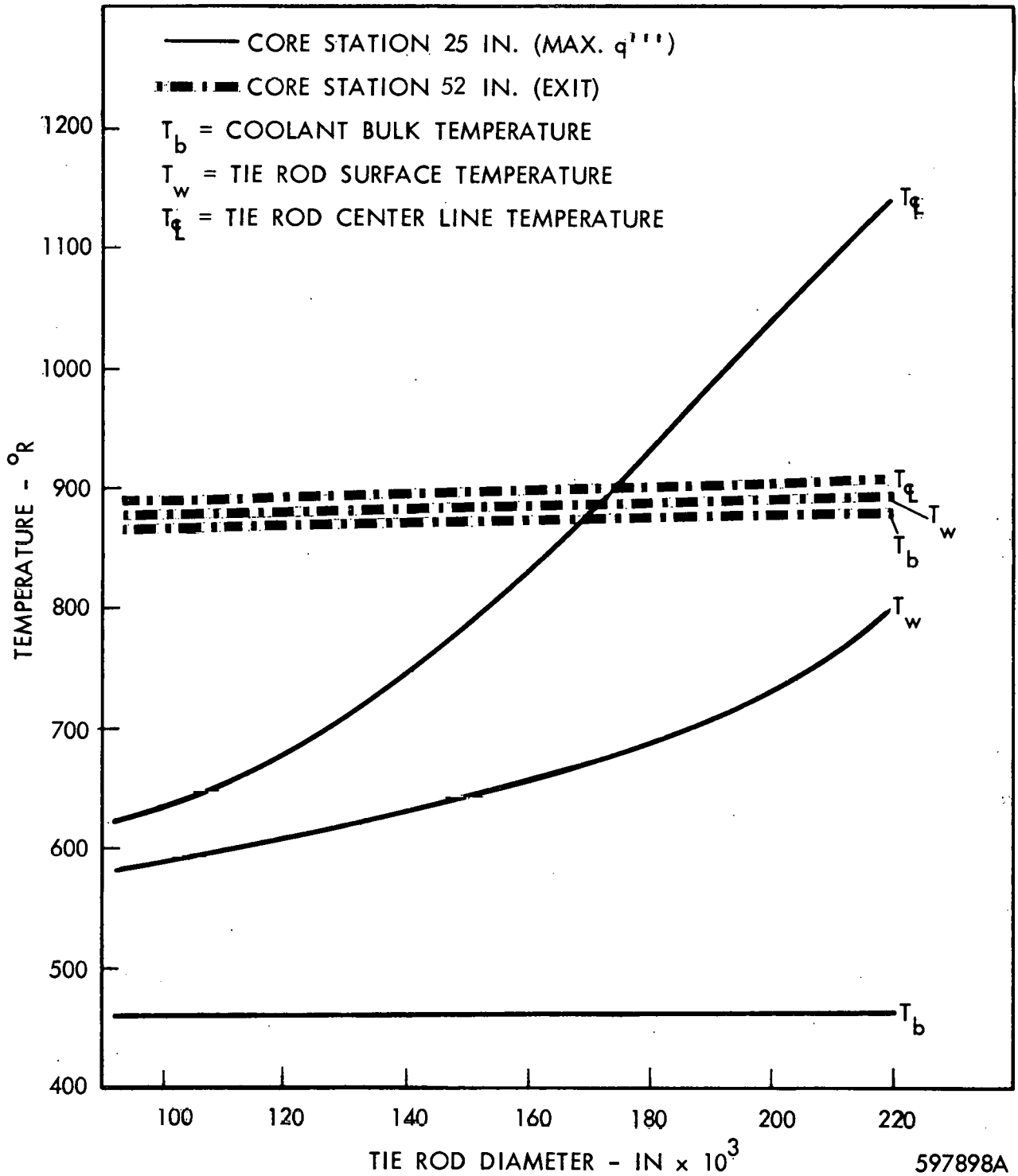
Figure 2-41 Tie Rod Channel Temperatures versus Tie Rod Diameter at Point of Maximum Radial Power Factor, Constant Inlet and Exit Pressure Drop

The second group includes:

1) Variation in internal heat generation rates.

2) Variation in inlet and exit loss coefficients.

The variations in internal heat generation will affect the heat added to the coolant from both the unfueled element and from the tie rod. This effect will produce the same variation in coolant temperature for all tie rod diameters. However, the magnitude of the changes in the temperature differences in the tie rod will be greater for a large rod than for a small rod for the same percentage change in internal heat generation. The effect on coolant temperature due to variations in inlet loss coefficient will not change with tie rod diameter. Since it is assumed that the pressure drop at the inlet and exit is the same for all tie rod diameters, variations in the coefficients will cause the same change in flow for all rod diameters. Therefore, the changes in coolant temperature due to a given variation in inlet or exit loss coefficient will be the same for all tie rod diameters.

It can be concluded that:

1) tie rod and temperature limitations are not exceeded in the range studied (0.110 – 0.222 inch),

2) increasing tie rod diameter decreases axial tensile stress but also decreases lateral flexibility, and

3) increasing tie rod diameter offers no improvement in thermal performance.

D. Unmachined or As-extruded Elements

The current process for manufacturing fuel elements involves reaming of the coolant holes and machining of the exterior surfaces of the element after extrusion and graphitizing. To simplify manufacturing, elimination of the final machining is being considered. When final machining is eliminated, elements are produced which have wider dimensional tolerances than those currently being produced.

The variations in channel diameter which are present before coating, can cause changes in coolant exit temperature. This temperature perturbation will exist even though each individual channel in the core is orificed in an attempt to maintain the coolant exit

Astronuclear

temperature in all channels nearly the same. If the uncoated diameter of the channel is less than the nominal 0.098 inch, the coolant exit temperature will be higher than predicted. This increase in temperature is also a function of the radial power factor and the coated diameter of the channel. The increase in exit temperature above the nominal as a function of uncoated diameter with radial power factor as a parameter is shown in figure 2-42. All of the curves in the figure are calculated for channels with a coated diameter of 0.095 inch.

To compare the performance of a core composed of machined elements with the performance of a core of unmachined elements, a statistical analysis of fuel element maximum temperature was made. This procedure combines the variance in fuel element temperature from all manufacturing and operating deviations, including the variation in uncoated diameter to find the probable number of channels above 4960 and 5500°R. The results are calculated for a ± 0.0005 and ± 0.001 inch tolerances on the uncoated diameter. In the present process the uncoated diameter of the channels are held to a tolerance of ± 0.0005 inch. Inspection data of unmachined elements indicates that the tolerance on the uncoated diameter is ± 0.001 inch.

The results show that doubling the variation in channel diameter has a negligible effect on the statistical distribution of the fuel element maximum temperature. Within the accuracy of the calculation there is no increase in the number of channels above the specified temperature when the channel uncoated diameter variations increases from ± 0.0005 inch to ± 0.001 inch. This is true because the variation in temperature from the uncoated diameter of the channels is much less than the combination of all other effects.

Typically, the temperature variance due to a ± 0.001 inch variation in channel diameter is $256°R^2$. In comparison, the variance due to the 20 percent uncertainty in radial power distribution in the core periphery is $335,000°R^2$.

In can be concluded that:

1) The variation in exit temperature from the uncertainty in uncoated channel diameter is not detrimental to core integrity.

2) The use of as-extruded elements eliminated the leaching of the coolant channels. The large uranium loss and variations in fuel element concentration caused by leaching are therefore eliminated.
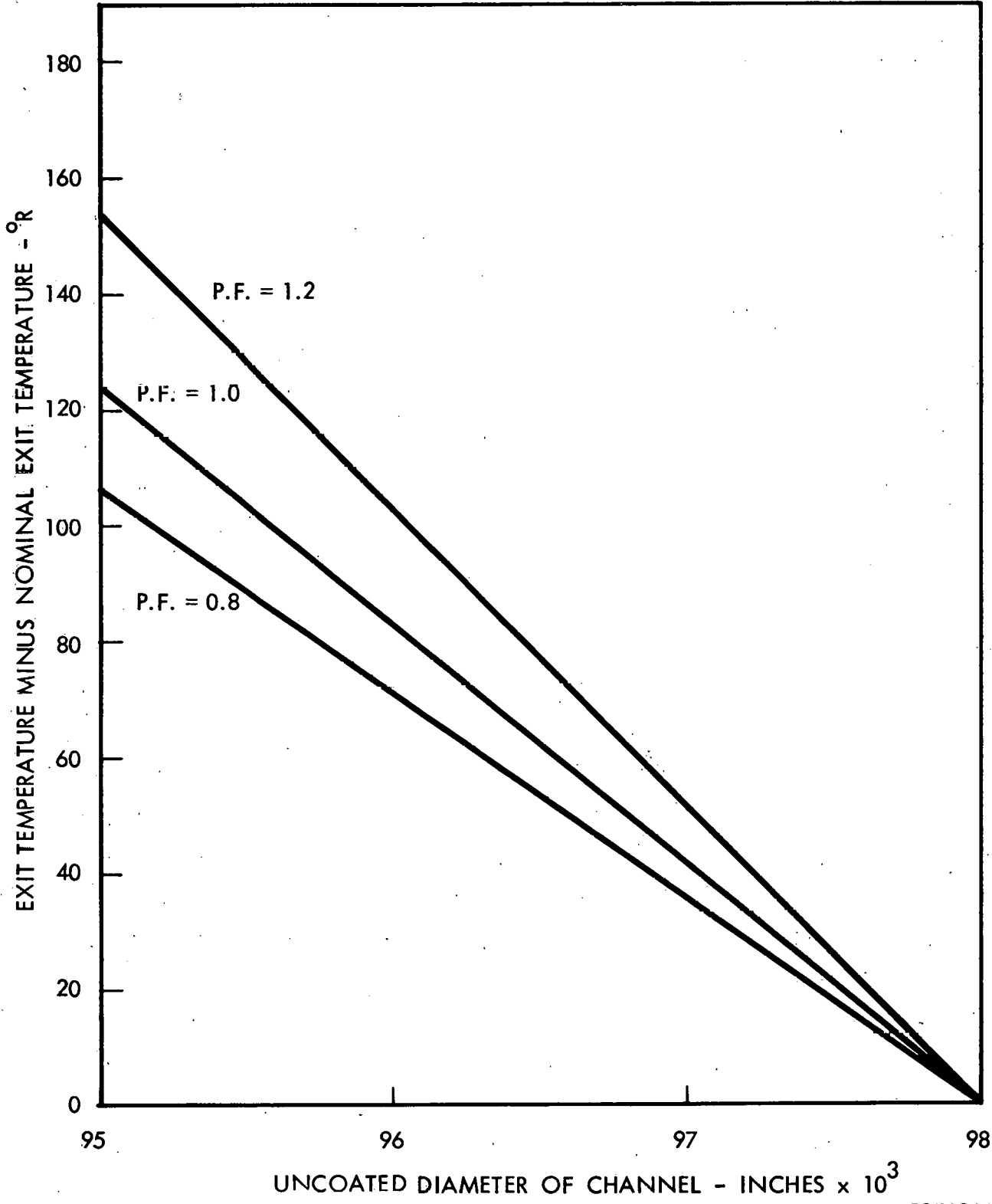
Astronuclear

Figure 2-42 Hydrogen Exit Temperature Minus Nominal Exit Temperature Versus Uncoated
Diameter of Channel for Three Radial Power Factors and 0.095 Inch Coated Diameter

597696A

Astronuclear

SECTION 3

NUCLEAR ANALYSIS

The primary NRX-A5 nuclear design effort has been the investigation of several candidate reactor types. The nuclear characteristics of each reactor type was determined, and a range of acceptability established. Major areas of possible redesign which will affect the neutronics of the reactor are the core periphery, the filler strip region, and the inner reflector.

Core Periphery   Possibilities in this area include reducing the fueled core diameter, and elimination of irregularities in the core periphery. Generally, loss of part of the fueled core results in a loss of reactivity and control drum span. Introducing more regularity into the core periphery will result in a reduction in the local variation in power factors at the core edge.

Filler Strip Region   This area of redesign includes thickening of the filler strip region (in conjunction with a reduced core diameter), the addition of coolant holes and coolant hole liners, and the use of a metallic wrapper (5 to 10 mils) surrounding the filler strip region.

Inner Reflector   The major change being considered here consists of replacing the graphite cylinder with a composite beryllium-aluminum or graphite-aluminum structure. The effect of graphite removal, or replacement of graphite by aluminum, is a reduction in both reactivity and control drum span. The effect of replacing graphite with beryllium is to increase both reactivity and drum span; a considerable uncertainty is attached to these calculations however, because of the lack of confirming experimental data.

Within these broad areas of possible redesign, seven specific core-reflector combinations were calculated in detail. They are the following:

1)   The KIWI B-4D reactor as designed by LASL.

2)   A KIWI B-4D, NRX-A2 combination; this reactor consists of a B-4D sized core but with the NRX-A2 loading scheme, thickened filler strips containing lined coolant holes, a metallic wrapper around the filler strip region, and the NRX-A2 inner and outer reflectors.

3) The NRX-A2 reactor, modified by use of thickened filler strips with lined coolant channels, and by addition of a metallic wrapper.

4 & 5) The NRX-A2 reactor but with an aluminum-graphite structure replacing the graphite inner reflector cylinder. Cases (4) and (5) have respectively 40 and 75 volume percent aluminum in the inner reflector cylinder.

6 & 7) The NRX-A2 reactor but with an aluminum-beryllium structure replacing the graphite inner reflector cylinder. Cases (6) and (7) have respectively 40 and 75 volume percent aluminum in the inner reflector cylinder.

3-1 GENERAL CONSIDERATIONS

In order to indicate generally the sensitivity and control drum span to changes in the above areas of redesign, the following experimental results are presented. Table 3-1 presents experimental data obtained from both LASL-KIWI and WANL-PAX experiments. The experimental data applies only for very small perturbations. Where major changes are anticipated, such as the substitution of aluminum or beryllium for a large part of the graphite cylinder, analytical methods are required. The methods in use have been proven reliable for analyzing KIWI-type reactors including the NRX-A2.

3-2 NRX-A5 CALCULATIONS

In order to evaluate the candidate reactor types for acceptability from a nuclear standpoint, tentative minimum requirements for room temperature reactivity and control drum span were established.

The following table summarizes the requirements which establish the excess reactivity which must be available in the cold reactor by rotating the control drums out from the cold critical position.

Excess Reactivity Requirements in Cold Reactor

$0.9	maximum cold-to-hot reactivity loss (includes $0.4 uncertainty)
1.5	reactivity loss during operation
1.7	excess reactivity required at end of test
$\overline{\$4.1}$	total reactivity requirement

The cold-to-hot reactivity loss is based on current NRX-A2 calculations for full power operation.

The operating reactivity loss represents an extrapolation from current weight loss data to 20 min. operation assuming all of the material lost to be carbon. It is hoped that materials development may reduce this number even for longer operating times since the resulting swing in control drum position causes the power density at the core edge to increase by 5 - 10 percent during operation. In order to avoid overtemperaturing the edge elements, the core periphery must accordingly be derated at the start of the test by this amount.

The final item in the table derives from the requirement that the reactor should still have at least $0.5 reactivity available for maneuvering and the control drums should not exceed 130 degrees. Although the latter figure might be relaxed somewhat, it is unsatisfactory to operate at large angles since the control worth per degree of rotation is approaching zero. Implicit also is the need for a margin since control worth measurements must be made at room temperature and by using only a few drums, which contributes to error.

The control drum worth must be sufficient so that in the condition of highest reactivity, the drums must be able to provide at least $2.80 shutdown.* Providing that transient conditions do not occur in which the propellant reactivity feedback exceeds the operating value the reactor has the highest reactivity in the cold, dry condition. Under this assumption the required control worth is just the $4.1 previously developed, plus $2.8, or a total of $6.9.

The above requirements are based on presently available data for the NRX-A2 reactor. Although these will vary slightly for the different reactor systems being evaluated, the comparison is believed to be valid.

---

* This is the current limitation governing operations at WANEF.

The calculated nuclear characteristics for the seven reactors investigated are summarized in Tables 3-2 through 3-8. Included is a brief description of the particular reactor, the calculated excess reactivity and control drum span, and an indication of the radial power shape, given by the centerline and edge power factors. The compensating changes in central loading necessary to increase the calculated excess reactivity at 180 degree drum angle to the minimum level of $4.1, and the edge loading necessary to raise the edge power factor to the centerline value are given.

The reactivity is based in each case on a standard configuration using the NRX-A2 multihole unfueled element throughout the core. Additional positive reactivity is available either by introducing graphite shim pencils, or by substituting single hole unfueled modules. Negative shimming would be accomplished by using tantalum carbide-loaded pencils as in NRX-A2, or by inserting tantalum carbide - loaded single hole modules as in the KIWI B-4D and B-4E reactors.

Table 3-2, which describes the KIWI B-4D design, also has a comparison of WANL calculations for reactivity, control drum span, and radial power shape, versus the measured values. As can be seen in Table 3-2, the agreement between experimental and calculated drum span and radial power shape is very good. The discrepancy between the calculated and experimental excess reactivity is thought to be due in part to smearing the 4.5 kilograms of tantalum homogeneously in the calculation. Emphasis was placed on the KIWI B-4D calculations both because it contains design features considered for NRX-A5 and because experimental data for this reactor are available to verify calculations. The tables indicate that all of the designs are feasible from a nuclear standpoint.

The reactivity losses are not prohibitive in any of the cases studied. The highest central loading required, in the case of the 75 percent aluminum barrel, is only 462 mg/cc. Elements of this loading have already been fabricated by Los Alamos, using the current fabrication process, which entails a process loss of uranium of 9 - 10 percent. If the NRX-A5 elements are not reamed, there is believed to be very little process loss so that the present pellet-graphite proportions should produce uranium densities approaching 450 mg/cc. The mechanical properties of the beaded fuel element are believed to be essentially unimpaired until the loading is increased to the order of 600 mg/cc.

Ⓦ △stronuclear

The effects on radial power shape are also moderate.

The loss of control span is of more concern in the studies making extensive use of aluminum in the reflector cylinder. In view of the uncertainty in control drum calculations, which is considerable, experimental measurement of the control span in this configuration should be made.

3-3   EFFECT OF COLD-TO-HOT CHANGES ON REACTOR NEUTRONICS

Calculations to describe the effects of cold-to-hot changes on the candidate designs have been made. Figure 3-1 shows the comparison between a WANL calculation and experimental results for the relative power in KIWI B-4D at room temperature, in terms of fissions per gram uranium. The good agreement lends assurance that the edge fuel loadings given in Tables 3-2 through 3-8 are reasonable. Figure 3-2 shows the calculated versus experimental change in radial power shape for an 8 degree outward rotation of the control drums, and again the agreement is good. The effect of operating temperature on edge power is not well defined experimentally (LASL is using one-dimensional transport theory to estimate this effect in KIWI B-4D). Although this effect has not yet been calculated by WANL for the KIWI B-4D, calculations on the NRX-A2 show good agreement.

Using the LASL predictions for radial fissions per gram uranium at operating conditions, and their experimental local corrections, channel by channel power factors were generated for a 60 degree sector of KIWI B-4D. The factors range from 0.74 to 1.23. In general, however, the power factors lie between 0.80 and 1.20.

In summary it is concluded that:

1)   None of the designs considered involve reactivity losses which cannot be compensated with reasonable fuel loading increases, without exceeding the range of loadings already fabricated.

2)   The power shape is not worsened in these designs.

3)   An undesirable loss in control drum span occurs when aluminum is used extremely in the reflector cylinder. Calculations indicate that the loss can be tolerated in view of print requirements.

Astronuclear
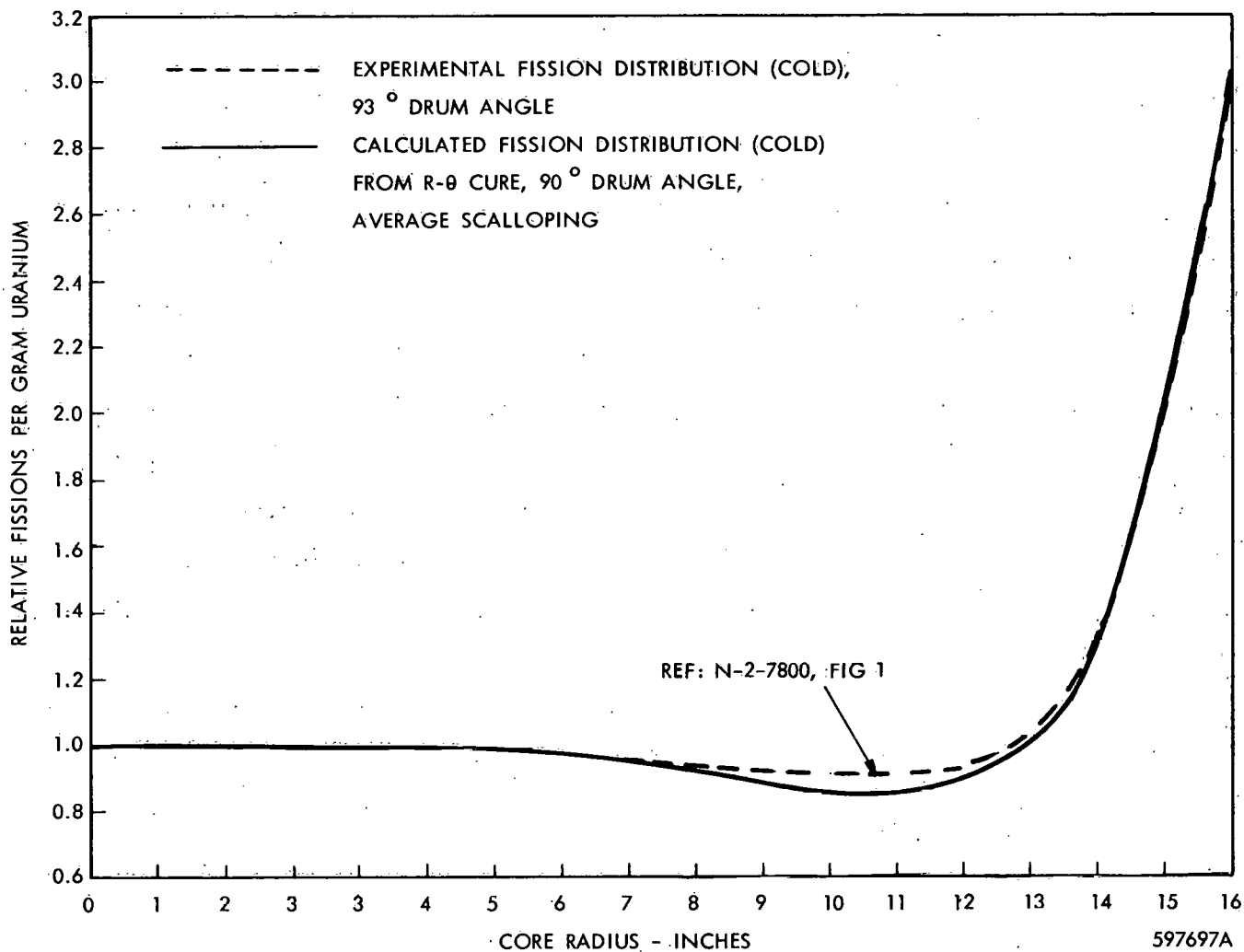
Figure 3-1 KIWI B4D KIVA Calculated Versus Experimental Fissions Per Gram

CONFIDENTIAL
RESTRICTED DATA
Atomic Energy Act 1954

CONFIDENTIAL
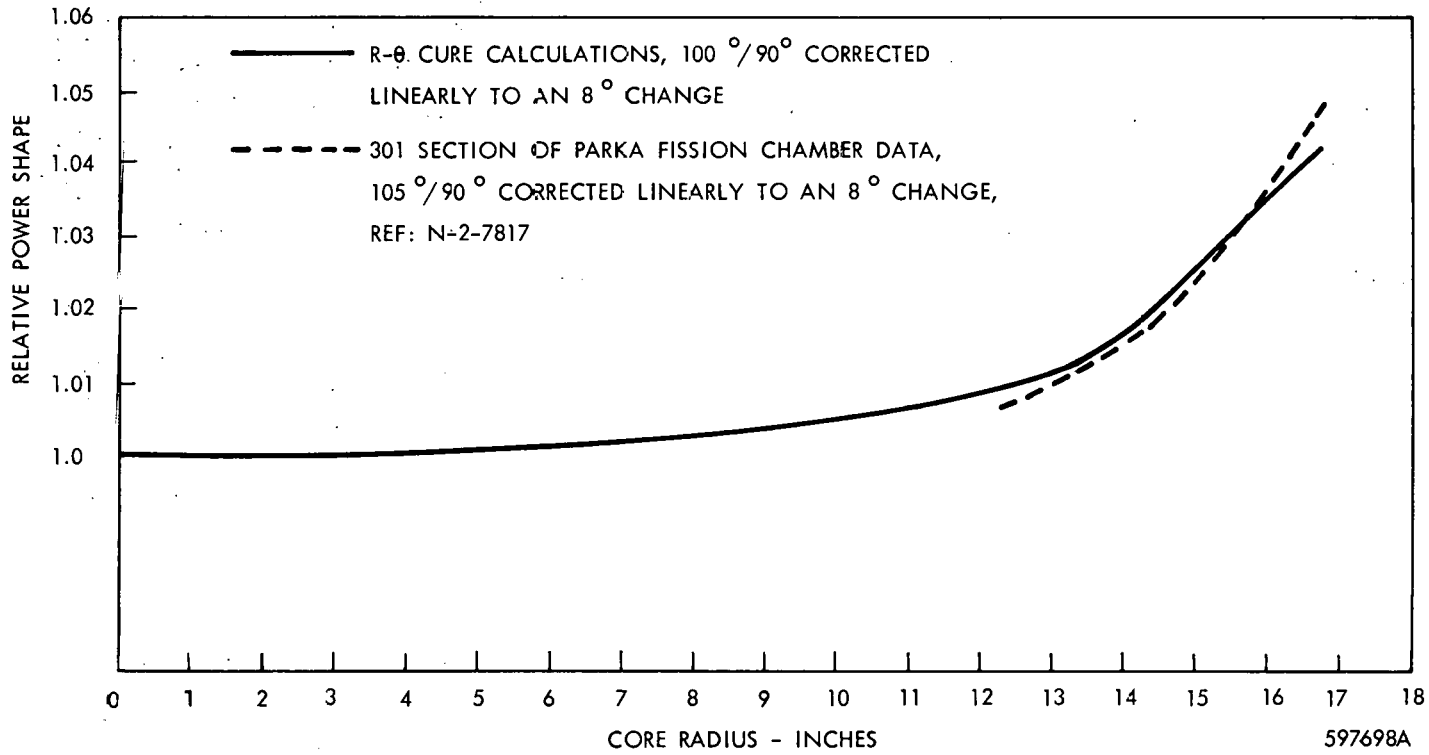RESTRICTED DATA
Atomic Energy Act 1954

Figure 3-2 Change in Radial Power Shape with 8 Degree Drum Angle Change
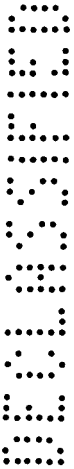
Astronuclear

TABLE 3-1

EXPERIMENTAL REACTIVITY AND DRUM SPAN COEFFICIENTS

Material	Description	Mass	Reactivity Change	Reactivity Coefficient	Drum Span Change	Drum Span Coefficient	Reference
Aluminum (added)	KIWI B-4A ZEPO; 0.25 in thick annulus adjacent to core; I.D. 44.7 cm	63.6 kg	+ $0.50	+0.79 /kg	$0.00	0.0 /kg	N-2-7612
Beryllium (added)	KIWI B-4A ZEPO; thin annuli,						
	a) Adjacent to core, I.D.= 18 in			+ 5.2 /kg			N-2-7612
	b) Between C and Be Ref's, I.D.= 20.2 in			+ 3.5 /kg			N-2-7612
	c) Outside Be Ref. I.D. 20.2 in			+ 0.9 /kg			N-2-7612
	d) 0.25 in. thick, I.D. 20.2 in	50.0 kg			+ $0.15	+ 0.3 /kg	N-2-7612
Carbon (removed)	KIWI B-4A ZEPO; 0.19 in thick annulus adjacent to core; I.D. 44.7 cm	31.9 kg	- $1.00	+ 3.1 /kg	- $0.4	+ 1.2 /kg	N-2-7612
Carbon (removed)	WANL-PAX; filler strips removed in front of one control drum	2.092 kg (25.10 kg)*			- $ .022 (- $ .27)	+ 1.06 /kg (+ 1.06 /kg	WANEF - 182
Carbon (removed)	WANL-PAX; filler strip average I.D.=43.8 cm, O.D.=45.2 cm			+ 3.39 /kg			WANEF - 182
	graphite reflector average I.D.=45.2 cm, O.D.=51.0 cm			+ 2.22 /kg			WANEF - 182
Nickel (added)	KIWI B-4D ZEPO; 0.007 in thick foil around core; I.D. 44.7 cm	5.87 kg	- $ 0.19	- 3.2 /kg			N-2-7705

TABLE 3-1 (Cont)

Material	Description	Mass	Reactivity Change	Reactivity Coefficient	Drum Span Change	Drum Span Coefficient	Reference
Stainless Steel (added)	WANL-PAX: 5 " O.D. Stainless steel rods in filler strip region	9.14 kg	- $0.11	- 1.2 /kg			WANEF - 167
Stainless Steel (added)	KIWI B-4D ZEPO; .056 in thick annulus between C and Be Ref's.	43.5 kg	- $0.23	-0.5 /kg	- $0.40	- .82 /kg	N-2-7705
Stainless Steel (added)	KIWI B-4 ZEPO; 0.62 in annulus between C and Be Ref's. I.D. 20.2 in, 90° core sector	12.385 kg (51.18 kg)	- $0.28 (- $1.16)	- 2.27 /kg (- 2.27 /kg)	- $0.16 per drum (- $1.90)	- 3.71 /kg (- 3.71 /kg)	N-2-7705

* Numbers in parenthesis are extrapolations from actual experiments to a 360° core sector.

Astronuclear

Astronuclear

TABLE 3-2

DESCRIPTION AND NUCLEAR CHARACTERISTICS OF KIWI B4-D LASL DESIGN

Description

Core	Fueled core diameter reduced loading: approximately 400 mg/cc central, 175 to 145 mg/cc edge with 100 centermost elements approximately 460 mg/cc
Lateral Support	Cooled filler strips and wrapper NRX type leaf springs
Outer Reflector	B-4A type

Excess Reactivity	Experimental	Calculated
	$3.80	$2.05
Control Drum Span	$7.40	$7.50
Radial Power Shape (Fiss/Gm.U) edge to center line	3.04 (93°)	2.98 (90°)

Compensating Changes (To Achieve Desired Reactivity and Radial Power Shape)

Central Loading	-
Edge Loading	-

Reactivity Available by
Employing Single Hole Tie
Rod Elements

Astronuclear

TABLE 3-3

DESCRIPTION AND NUCLEAR CHARACTERISTICS OF

NRX-A2, KIWI B-4D COMBINATION

Description

Core	KIWI B-4D core geometry, NRX-A2 loadings, i.e., 417 mg/cc central, 136 mg/cc edge
Lateral Support	KIWI B-4D filler strips NRX-A2 inner reflector
Outer Reflector	NRX-A2

Excess Reactivity (13 Hole Tie Rod Elements) $3.86

Control Drum Span $7.53

Radial Power Shape

Center line to average	1.19
Edge to average	1.06

Compensating Changes (To Achieve Desired Reactivity and Radial Power Shape)

Central Loading	421 mg/cc
Edge Loading	152 mg/cc

Reactivity Available by
Employing Single Hole Tie $2.18
Rod Elements

Astronuclear

TABLE 3-4

DESCRIPTION AND NUCLEAR CHARACTERISTICS OF

NRX-A2, KIWI B-4D COMBINATION

Description

Core	NRX-A2
Lateral Support	Cooled filler strips, wrapper NRX-A2 inner reflector
Outer Reflector	NRX-A2

Excess Reactivity (13 Hole Tie Rod Elements) $4.49

Control Drum Span $8.55

Radial Power Shape

Center line to average	1.20
Edge to average	1.05

Compensating Changes (To Achieve Desired Reactivity and Radial Power Shape)

Central Loading	4.17 mg/cc
Edge Loading	145 mg/cc

Reactivity Available by Employing Single Hole Tie Rod Elements $2.43

Astronuclear

TABLE 3-5

DESCRIPTION AND NUCLEAR CHARACTERISTICS OF

NRX-A2 WITH ALUMINUM GRAPHITE INNER REFLECTOR - 40 v/o

Description

Core	NRX-A2
Lateral Support	NRX-A2 filler strips 40 v/o aluminum in graphite cylinder
Outer Reflector	NRX-A2

Excess Reactivity (13 Hole Tie Rod Elements) $3.22

Control Drum Span $7.85

Radial Power Shape

Center line to average	1.24
Edge to average	0.96

Compensating Changes (To Achieve Desired Reactivity
and Radial Power Shape)

Central Loading	432 mg/cc
Edge Loading	180 mg/cc

Reactivity Available by
Employing Single Hole Tie $2.43
Rod Elements

Astronuclear

TABLE 3-6

DESCRIPTION AND NUCLEAR CHARACTERISTICS OF

NRX-A2 WITH ALUMINUM GRAPHITE INNER REFLECTOR - 75 v/o

Description

Core	NRX-A2
Lateral Support	NRX-A2 filler strips 75 v/o aluminum in graphite cylinder
Outer Reflector	NRX-A2

Excess Reactivity (13 Hole Tie Rod Elements) $1.32

Control Drum Span $7.10

Radial Power Shape

Center line to average	1.28
Edge to average	0.87

Compensating Changes (To Achieve Desired Reactivity
and Radial Power Shape)

Central Loading	462 mg/cc
Edge Loading	220 mg/cc

Reactivity Available by $2.43
Employing Single Hole Tie
Rod Elements

Astronuclear

TABLE 3-7

DESCRIPTION AND NUCLEAR CHARACTERISTICS OF

NRX-A2 WITH ALUMINUM BERYLLIUM INNER REFLECTOR - 40 v/o

Description

Core	NRX-A2	
Lateral Support	NRX-A2 filler strips 40 v/o aluminum in beryllium cylinder	
Outer Reflector	NRX-A2	

Excess Reactivity (13 Hole Tie Rod Elements) $4.92

Control Drum Span $8.37

Radial Power Shape

Center line to average   1.20

Edge to average   1.00

Compensating Changes (To Achieve Desired Reactivity and Radial Power Shape)

Central Loading   417 mg/cc

Edge Loading   160 mg/cc

Reactivity Available by Employing Single Hole Tie Rod Elements $2.43

DECLASSIFIED

Astronuclear

TABLE 3-8

DESCRIPTION AND NUCLEAR CHARACTERISTICS OF

NRX-A2 WITH ALUMINUM BERYLLIUM INNER REFLECTOR - 75 v/o

Description

Core	NRX-A2
Lateral Support	NRX-A2 filler strips 75 v/o aluminum in beryllium cylinder
Outer Reflector	NRX-A2

Excess Reactivity (13 Hole Tie Rod Elements) $2.12

Control Drum Span $7.80

Radial Power Shape

Center line to average	1.26
Edge to average	0.91

Compensating Changes (To Achieve Desired Reactivity and Radial Power Shape)

Central Loading	449 mg/cc
Edge Loading	200 mg/cc

Reactivity Available by $2.43
Employing Single Hole Tie
Rod Elements

It is recommended that a confirmation of the control drum worth be made experimentally for designs utilizing aluminum-graphite and aluminum-beryllium inner reflectors.

THIS PAGE

WAS INTENTIONALLY

LEFT BLANK

SECTION 4

DEFINITION OF REDESIGN EFFORT

A strong emphasis was made in the redesign effort on the increase of the performance and mission capability of the NRX-A reactor. The three primary objectives were:

1) capability of twice NRX-A2 power density,

2) capability of 1.7 diametrical scaling, and

3) capability of 60 minutes of full power operation.

If the existing nozzle and reactor geometry remain unchanged, flows and pressure levels will have to be doubled to maintain the same exit temperature in the nozzle chamber. Consequently, fluid loading of many structural components will increase by about a factor of two.

Also, if the coolant flow area is increased at the expense of fuel to reduce the core pressure drop, the uranium loading in the fuel increases rapidly. In addition to the obvious changes, as in the strength of the web between channels, there are significant nuclear and materials problems associated with the use of increased channel diameter.

The thermal effects of doubling the power density can be discussed in general terms. Temperature gradients in both fuel and structural components are proportional to volumetric generation rate, and hence will double. Thickening structural members to handle the higher hydraulic forces may be limited as a consequence. Maximum temperatures may generally increase over the NRX-A2 for many components. Fuel element temperatures should increase only slightly because the distance from the point of maximum temperature to the coolant surface is relatively small. In regions of low thermal conductivity, such as the titanium support structure, and in regions relatively distant from coolant surfaces, substantial increases in maximum temperature may be experienced. This is illustrated in figures 2-31 and 2-32 in which inner reflector temperatures were calculated at twice the current design power. The maximum temperature in pyrolytic graphite (insulating tiles) exceeds $8000^\circ R$ indicating redesign may be required here.

From a nuclear standpoint, the increased propellant density may increase control requirements since the operating reactivity is much increased and the problem of propellant reactivity feedback is aggravated. A complete analysis of the reactivity during operation is indicated. The fission power distribution is also affected by the change in propellant distribution in both core and reflector. In a 60 minute operation, loss of fuel by corrosion may be a limiting factor determining both initial reactivity and control requirements.

For a detailed discussion of changes to the NRX-A2 reactor design to define the NRX-A5 reactor, the reader is referred to WANL-TME-784, which summarizes the Mechanical Design Review held April 9, 1964.

SECTION 5

CONCLUSIONS

Two types of seal systems, the cooled periphery and the hot periphery, have been studied and shown to be thermally feasible. Either concept could be adapted to the NRX-A2 type of design with perhaps more development necessary for the "hot periphery", than for the "cooled periphery" concept. The experience of LASL with the KIWI B-4D wrapper could be used to supplement the "cooled periphery" concept. The NRX-A5 design, as currently combined, will basically have the NRX-A2 type periphery and inner reflector modified to reflect design improvements over NRX-A2 reactor.

In reflector component design, calculations have shown that convection cooling of the lateral support springs is necessary and the use of an aluminum inner reflector is thermally possible.

No immediate change in core component design is anticipated as a result of the studies made. However, the use of as-extruded elements is recommended.

From a nuclear standpoint none of the inner reflector designs of various combinations of graphite, beryllium and/or aluminum can be eliminated from their effects on reactivity and control drum span.

THIS PAGE

WAS INTENTIONALLY

LEFT BLANK

Astronuclear

APPENDIX A

ATTENDEES AT NRX-A5 THERMAL AND NUCLEAR DESIGN REVIEW
MEETING ON APRIL 10, 1964

AGC

R. W. Hardy

H. A. Lamonds

G. E. Moore

R. Pickering

C. M. Rice

J. R. Smith

SNPO-Cleveland

E. W. Bosse

M. R. Fleishman

R. C. Wilke

E. J. Ziurys

SNPO-Washington

I. Helms

DECLASSIFIED